Universität Potsdam

Mathematisch-Naturwissenschaftliche Fakultät

Institut für Physik und Astronomie

SIGNATURES OF NON-CLASSICALITY IN OPTOMECHANICAL SYSTEMS

Promotion an der Math.-Nat. Fakultät der Universität Potsdam
Kumulative Dissertation

Kandidat:
Andrea Mari

Supervisor:
Prof. Jens Eisert

Potsdam, Januar 2012

Published online at the
Institutional Repository of the University of Potsdam:
URL http://opus.kobv.de/ubp/volltexte/2012/5981/
URN urn:nbn:de:kobv:517-opus-59814
http://nbn-resolving.de/urn:nbn:de:kobv:517-opus-59814

Abstract

This thesis contains several theoretical studies on optomechanical systems, *i.e.* physical devices where mechanical degrees of freedom are coupled with optical cavity modes. This optomechanical interaction, mediated by radiation pressure, can be exploited for cooling and controlling mechanical resonators in a quantum regime.

The goal of this thesis is to propose several new ideas for preparing mesoscopic mechanical systems (of the order of 10^{15} atoms) into highly *non-classical states*. In particular we have shown new methods for preparing optomechanical *pure states*, *squeezed states* and *entangled states*. At the same time, procedures for experimentally detecting these quantum effects have been proposed. In particular, a quantitative measure of non classicality has been defined in terms of the negativity of phase space quasi-distributions. An operational algorithm for experimentally estimating the non-classicality of quantum states has been proposed and successfully applied in a quantum optics experiment.

The research has been performed with relatively advanced mathematical tools related to differential equations with periodic coefficients, classical and quantum Bochner's theorems and semidefinite programming. Nevertheless the physics of the problems and the experimental feasibility of the results have been the main priorities.

Contents

List of publications

- **Quantum effects in optomechanical systems**,
  C. Genes, A. Mari, D. Vitali and P. Tombesi,
  Advances in Atomic, Molecular, and Optical Physics 57, 33 (2009).

- **Gently modulating opto-mechanical systems**,
  A. Mari and J. Eisert,
  Physical Review Letters 103, 213603 (2009).

- **Directly estimating non-classicality**,
  A. Mari, K. Kieling, B. M. Nielsen, E. S. Polzik and J. Eisert,
  Physical Review Letters 106, 010403 (2011).

- **Cooling by heating**,
  A. Mari and J. Eisert,
  arXiv:1104.0260, submitted (2011).

- **Opto- and electro-mechanical entanglement improved by modulation**,
  A. Mari and J. Eisert,
  arXiv:1111.2415, submitted (2011).

Introduction

What is quantum optomechanics?

The aim of this thesis is to theoretically investigate the possibility of inducing and observing quantum effects in mesoscopic mechanical systems. Most of the investigation is focused on the prototypical experimental scenario of a mechanical resonator coupled to quantum light modes. The study of this kind of setting became in the last decades a very flourishing research field called *quantum optomechanics* [6, 7]. Probably the main question that strongly motivates the scientific effort in this field is the following: *at which mass and length scales do mechanical systems behave according to quantum mechanics rather than to classical mechanics?* This question can be interpreted in two different ways which are both interesting and stimulating. One point of view is to better understand some fundamental aspects of quantum mechanics, in particular the controversial origin of decoherence or more generally the transition from the quantum to the classical world. On the other hand, one can look at the same question more pragmatically as a technical challenge to push the limits of quantum controllability over larger and larger systems. This second point of view can be well expressed by quoting A. Zeilinger: *"The border between classical and quantum phenomena is just a question of money"* [8]. In any case, whatever it is the philosophical approach, the previous question is worth being tackled and the aim of thesis is to give a contribution to this challenge by providing new methods for preparing and rigorously detecting macroscopic quantum states of mechanical degrees of freedom.

One of the more interesting and promising ways in which a mechanical system can interact with an optical or microwave field is via the phenomenon of *radiation pressure*. The simple reflection of a light beam on a mechanical system can transfer a very weak momentum to it. This was assumed for the first time by Kepler in order to justify the characteristic bending of the tails of comets and later theoretically established within the framework of

Maxwell equations [11]. From a classical point of view, the radiation pressure interaction is nowadays well known and also conveniently applied: see for example the recently launched spacecraft IKAROS making use of the solar pressure as main propulsion [10].

Probably the first intersection of the concept of radiation pressure with quantum mechanics can be traced back to a *Gedankenexperiment* proposed by Einstein in 1909 [12] where, for the first time, the concept of single quanta of light exchanging momentum with a moving membrane was prophetically introduced. Much later, in 1970, Braginsky studied the quantum fundamental limits that radiation pressure induces when sensing mechanical motion with light [13]. However, only in the last twenty years, thanks to the theoretical background of quantum optics and to the experimental progress in micro and nano-technologies, the research field of optomechanics strongly emerged and acquired the large scientific attention that it has in our days [6, 7]. After several pioneering theoretical ideas related to mechanical Kerr effects [14, 15], photon number measurements [16], laser cooling [17] and mechanical superpositions [18], many experiments where done involving micro and nano-mechanical resonators controlled closer and closer to their quantum regime [19, 20, 21, 22, 23]. Only very recently one of the most exciting quest in the context of quantum optomechanics has been reached by several experimental groups: the cooling of a mesoscopic mechanical resonator down to its quantum ground state [24, 25, 26]. The present experimental ability to achieve high level of mechanical purity and control is opening the road to many other research directions like non-classical state preparation [27], quantum transducers [30], optomechanical entanglement [28, 29] *etc.*. It is exactly this relatively short distance between theoretical ideas and experiments, together with the wide range of possible applications, what makes the field of quantum optomechanics particularly lively and attractive.

Structure of the thesis

This is a cumulative thesis and it is structured in the following way: two introductory chapters, five attached publications [1, 2, 3, 4, 5] (in their original layout) and a final discussion. The first two chapters have the role of introducing the reader to the main concepts and methods of this thesis. The first chapter is an introduction to the theory of optomechanics, setting the stage for a quantum mechanical description of these devices. The second chapter contains a brief overview of mathematical methods used within the various

publications: phase space methods, classical and quantum Bochner's theorems and differential equations with periodic coefficients. The publications are attached in a chronological order with respect to their submission date. In the conclusion all the publications are schematically summarized and followed by a general discussion connecting the different results and giving the global motivation of the thesis.

Chapter 1

Quantum theory of optomechanics

1.1 Fabry-Pérot cavity with a moving mirror

The canonical model of an optomechanical device is an optical cavity where one mirror is fixed while the other one is free to move in a harmonic potential (see Fig. 1.1). One of the optical modes is driven with a laser and the light inside the cavity will push the mirror due to radiation pressure. At the same time, any movement of the mirror will change the length of the cavity modulating the phase of the light. It is the combination of these two mechanisms that, if used in a convenient way, can generate a very rich variety of optomechanical phenomena. Real experimental devices reproducing exactly this structure have been realized [22], but many other configurations are also possible: optomechanical micro-toroids [21, 23], optical cavities with vibrating

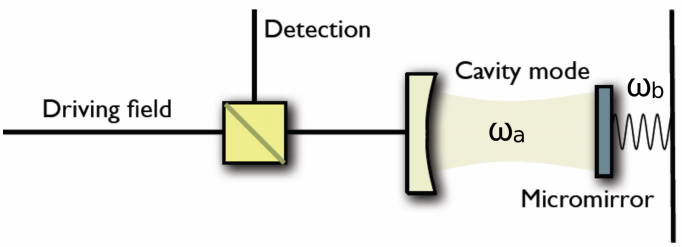

Figure 1.1: Typical model of an optomechanical system. A cavity mode of frequency ω_a is driven by a laser. The light mode interacts via radiation pressure with the mechanical motion of the right mirror. The mirror oscillates in a harmonic potential of frequency ω_b.

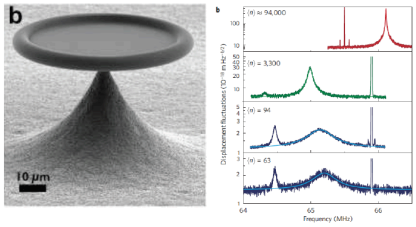

Schliesser, Arcizet, Rivière, Anetsberger, Kippenberg, Nature Physics 5 (2009)

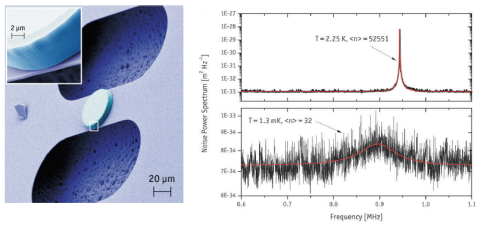

Gröblacher, Hertzberg, Vanner, Cole, Gigan, Schwab, Aspelmeyer, *Nature Physics* 5 (2009)

Figure 1.2: Experimental examples of optomechanical systems. On the left a micro-toroidal realization of an optomechanical system [21, 23]. On the right a micro-mirror attached to a cantilever [22] as in the scheme of Fig. 1.1.

membranes [32], spheres in optical tweezers [31], *etc.*. Even if experimentally very different (see *e.g.* Fig. 1.2), all the mentioned devices can be theoretically described by the same basic model of Fig. 1.1.

1.1.1 Coherent dynamics

In a quantum mechanical picture of the setup, the laser driven optical mode and the mechanical motion of the mirror are formally described by two harmonic oscillators of frequencies ω_a and ω_b with respective creation and annihilation operators a, $a^\dagger$ and b, $b^\dagger$ obeying bosonic commutation rules $[a, a^\dagger] = [b, b^\dagger] = 1$. Since we are dealing with harmonic modes, all the theoretical formalism will be essentially the one generally used in quantum optics. It can be shown [33] that, if ω_b is much smaller than the free spectral range of the optical cavity, the dynamics of the system is well approximated by the following Hamiltonian:

$$H = \hbar\omega_a a^\dagger a + \hbar\omega_b b^\dagger b - \hbar g a^\dagger a(b + b^\dagger) + E(ae^{-i\omega_l t} + a^\dagger e^{i\omega_l t}), \qquad (1.1)$$

where the first two terms represent the energy of the optical and mechanical modes, the third term is the interaction potential and the last one describes the coherent driving of a laser of frequency ω_l.

By direct inspection of the third term we can recognize a potential of the form $-Fq$, where $q = (b + b^\dagger)/\sqrt{2}$ is the position operator of the mirror and F a force pushing the mirror to the right with a modulus proportional to the intensity $\hbar\omega_a a^\dagger a$ of the light. This is the standard non-linear radiation pressure interaction that is at the basis of every optomechanical device.

The coupling constant g depends non-trivially on the experimental apparatus and it is usually determined via a direct measurement. However in the

particular setup of Fig. 1.1, this coupling can be indirectly estimated [33]: $g = \frac{\omega_a}{L}\sqrt{\frac{2\hbar}{m\omega_b}}$ where L is the length of the cavity and m is the effective mass of the mechanical mode. In general the coupling constant is very small $g << \omega_b$, nevertheless strong effective couplings can be achieved via strong laser pumping, *i.e.* $E >> \omega_b$.

1.1.2 Dissipative dynamics

The previous Hamiltonian is a good description of the coherent dynamics however both the optical and the mechanical modes will be subject to decoherence and these non unitary processes should also be included in the description of the system. In the Schrödinger picture, dissipation and decoherence can be taken into account with a *master equation* [34] describing the evolution of the density operator:

$$\begin{aligned}\dot{\rho} &= -\frac{i}{\hbar}[H,\rho] \\ &\quad +\kappa(n_a+1)(2a\rho a^\dagger - a^\dagger a\rho - \rho a^\dagger a) + \kappa n_a(2a^\dagger\rho a - aa^\dagger\rho - \rho aa^\dagger) \\ &\quad +\gamma(n_b+1)(2b\rho b^\dagger - b^\dagger b\rho - \rho b^\dagger b) + \gamma n_b(2b^\dagger\rho b - bb^\dagger\rho - \rho bb^\dagger), \quad (1.2)\end{aligned}$$

where the first line corresponds to the unitary Schrödinger equation while the second and third lines are responsible for the dissipative processes of the optical and mechanical modes respectively. The constants κ and γ are the optical and mechanical decay rates, while $n_x = [\exp(\frac{\hbar\omega_x}{k_B T}) - 1]^{-1}$ are the bath mean occupation numbers at the respective frequencies and at temperature T.

In the previous master equation the dissipative structure of the mechanical mode is assumed to be the same of the optical mode. This is a justified approximation if we are dealing with good mechanical quality factors $\omega_b >> \gamma$. A more realistic model for the mechanical decoherence is that of *quantum Brownian motion* [34] where the symmetry between the mechanical position operator $q = (b+b^\dagger)\sqrt{2}$ and the momentum operator $p = i(b^\dagger - b)\sqrt{2}$ is broken. This symmetry breaking is motivated by the classical intuition that mechanical friction and noise are invariant for spatial translations and are related only to the velocity of the system. More rigorously, from a microscopic model of a large bath of harmonic oscillators coupled to the mechanical mirror, a quantum analogue of classical *Langevin equations* can be derived well reproducing the mechanical dissipation and decoherence [34, 29]. This is a set of Heisenberg equations of motion of the system operators that can be used in place of the

previous master equation:

$$\dot{q} = \omega_b\, p, \tag{1.3}$$

$$\dot{p} = -\omega_b\, q - 2\gamma\, p + g a^\dagger a + \xi, \tag{1.4}$$

$$\dot{a} = -(\kappa + i\omega_a)a + i\sqrt{2}gaq + Ee^{-i\omega_l t} + \sqrt{2\kappa}a^{in}, \tag{1.5}$$

where ξ and a^{in} are noise operators modeling the sources of mechanical and optical fluctuations. These noise operators are assumed to be Gaussian, *i.e.* completely described by their first and second order correlation functions which are

$$\langle \xi(t) \rangle = \langle a^{in}(t) \rangle = 0, \tag{1.6}$$

$$\langle \xi(t)\xi(t') \rangle = 2\gamma[(2n_b + 1)\delta(t - t') + i\frac{d}{dt}\delta(t - t')], \tag{1.7}$$

$$\langle a^{in}(t)^\dagger a^{in}(t') \rangle = (n_a + 1)\delta(t - t'), \tag{1.8}$$

$$\langle a^{in}(t) a^{in}(t')^\dagger \rangle = \delta(t - t'), \tag{1.9}$$

and all the other second order correlations are zero.

In the limit of $\omega_m \to \infty$, these quantum Langevin equations become equivalent to the master equation (1.2). Both the Schrödinger and Heisenberg picture approaches introduced in this section are used as starting points in most of the publications included in this thesis.

Chapter 2

Mathematical tools

This chapter contains an introductory overview of the main mathematical methods which have been used in the attached publications.

2.1 The Wigner function

The Wigner function [34, 35, 36, 37] is a mathematical description of a quantum state that is particularly convenient in quantum optics, optomechanics and more generally each time the system under investigation is described in terms of *continuous variable* operators like position and momentum. The main idea is to associate to a quantum state something similar to a phase space distribution. The Wigner function is the closest quantum analogue of a phase space density in the sense that it is a phase-space function that contains all the information that we can have about a quantum state. However, differently form its classical counterpart, the Wigner function can have negative values in some small phase space regions at the quantum scale of $\hbar$. It is exactly the negativity of this function that it is often used as a figure of merit of "quantumness" of a state. The intuition is that, whenever the Wigner function is positive, this could be interpreted as a classical probability distribution associated to a system described in terms of classical canonical coordinates. The negativity of the Wigner function can then be used as a reasonable criterion to distinguish classical states from non-classical ones.

Formally, given N quantum systems, if we define a vector containing the position and momentum operators $R = (q_1, p_1, q_2, p_2, ...q_N, p_N)^T$ we can express the canonical commutation relations in matrix form

$$[R_k, R_l] = i\sigma_{k,l}\,, \tag{2.1}$$

where σ is the $2N \times 2N$ symplectic matrix given by

$$\sigma = \bigoplus_{k=1}^{N} \begin{pmatrix} 0 & 1 \\ -1 & 0 \end{pmatrix}. \tag{2.2}$$

Given this vector R of canonical operators, one can introduce a family of *displacement* or *Weyl operators* [36, 37]:

$$D_\xi = e^{i\xi^T \sigma R}, \quad \xi \in \mathbb{R}^{2N}. \tag{2.3}$$

Through these operators one can apply to the density matrix ρ a quantum analogue of the Fourier transform:

$$\chi(\xi) = \mathrm{Tr}(\rho D_\xi). \tag{2.4}$$

The function $\chi(\xi)$ is called *quantum characteristic function* and it shares many properties with its classical counterpart, *e.g.*:

$$\chi(0) = 1, \tag{2.5}$$

$$\frac{1}{(2\pi)^N} \int |\chi(\xi)|^2 d\xi \leq 1, \tag{2.6}$$

where the last integral is equal to 1 if and only if the state ρ is pure. The characteristic function maps each operator to a unique function in $\mathcal{L}^2$ however, if we want something which is analogous to a probability distribution in a phase space, we need the inverse Fourier transform of it:

$$W(r) = \frac{1}{(2\pi)^{2N}} \int \chi(\xi) e^{-i\xi^T \sigma r} d\xi, \tag{2.7}$$

which is called the *Wigner function*.

2.1.1 Gaussian states and covariance matrices

A quantum state ρ is defined to be *Gaussian* if its characteristic function (or equivalently its Wigner function) is a Gaussian. Given the displacement vector $d = \mathrm{Tr}\{\rho R\}$, and the symmetrically ordered covariance matrix $V_{k,l} = \mathrm{Tr}\{\rho[R_k - d_k, R_l - d_l]_+\}$, the most general Gaussian characteristic function can be written as:

$$\chi(\xi) = e^{-\frac{1}{4}(\sigma\xi)^T V \sigma\xi + i d^T \sigma\xi}, \tag{2.8}$$

where the first moments d and the second moments V completely characterize the state. From the definition (2.7), the associated *Wigner function* will also be Gaussian and equal to [36, 37]:

$$W(r) = \pi^{-N} |V|^{-\frac{1}{2}} e^{-(r-d)^T \sigma^T V^{-1} \sigma (r-d)}, \tag{2.9}$$

where $|V|$ is the determinant of the covariance matrix. Not every Gaussian function can be a Wigner function of a physical state. The Heisenberg principle implies the following constraint [36, 37] on the correlation matrix

$$V + i\sigma \geq 0. \tag{2.10}$$

We have seen that through the Wigner function one can have a rigorous and complete phase space representation of a quantum state ρ. In general, however, it is difficult to compute how the Wigner function behaves when general quantum operations are applied to ρ. This problem is much easier if we consider only *Gaussian operations*, which are the transformations mapping Gaussian states into Gaussian states. Since a Gaussian state is determined by its first and second moments we can completely define a Gaussian operation via its effect on the correlation matrix V and on the displacement vector d. Since strongly driven optomechanical systems evolve according to a Gaussian dissipative dynamic, this formalism based only on first and second moments is particularly convenient and it is indeed heavily used in many of the attached publications.

2.2 Classical and quantum Bochner's theorems

Classical [40] and quantum [38, 39] Bochner's theorems are the two main mathematical tools used in the publication *Directly estimating non-classicality* [3]. They are related to characteristic functions and they answer to the following two questions:

1. How can we test if a characteristic function corresponds to a positive Wigner function?

2. How can we test if a characteristic function corresponds to a physical quantum state (*i.e.* to a positive density matrix)?

Theorem 1 (Classical Bochner's theorem [40])**.** *A characteristic function $\chi(\xi)$ is the Fourier transform of a positive function (e.g. the Wigner function) if and only if, for every $m \in \mathbb{N}$ and for every set of real vectors $T = (\xi_1, \xi_2, \ldots, \xi_m)$, the $m \times m$ matrix $M^{(0)}$ with entries*

$$M^{(0)}_{k,l} = \chi(\xi_k - \xi_l) \tag{2.11}$$

is positive semidefinite, i.e. $M^{(0)} \geq 0$.

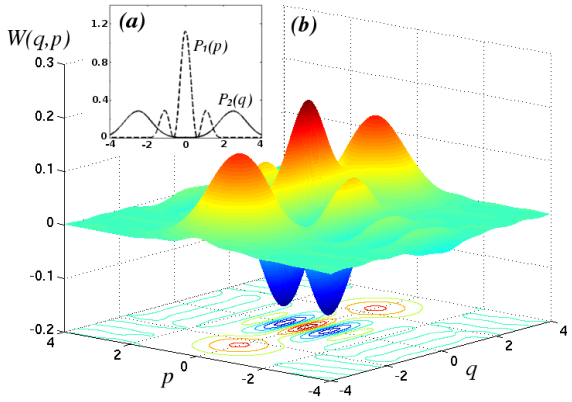

Figure 2.1: Example of a Wigner function of a non-classical state (b). By measuring position and momentum distributions only (a), classical and quantum Bochner's theorems allow to certify the negativity of the Wigner funciton. This figure is taken from [3].

Theorem 2 (Quantum Bochner's theorem [38, 39])**.** *A characteristic function* $\chi(\xi)$ *is the the quantum Fourier transform of a positive operator (e.g. a density matrix) if and only if, for every* $m \in \mathbb{N}$ *and for every set of real vectors* $T = (\xi_1, \xi_2, \ldots, \xi_m)$*, the* $m \times m$ *matrix* $M^{(1)}$ *with entries*

$$M^{(1)}_{k,l} = \chi(\xi_k - \xi_l) e^{-i\xi_k \cdot \sigma \xi_l / 2} \tag{2.12}$$

is positive semidefinite, i.e. $M^{(1)} \geq 0$*.*

As we have already anticipated, Wigner functions can take negative values. As a consequence, every quantum state must have a characteristic function satisfying the quantum Bochner's theorem but not necessarily the positivity condition given in the classical version of theorem. This means that a violation of the semi-positivity of the matrix $M^{(0)}$ given in Eq. (2.11) provides a valid and rigorous test for the negativity of the Wigner function. This test has been used in the publication *Directly measuring non-classicality* [3] in order to certify and to quantify the non-classicality of continuous variable quantum states (see Fig. 2.1).

2.3 Differential equations with periodic coefficients

In the publications *Gently modulating optomechanical systems* [2] and *Opto and electro-mechanical entanglement improved by modulation* [5], a scheme similar to the one introduced in the previous chapter (see Eq. (1.1)) has been

analyzed where the amplitude E of the driving laser is not constant but it has some periodic time dependence $E(t) = E(t+\tau)$ with period $\tau > 0$. For this reason several differential equations with periodic coefficients appears in the equations of motion of the optomechanical system.

In this section we explicitly analyze, abstracting from the original physical situation, the mathematical properties of differential equations with time periodic coefficients [41]. Consider a linear first-order system,

$$\dot{x}(t) = B(t)x(t), \tag{2.13}$$

where $x(\cdot)$ is a time dependent vector with n components and $B(\cdot)$ is some complex square matrix with entries dependent on $t \geq t_0$ with some $t_0 > 0$. Then the linear first-order system has a unique solution for $x(t_0) = x_0$ for all times $t > t_0$. The principal matrix solution is the solution of

$$\dot{P}(t, t_0) = B(t)P(t, t_0), \tag{2.14}$$

with $P(t, t_0) = \mathbb{1}$. The solution to the inhomogeneous system $\dot{x}(t) = B(t)x(t) + g(t)$, with initial condition $x(t_0) = x_0$ is given by

$$x(t) = P(t, t_0)x_0 + \int_{t_0}^{t} ds P(t, s)g(s). \tag{2.15}$$

Theorem 3 (Floquet's theorem [41])**.** *If $B(.)$ is periodic, $B(t) = B(t+\tau)$ for some $\tau > 0$ for all $t \geq t_0$, then the principal matrix solution has the form $P(t, t_0) = X(t, t_0)e^{(t-t_0)Y(t_0)}$, where the matrices $X(.,.)$ and $Y(.)$ are τ-periodic in all their arguments and $X(t_0, t_0) = \mathbb{1}$.*

The eigenvalues λ_i of the matrix Y are known as Floquet exponents. A negative value of $\lambda = \max_j \mathrm{re}(\lambda_j)$ implies asymptotic periodic solutions:

Theorem 4 (Asymptotic periodicity)**.** *For stable systems, if both $B(.)$ and $g(.)$ are τ-periodic then, for $t - t_0 > 1$ we have*

$$\begin{aligned} \|x(t+\tau) - x(t)\| \quad &\leq \quad e^{\lambda(t-t_0)} mcn\,(t - t_0 + \tau)^{n-1} \\ &\quad \times \Big(2\|x_0\| + \tau \max_{v \in I} \|g(v)\|\Big), \end{aligned} \tag{2.16}$$

where n is the dimension of the vector space, $I = [0, \tau]$, $m = \max_{t,t' \in I} \|X(t, t')\|$ and $c = \max_{u \in I} \|W(u)\| \, \|W^{-1}(u)\|$, where $W(u)$ is a similarity transformation that brings $Y(u)$ to a Jordan form. Here the norm $\|.\|$ is the one induced by

the Euclidean vector norm. (For a proof of this theorem see the appendix of the preprint version of [2]).

This final result on asymptotic periodicity of differential equations is used in the following publications to theoretically predict the emergence of periodic limit cycles in modulated optomechanical systems [2, 5].

Chapter 3

Quantum effects in optomechanical systems

Quantum effects in optomechanical systems

C. Genes [a], A. Mari [b], D. Vitali [c], and P. Tombesi [c]

[a] *Institute for Theoretical Physics, University of Innsbruck, and Institute for Quantum Optics and Quantum Information, Austrian Academy of Sciences, Technikerstrasse 25, A-6020 Innsbruck, Austria*

[b] *Institute of Physics and Astronomy, University of Potsdam, 14476 Potsdam, Germany*

[c] *Dipartimento di Fisica, Università di Camerino, via Madonna delle Carceri, I-62032, Camerino (MC) Italy*

Abstract

The search for experimental demonstrations of the quantum behavior of macroscopic mechanical resonators is a fastly growing field of investigation and recent results suggest that the generation of quantum states of resonators with a mass at the microgram scale is within reach. In this chapter we give an overview of two important topics within this research field: cooling to the motional ground state, and the generation of entanglement involving mechanical, optical and atomic degrees of freedom. We focus on optomechanical systems where the resonator is coupled to one or more driven cavity modes by the radiation pressure interaction. We show that robust stationary entanglement between the mechanical resonator and the output fields of the cavity can be generated, and that this entanglement can be transferred to atomic ensembles placed within the cavity. These results show that optomechanical devices are interesting candidates for the realization of quantum memories and interfaces for continuous variable quantum communication networks.

Key words: radiation pressure, optical cavities, micromechanical systems, optomechanical devices, ground state cooling, quantum entanglement, atomic ensembles
PACS: 03.67.Mn, 85.85.+j, 42.50.Wk, 42.50.Lc

Contents

1 Introduction

Mechanical resonators at the micro- and nano-meter scale are widely employed for a large variety of applications, more commonly as sensors or actuators in integrated electrical, optical, and opto-electronical systems [1,2,3,4]. Modifications of the resonator motion can be detected with high sensitivity by looking at the radiation (or electric current) which interacted with the resonator. For example, small masses can be detected by measuring the frequency shift induced on the resonator, while tiny displacements (or weak forces inducing such displacements) can be measured by detecting the corresponding phase shift of the light interacting with it [2]. The resonators are always subject to thermal noise, which is due to the coupling with internal and/or external degrees of freedom and is one of the main factors limiting the sensitivity of these devices. However, due to the progress in nanofabrication techniques, the mechanical quality factor $\mathcal{Q}_m$ (which quantifies this undesired coupling to environmental degrees of freedom) is steadily improving, suggesting that in the near future these devices will reach the regime in which their sensitivity is limited by the ultimate quantum limits set by the Heisenberg principle. The importance of the limits imposed by quantum mechanics on the resonator motion was first pointed out by Braginsky and coworkers [5] in the completely different context of *massive* resonators employed in the detection of gravitational waves [6]. However, in recent years the quest for the experimental demonstration of genuine quantum states of macroscopic mechanical resonators has spread well beyond the gravitational wave physics community and has attracted a

wide interest. In fact, the detection of an unambiguous signature of the quantum behavior of a macroscopic oscillator, with a mass at least of the order of a microgram, would shed further light onto the quantum-classical boundary problem [7]. In fact, nothing in the principles of quantum mechanics prevents macroscopic systems to be prepared in genuine quantum states. However, it is not yet clear how far one can go in this direction [8], and a complete understanding of how classical behavior emerges from the quantum substrate requires the design and the implementation of dedicated experiments. Examples of this kind are single-particle interference of macro-molecules [9], the demonstration of entanglement between collective spins of atomic ensembles [10], and of entanglement in Josephson-junction qubits [11]. For what concerns mechanical resonators, the experimental efforts are currently focusing on cooling them down to their motional ground state [2]. This goal has not been achieved yet, but promising results in this direction have been obtained in different setups [12,13,14,15,16,17,18,19,20,21,22,23,24,25,26,27,28,29,30,31], involving different examples of mechanical resonators coupled either to radiative or to electrical degrees of freedom. Ground state cooling of microgram-scale resonators seems to be within reach, as already suggested by various theoretical proposals [32,33,34,35,36,37,38,39,40,41,42,43] which showed how a mechanical oscillator can be coupled to another system so that the latter can act as an effective zero-temperature reservoir. In the first part of this chapter we shall review the problem of ground state cooling of a mechanical resonator, by focusing onto the case where the role of effective zero-temperature "fridge" is played by an optical cavity mode, coupled to the resonator by radiation pressure. In this case this interaction can be exploited for cooling in two different ways: i) back-action, or self-cooling [33,39,40,41,42,43] in which the off-resonant operation of the cavity results in a retarded back action on the mechanical system and hence in a "self"-modification of its dynamics [14,17,18,20,21,23,24,25,26,27,29,30,31]; ii) cold-damping quantum feedback, where the oscillator position is measured through a phase-sensitive detection of the cavity output and the resulting photocurrent is used for a real-time correction of the dynamics [12,16,19,22,28]. We shall compare the two approaches and see that while back-action cooling is optimized in the good cavity limit where the resonator frequency is larger than the cavity bandwidth, cold damping is preferable in the opposite regime of larger cavity bandwidths [41]. It should be noticed that the model Hamiltonian based on radiation pressure coupling between an optical cavity mode and one movable cavity mirror is quite general and immediately extendible to other situations, such as the toroidal microcavities of Refs. [20,25], the capacitively coupled systems of Refs. [23,27] and even atomic condensate systems [44].

From the theory side, the generation of other examples of quantum states of a micro-mechanical resonator has been also considered. The most relevant examples are given by squeezed and resonator-field (or atoms) entangled states. Squeezed states of nano-mechanical resonators [45] are potentially useful for

surpassing the standard quantum limit for position and force detection [5], and could be generated in different ways, either by coupling to a qubit [46], or by measurement and feedback schemes [36,47]. Entanglement is instead the characteristic element of quantum theory, because it is responsible for correlations between observables that cannot be understood on the basis of local realistic theories [48]. For this reason, there has been an increasing interest in establishing the conditions under which entanglement between macroscopic objects can arise. Relevant experimental demonstration in this directions are given by the entanglement between collective spins of atomic ensembles [10], and between Josephson-junction qubits [11]. Then, starting from the proposal of Ref. [49] in which two mirrors of a ring cavity are entangled by the radiation pressure of the cavity mode, many proposals involved nano- and micro-mechanical resonators, eventually entangled with other systems. One could entangle a nanomechanical oscillator with a Cooper-pair box [50], while Ref. [51] studied how to entangle an array of nanomechanical oscillators. Further proposals suggested to entangle two charge qubits [52] or two Josephson junctions [53] via nanomechanical resonators, or to entangle two nanomechanical resonators via trapped ions [54], Cooper pair boxes [55], or dc-SQUIDS [56]. More recently, schemes for entangling a superconducting coplanar waveguide field with a nanomechanical resonator, either via a Cooper pair box within the waveguide [57], or via direct capacitive coupling [58], have been proposed. After Ref. [49], other optomechanical systems have been proposed for entangling optical and/or mechanical modes by means of the radiation pressure interaction. Ref. [59] considered two mirrors of two different cavities illuminated with entangled light beams, while Refs. [60,61,62,63] considered different examples of double-cavity systems in which entanglement either between different mechanical modes, or between a cavity mode and a vibrational mode of a cavity mirror have been studied. Refs. [64,65] considered the simplest scheme capable of generating stationary optomechanical entanglement, i.e., a single Fabry-Perot cavity either with one [64], or both [65], movable mirrors.

In the second part of the chapter we shall focus on the generation of stationary entanglement by starting from the Fabry-Perot model of Ref. [64], which is remarkable for its simplicity and robustness against temperature, and extend its study in various directions. In fact, entangled optomechanical systems could be profitably used for the realization of quantum communication networks, in which the mechanical modes play the role of local nodes where quantum information can be stored and retrieved, and optical modes carry this information between the nodes. Refs. [66,67,68] proposed a scheme of this kind, based on free-space light modes scattered by a single reflecting mirror, which could allow the implementation of continuous variable (CV) quantum teleportation [66], quantum telecloning [67], and entanglement swapping [68]. Therefore, any quantum communication application involves *traveling output* modes rather than intracavity ones, and it is important to study how the optomechanical entanglement generated within the cavity is transferred to the output field.

Furthermore, by considering the output field, one can adopt a multiplexing approach because, by means of spectral filters, one can always select many different traveling output modes originating from a single intracavity mode. One can therefore manipulate a multipartite system, eventually possessing multipartite entanglement. We shall develop a general theory showing how the entanglement between the mechanical resonator and optical output modes can be properly defined and calculated [69]. We shall see that, together with its output field, the single Fabry-Perot cavity system of Ref. [64] represents the "cavity version" of the free-space scheme of Refs. [66,67]. In fact, as it happens in this latter scheme, all the relevant dynamics induced by radiation pressure interaction is carried by the two output modes corresponding to the first Stokes and anti-Stokes sidebands of the driving laser. In particular, the optomechanical entanglement with the intracavity mode is optimally transferred to the output Stokes sideband mode, which is however robustly entangled also with the anti-Stokes output mode. We shall see that the present Fabry-Perot cavity system is preferable with respect to the free space model of Refs. [66,67], because entanglement is achievable in a much more accessible experimental parameter region. We shall then extend the analysis to the case of a doubly-driven cavity mode. We shall see that a peculiar parameter regime exists where the optomechanical system, owing to the combined action of the two driven modes, is always stable and is characterized by robust entanglement between the resonator and the cavity output fields.

In the last Section we shall investigate the possibility to couple and entangle in a robust way optomechanical systems to atomic ensembles, in order to achieve a strongly-coupled hybrid multipartite system [70,71]. We shall see that this is indeed possible, especially when the atomic ensemble is resonant with the Stokes sideband induced by the resonator motion. Such hybrid systems might represent an important candidate for the realization of CV quantum interfaces within CV quantum information networks.

2 Cavity optomechanics via radiation pressure

The simplest cavity optomechanical system consists of a Fabry-Perot cavity with one heavy, fixed mirror through which a laser of frequency ω_l drives a cavity mode, and another light end-mirror of mass m (typically in the micro or nanogram range), free to oscillate at some mechanical frequency ω_m. Our treatment is however valid also for other cavity geometries in which one has an optical mode coupled by radiation pressure to a mechanical degree of freedom. A notable example is provided by silica toroidal optical microcavities which are coupled to radial vibrational modes of the supporting structure [20,72]. Radiation pressure typically excites several mechanical degrees of freedom of the system with different resonant frequencies. However, a single mechanical

mode can be considered when a bandpass filter in the detection scheme is used [73] and coupling between the different vibrational modes can be neglected. One has to consider more than one mechanical mode only when two close mechanical resonances fall within the detection bandwidth (see Ref. [74] for the effect of a nearby mechanical mode on cooling and entanglement). The Hamiltonian of the system describes two harmonic oscillators coupled via the radiation pressure interaction, and reads [75]

$$H = \hbar\omega_c a^\dagger a + \frac{1}{2}\hbar\omega_m(p^2+q^2) - \hbar G_0 a^\dagger a q + i\hbar\mathcal{E}(a^\dagger e^{-i\omega_l t} - a e^{i\omega_l t}). \quad (1)$$

The first term describes the energy of the cavity mode, with lowering operator a ($[a, a^\dagger] = 1$), frequency ω_c (and therefore detuned by $\Delta_0 = \omega_c - \omega_l$ from the laser), and decay rate κ. The second term gives the energy of the mechanical mode, described by dimensionless position and momentum operators q and p ($[q, p] = i$). The third term is the radiation-pressure coupling of rate $G_0 = (\omega_c/L)\sqrt{\hbar/m\omega_m}$, where m is the effective mass of the mechanical mode [73], and L is an effective length that depends upon the cavity geometry: it coincides with the cavity length in the Fabry-Perot case, and with the toroid radius in the case of Refs. [20,72]. The last term describes the input driving by a laser with frequency ω_l, where $\mathcal{E}$ is related to the input laser power $\mathcal{P}$ by $|\mathcal{E}| = \sqrt{2\mathcal{P}\kappa/\hbar\omega_l}$. One can adopt the single cavity mode description of Eq. (1) as long as one drives only one cavity mode and the mechanical frequency ω_m is much smaller than the cavity free spectral range $FSR \sim c/2L$. In this case, in fact, scattering of photons from the driven mode into other cavity modes is negligible [76].

2.1 Langevin equations formalism

The dynamics are also determined by the fluctuation-dissipation processes affecting both the optical and the mechanical mode. They can be taken into account in a fully consistent way [75] by considering the following set of nonlinear QLE (quantum Langevin equations), written in a frame rotating at ω_l

$$\dot{q} = \omega_m p, \quad (2)$$
$$\dot{p} = -\omega_m q - \gamma_m p + G_0 a^\dagger a + \xi, \quad (3)$$
$$\dot{a} = -(\kappa + i\Delta_0)a + iG_0 a q + \mathcal{E} + \sqrt{2\kappa}a^{in}. \quad (4)$$

The mechanical mode is affected by a viscous force with damping rate γ_m and by a Brownian stochastic force with zero mean value $\xi(t)$, possessing the

correlation function [75,77]

$$\langle \xi(t)\xi(t')\rangle = \frac{\gamma_m}{\omega_m}\int \frac{d\omega}{2\pi} e^{-i\omega(t-t')}\omega \left[\coth\left(\frac{\hbar\omega}{2k_B T_0}\right)+1\right], \tag{5}$$

where k_B is the Boltzmann constant and T_0 is the temperature of the reservoir of the micromechanical oscillator. The correlation function and the commutator of the Gaussian stochastic force $\xi(t)$ are not proportional to a Dirac delta and therefore $\xi(t)$ is a non-Markovian stochastic process. This fact guarantees that the QLE of Eqs. (2)-(4) preserve the correct commutation relations between operators during the time evolution [75]. However, a Markovian description of the symmetrized correlations of $\xi(t)$ is justified in two different limits, which are both met in typical experimental situations: i) not too low temperatures $k_B T_0/\hbar\omega_m \gg 1$, which for typical values is satisfied even at cryogenic temperatures; ii) high mechanical quality factor $\mathcal{Q} = \omega_m/\gamma_m \to \infty$ [78], which is an important condition for the observation of quantum effects on the mechanical resonator. In this case the correlation function of Eq. (5) can be approximated as

$$\langle \xi(t)\xi(t')\rangle \simeq \gamma_m \left[(2n_0+1)\delta(t-t') + i\frac{\delta'(t-t')}{\omega_m}\right], \tag{6}$$

where $n_0 = (\exp\{\hbar\omega_m/k_B T_0\}-1)^{-1}$ is the mean thermal excitation number of the resonator and $\delta'(t-t')$ denotes the derivative of the Dirac delta.

The cavity mode amplitude instead decays at the rate κ and is affected by the vacuum radiation input noise $a^{in}(t)$, whose correlation functions are given by [79]

$$\langle a^{in}(t)a^{in,\dagger}(t')\rangle = [N(\omega_c)+1]\,\delta(t-t'). \tag{7}$$
$$\langle a^{in,\dagger}(t)a^{in}(t')\rangle = N(\omega_c)\delta(t-t'), \tag{8}$$

where $N(\omega_c) = (\exp\{\hbar\omega_c/k_B T_0\}-1)^{-1}$ is the equilibrium mean thermal photon number. At optical frequencies $\hbar\omega_c/k_B T_0 \gg 1$ and therefore $N(\omega_c) \simeq 0$, so that only the correlation function of Eq. (7) is relevant.

Equations (2)-(4) are not easy to analyze owing to the nonlinearity. However, one can proceed with a linearization of operators around the steady state. The semiclassical steady state is characterized by an intracavity field amplitude α_s ($|\alpha_s| \gg 1$), and a new equilibrium position for the oscillator, displaced by q_s. The parameters α_s and q_s are the solutions of the nonlinear algebraic equations obtained by factorizing Eqs. (2)-(4) and setting the time derivatives to zero:

$$q_s = \frac{G_0|\alpha_s|^2}{\omega_m}, \tag{9}$$

$$\alpha_s = \frac{\mathcal{E}}{\kappa + i\Delta}, \tag{10}$$

where the latter equation is in fact the nonlinear equation determining α_s, since the effective cavity detuning Δ, including radiation pressure effects, is given by [80]

$$\Delta = \Delta_0 - \frac{G_0^2|\alpha_s|^2}{\omega_m}. \tag{11}$$

Rewriting each Heisenberg operator of Eqs. (2)-(4) as the c-number steady state value plus an additional fluctuation operator with zero mean value, one gets the exact QLE for the fluctuations

$$\delta\dot{q} = \omega_m \delta p, \tag{12}$$

$$\delta\dot{p} = -\omega_m \delta q - \gamma_m \delta p + G_0\left(\alpha_s \delta a^\dagger + \alpha_s^* \delta a\right) + \delta a^\dagger \delta a + \xi, \tag{13}$$

$$\delta\dot{a} = -(\kappa + i\Delta)\delta a + iG_0\left(\alpha_s + \delta a\right)\delta q + \sqrt{2\kappa}a^{in}. \tag{14}$$

Since we have assumed $|\alpha_s| \gg 1$, one can safely neglect the nonlinear terms $\delta a^\dagger \delta a$ and $\delta a \delta q$ in the equations above, and get the linearized QLE

$$\delta\dot{q} = \omega_m \delta p, \tag{15}$$

$$\delta\dot{p} = -\omega_m \delta q - \gamma_m \delta p + G\delta X + \xi, \tag{16}$$

$$\delta\dot{X} = -\kappa\delta X + \Delta\delta Y + \sqrt{2\kappa}X^{in}, \tag{17}$$

$$\delta\dot{Y} = -\kappa\delta Y - \Delta\delta X + G\delta q + \sqrt{2\kappa}Y^{in}. \tag{18}$$

Here we have chosen the phase reference of the cavity field so that α_s is real and positive, we have defined the cavity field quadratures $\delta X \equiv (\delta a + \delta a^\dagger)/\sqrt{2}$ and $\delta Y \equiv (\delta a - \delta a^\dagger)/i\sqrt{2}$ and the corresponding Hermitian input noise operators $X^{in} \equiv (a^{in} + a^{in,\dagger})/\sqrt{2}$ and $Y^{in} \equiv (a^{in} - a^{in,\dagger})/i\sqrt{2}$. The linearized QLE show that the mechanical mode is coupled to the cavity mode quadrature fluctuations by the effective optomechanical coupling

$$G = G_0\alpha_s\sqrt{2} = \frac{2\omega_c}{L}\sqrt{\frac{\mathcal{P}\kappa}{m\omega_m\omega_l\left(\kappa^2 + \Delta^2\right)}}, \tag{19}$$

which can be made very large by increasing the intracavity amplitude α_s. Notice that together with the condition $\omega_m \ll c/L$ which is required for the single cavity mode description, $|\alpha_s| \gg 1$ is the *only* assumption required by the linearized approach. This is in contrast with the perturbative approaches described in [40], where a reduced master equation of the mechanical resonator is derived under the weak-coupling assumption $G \ll \omega_m$.

2.2 Stability analysis

The stability analysis can be performed on the linearized set of equations Eqs. (2)-(4) by using the Routh-Hurwitz criterion [81]. Two conditions are obtained

$$s_1 = 2\gamma_m\kappa\left\{\left[\kappa^2+(\omega_m-\Delta)^2\right]\left[\kappa^2+(\omega_m+\Delta)^2\right]\right. \tag{20}$$

$$\left.+\,\gamma_m\left[(\gamma_m+2\kappa)\left(\kappa^2+\Delta^2\right)+2\kappa\omega_m^2\right]\right\}+\Delta\omega_m G^2\left(\gamma_m+2\kappa\right)^2>0, \tag{21}$$

$$s_2 = \omega_m\left(\kappa^2+\Delta^2\right)-G^2\Delta>0. \tag{22}$$

The violation of the first condition, $s_1 < 0$, indicates instability in the domain of blue-detuned laser ($\Delta < 0$) and it corresponds to the emergence of a self-sustained oscillation regime where the mirror effective damping rate vanishes. In this regime, the laser field energy leaks into field harmonics at frequencies $\omega_l \pm r\omega_m\,(r = 1, 2...)$ and also feeds the mirror coherent oscillations. A complex multistable regime can emerge as described in [82]. The violation of the second condition $s_2 < 0$ indicates the emergence of the well-known effect of bistable behavior observed in [83] and occurs only for positive detunings ($\Delta > 0$). In the following we restrict our analysis to positive detunings in the stable regime where both s_1 and s_2 conditions are fulfilled. A parametric plot showing the domain of stability in the red-detuning regime $\Delta > 0$ is shown in Fig. 1 where we have plotted the stability parameter

$$\eta = 1-\frac{G^2\Delta}{\omega_m\left(\kappa^2+\Delta^2\right)}. \tag{23}$$

Negative values of η indicate the emergence of instability. We have chosen the following set of parameters which will be used extensively throughout the chapter and which is denoted by p_0=$(\omega_m, Q_m, m, L, \lambda_c, T_0)$ = ($2\pi \times 10$ MHz, 10^5, 30 ng, 0.5 mm, 1064 nm, 0.6 K). These values are comparable to those used in recent experiments [17,18,19,24,25,26,30,31].

2.3 Covariance matrix and logarithmic negativity

The mechanical and intracavity optical mode form a bipartite continuous variable (CV) system. We are interested in the properties of its steady state which, due to the linearized treatment and to the Gaussian nature of the noise operators, is a zero-mean Gaussian state, completely characterized by its symmetrized covariance matrix (CM). The latter is given by the 4×4 matrix with elements

$$\mathcal{V}_{lm} = \frac{\langle u_l(\infty)\,u_m(\infty)+u_m(\infty)\,u_l(\infty)\rangle}{2}, \tag{24}$$

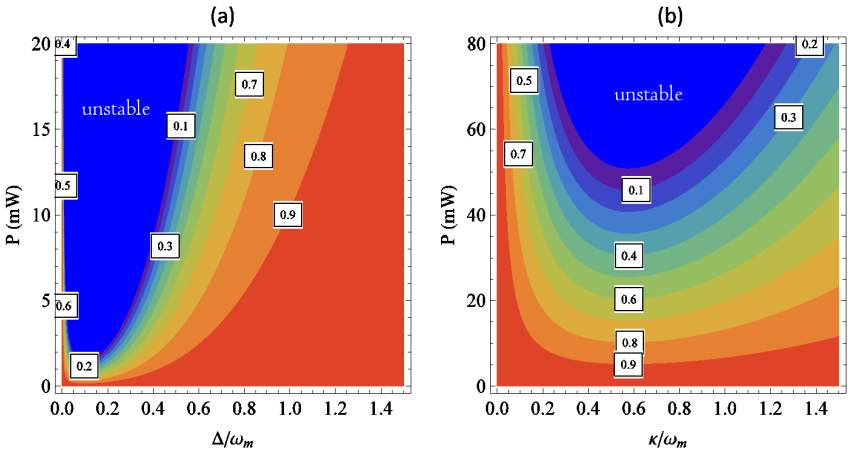

Fig. 1. Stability condition in the red-detuning region. (a) Contour plot of the stability parameter η of Eq. (23) as a function of input power $\mathcal{P}$ and normalized detuning Δ/ω_m. The parameter set p_0=$(\omega_m, Q_m, m, L, \lambda_c, T_0)$ = $(2\pi \times 10$ MHz, 10^5, 30 ng, 0.5 mm, 1064 nm, 0.6 K has been used, together with $\mathcal{F} = 8 \times 10^4$ (corresponding to $\kappa = 0.37\omega_m$). The blue area corresponds to the unstable regime. (b) Stability parameter η versus $\mathcal{P}$ and the normalized cavity decay rate κ/ω_m at $\Delta = \omega_m$.

where $u_m(\infty)$ is the asymptotic value of the m-th component of the vector of quadrature fluctuations

$$u(t) = (\delta q(t), \delta p(t), \delta X(t), \delta Y(t))^{\intercal}. \tag{25}$$

Its time evolution is given by Eqs. (15)-(18), which can be rewritten in compact form as

$$\frac{d}{dt}u(t) = Au(t) + v(t), \tag{26}$$

with A the drift matrix

$$A = \begin{pmatrix} 0 & \omega_m & 0 & 0 \\ -\omega_m & -\gamma_m & G & 0 \\ 0 & 0 & -\kappa & \Delta \\ G & 0 & -\Delta & -\kappa \end{pmatrix}, \tag{27}$$

and $v(t)$ the vector of noises

$$v(t) = \left(0, \xi(t), \sqrt{2\kappa}X^{in}(t), \sqrt{2\kappa}Y^{in}(t)\right)^{\intercal}. \tag{28}$$

The steady state CM can be determined by solving the Lyapunov equation

$$A\mathcal{V} + \mathcal{V}A^{\intercal} = -D, \tag{29}$$

where D is the 4×4 diffusion matrix which characterizes the noise correlations and is defined by the relation $\langle n_l(t)\, n_m(t') + n_m(t')\, n_l(t)\rangle/2 = D_{lm}\delta(t-t')$. Using Eqs. (6)-(7), D can be written as

$$D = \mathrm{diag}[0, \gamma_m(2n_0+1), \kappa, \kappa]. \tag{30}$$

Eq. (29) is a linear equation for $\mathcal{V}$ and it can be straightforwardly solved, but the general exact expression is very cumbersome and will not be reported here.

The CM allows to calculate also the entanglement of the steady state. We adopt as entanglement measure the logarithmic negativity $E_{\mathcal{N}}$, which is defined as [84]

$$E_{\mathcal{N}} = \max[0, -\ln 2\eta^-]. \tag{31}$$

Here $\eta^- \equiv 2^{-1/2}\left[\Sigma(\mathcal{V}) - [\Sigma(\mathcal{V})^2 - 4\det\mathcal{V}]^{1/2}\right]^{1/2}$ and $\Sigma(\mathcal{V}) \equiv \det\mathcal{V}_1 + \det\mathcal{V}_2 - 2\det\mathcal{V}_c$, with $\mathcal{V}_1, \mathcal{V}_2$ and $\mathcal{V}_c$ being 2×2 block matrices of

$$\mathcal{V} \equiv \begin{pmatrix} \mathcal{V}_1 & \mathcal{V}_c \\ \mathcal{V}_c^T & \mathcal{V}_2 \end{pmatrix}. \tag{32}$$

A bimodal Gaussian state is entangled if and only if $\eta^- < 1/2$, which is equivalent to Simon's necessary and sufficient entanglement non-positive partial transpose criterion for Gaussian states [85], which can be written as $4\det\mathcal{V} < \Sigma(\mathcal{V}) - 1/4$. Logarithmic negativity is a convenient entanglement measure because it is the only one which can always be explicitly computed and it is also additive. The drawback of $E_{\mathcal{N}}$ is that, differently from the entanglement of formation and the distillable entanglement, it is not strongly super-additive and therefore it cannot be used to provide lower-bound estimates of the entanglement of a generic state by evaluating the entanglement of Gaussian state with the same correlation matrix [86]. This fact however is not important in our case because the steady state of the system is Gaussian within the validity limit of our linearization procedure.

3 Ground state cooling

The steady state CM $\mathcal{V}$ determines also the mean energy of the mechanical resonator, which is given by

$$U = \frac{\hbar\omega_m}{2}\left[\left\langle\delta q^2\right\rangle + \left\langle\delta p^2\right\rangle\right] = \frac{\hbar\omega_m}{2}\left[\mathcal{V}_{11} + \mathcal{V}_{22}\right] \equiv \hbar\omega_m\left(n + \frac{1}{2}\right), \tag{33}$$

where $n = (\exp\{\hbar\omega_m/k_BT\} - 1)^{-1}$ is the occupancy corresponding to a bath temperature T. Obviously, in the absence of coupling to the cavity field it is $n = n_0$, where n_0 corresponds to the actual temperature of the environment T_0.

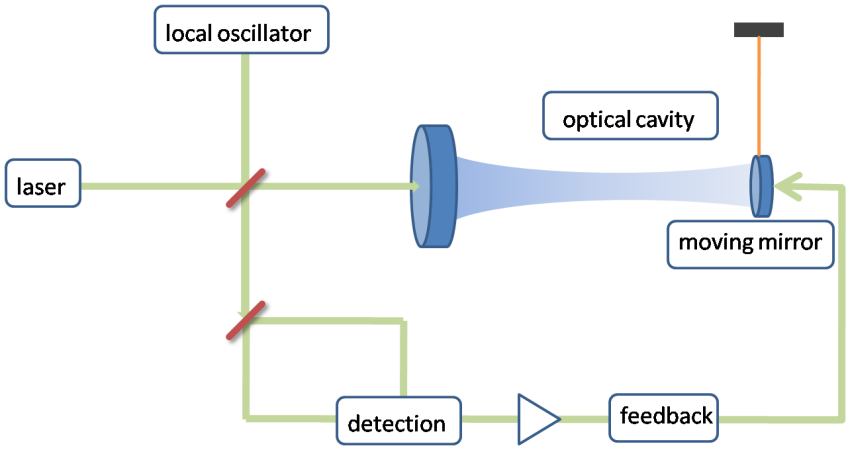

Fig. 2. Setup for feedback cooling (cold damping). The cavity output field is homodyne detected (thus acquiring information about the mirror position) and a force proportional to its derivative is fed back to the mirror.

The optomechanical coupling with the cavity mode can be used to 'engineer' an effective bath of much lower temperature $T \ll T_0$, so that the mechanical resonator is cooled. Let us see when it is possible to reach the ideal condition $n \ll 1$, which corresponds to ground state cooling.

3.1 Feedback cooling

A simple way for cooling an object is to continuously detect its momentum and apply 'corrective kicks' that continuously reduce it eventually to zero [32,35,36]. This is the idea of feedback cooling illustrated in Fig. 2 where the mirror position is detected via phase-sensitive homodyne detection of the cavity output field and a force proportional to the time derivative of the output signal (thus to the velocity) is fed back to it. By Fourier transforming Eq. (18) one obtains

$$\delta Y(\omega) = \frac{G(\kappa - i\omega)}{(\kappa - i\omega)^2 + \Delta^2}\delta q(\omega) + \text{noise terms}, \tag{34}$$

which shows that the intracavity phase-quadrature is sensitive to the mirror motion and moreover its optimal sensitivity is reached at resonance, when $\Delta = 0$. In this latter condition $\delta X(\omega)$ is not sensitive to the mirror motion, suggesting that the strongest feedback effect is obtained by detecting the output phase-quadrature Y^{out} and feeding it back to the resonator.

3.1.1 Phase quadrature feedback

As a consequence we set $\Delta = 0$ and add a feedback force in Eq. (16) so that

$$\delta\dot{p} = -\omega_m \delta q - \gamma_m \delta p + G\delta X + \xi - \int_{-\infty}^{t} ds g(t-s)\delta Y^{est}(s), \tag{35}$$

where $Y^{est}(s)$ is the estimated intracavity phase-quadrature, which, using input-output relations [79] and focusing onto the ideal scenario of perfect detection, is given by

$$\delta Y^{est}(t) = \frac{Y^{out}(t)}{\sqrt{2\kappa}} = \delta Y(t) - \frac{Y^{in}(t)}{\sqrt{2\kappa}}. \tag{36}$$

The filter function $g(t)$ is a causal kernel and $g(\omega)$ is its Fourier transform. We choose a simple standard derivative high-pass filter

$$g(t) = g_{cd}\frac{d}{dt}\left[\theta(t)\omega_{fb}e^{-\omega_{fb}t}\right] \qquad g(\omega) = \frac{-i\omega g_{cd}}{1 - i\omega/\omega_{fb}}, \tag{37}$$

so that ω_{fb}^{-1} plays the role of the time delay of the feedback loop, and $g_{cd} > 0$ is the feedback gain. The ideal derivative limit is obtained when $\omega_{fb} \to \infty$, implying $g(\omega) = -i\omega g_{cd}$ and therefore $g(t) = g_{cd}\delta'(t)$. In this limit the feedback force is equal (apart from an additional noise term) to $-g_{cd}\delta\dot{Y}$ which, due to Eq. (34), is an additional viscous force $-(g_{cd}G/\kappa)\delta\dot{q}$ only in the bad cavity limit $\kappa \gg \omega_m, \gamma_m$.

One can solve the Langevin equations supplemented with the feedback term in the Fourier domain. In fact, the two steady state oscillator variances $\langle \delta q^2 \rangle$ and $\langle \delta p^2 \rangle$ can be expressed by the following frequency integrals

$$\left\langle \delta q^2 \right\rangle = \int_{-\infty}^{\infty} \frac{d\omega}{2\pi} S_q^{cd}(\omega), \quad \left\langle \delta p^2 \right\rangle = \int_{-\infty}^{\infty} \frac{d\omega}{2\pi} \frac{\omega^2}{\omega_m^2} S_q^{cd}(\omega), \tag{38}$$

where $S_q^{cd}(\omega)$ is the position noise spectrum. Its explicit expression is given by

$$S_q^{cd}(\omega) = |\chi_{eff}^{cd}(\omega)|^2 [S_{th}(\omega) + S_{rp}(\omega) + S_{fb}(\omega)], \tag{39}$$

where the thermal, radiation pressure and feedback-induced contributions are respectively given by

$$S_{th}(\omega) = \frac{\gamma_m \omega}{\omega_m} \coth\left(\frac{\hbar\omega}{2k_B T_0}\right), \tag{40}$$

$$S_{rp}(\omega) = \frac{G^2\kappa}{\kappa^2 + \omega^2}, \tag{41}$$

$$S_{fb}(\omega) = \frac{|g(\omega)|^2}{4\kappa} \tag{42}$$

and $\chi_{eff}^{cd}(\omega)$ is the susceptibility of the mechanical oscillator modified by the feedback

$$\chi_{eff}^{cd}(\omega) = \omega_m \left[\omega_m^2 - \omega^2 - i\omega\gamma_m + \frac{g(\omega)G\omega_m}{\kappa - i\omega}\right]^{-1}. \tag{43}$$

This effective susceptibility contains the relevant physics of cold damping. In fact it can be rewritten as the susceptibility of an harmonic oscillator with effective (frequency-dependent) damping and oscillation frequency. The modification of resonance frequency (optical spring effect [21,36]) is typically small for the chosen parameter regime ($\omega_m \simeq 1$ MHz) and the only relevant effect of feedback is the modification of the mechanical damping which, in the case of the choice of Eq. (37), is given by

$$\gamma_m^{eff,cd}(\omega) = \gamma_m + \frac{g_{cd}G\omega_m\omega_{fb}(\kappa\omega_{fb} - \omega^2)}{(\kappa^2 + \omega^2)(\omega_{fb}^2 + \omega^2)}. \tag{44}$$

This expression shows that the damping of the oscillator may be significantly increased due to the combined action of feedback and of radiation pressure coupling to the field. In the ideal limit of instantaneous feedback and of a bad cavity, $\kappa, \omega_{fb} \gg \omega_m, \gamma_m$, effective damping is frequency-independent and given by $\gamma_m^{eff,cd} \simeq \gamma_m + g_{cd}G\omega_m/\kappa = \gamma_m(1 + g_2)$, where we have defined the scaled, dimensionless feedback gain $g_2 \equiv g_{cd}G\omega_m/\kappa\gamma_m$ [36].

The presence of cold-damping feedback also modifies the stability conditions. The Routh-Hurwitz criteria are equivalent to the conditions that all the poles of the effective susceptibility of Eq. (43) are in the lower complex half-plane. For the choice of Eq. (37) there is only one non-trivial stability condition, which reads

$$\begin{aligned} s_{cd} = &\left[\gamma_m\kappa\omega_{fb} + g_{cd}G\omega_m\omega_{fb} + \omega_m^2(\kappa + \omega_{fb})\right][(\kappa + \gamma_m)(\kappa + \omega_{fb})(\gamma_m + \omega_{fb}) \\ &+\gamma_m\omega_m^2 - g_{cd}G\omega_m\omega_{fb}\Big] - \kappa\omega_m^2\omega_{fb}(\kappa + \gamma_m + \omega_{fb})^2 > 0. \end{aligned} \tag{45}$$

This condition shows that the system may become unstable for large gain and finite feedback delay-time and cavity bandwidth because in this limit the feedback force can be out-of-phase with the oscillator motion and become an accelerating rather than a viscous force [41].

The performance of cold-damping feedback for reaching ground state cooling is analyzed in detail in Ref. [41], which shows that the optimal parameter regime is $\kappa \gg \omega_{fb} \sim \omega_m \gg \gamma_m$, which correspond to a bad-cavity limit and a finite-bandwidth feedback, i.e., with a feedback delay-time comparable to the resonator frequency. One gets in this case

$$\left\langle \delta q^2 \right\rangle \simeq \left[1 + g_2 + \frac{\omega_{fb}^2}{\omega_m^2}\right]^{-1} \left[\frac{g_2^2}{4\zeta} + \left(n_0 + \frac{1}{2} + \frac{\zeta}{4}\right)\left(1 + \frac{\omega_m^2}{\omega_{fb}^2}\right)\right] \tag{46}$$

$$\left\langle \delta p^2 \right\rangle \simeq \left[1 + g_2 + \frac{\omega_m^2}{\omega_{fb}^2}\right]^{-1} \left[\frac{g_2^2}{4\zeta}\left(1 + \frac{g_2\gamma_m\omega_{fb}}{\omega_m^2}\right) + \left(n_0 + \frac{1}{2} + \frac{\zeta}{4}\right)\left(1 + \frac{\omega_m^2}{\omega_{fb}^2} + \frac{g_2\gamma_m}{\omega_{fb}}\right)\right], \tag{47}$$

where we have defined the scaled dimensionless input power $\zeta = 2G^2/\kappa\gamma_m$. These two expressions show that with cold-damping feedback, $\langle \delta q^2 \rangle \neq \langle \delta p^2 \rangle$, i.e., energy equipartition does not hold anymore. The best cooling regime is achieved for $\omega_{fb} \sim 3\omega_m$ and $g_2 \simeq \xi$ (i.e. $g_{cd} \simeq 2G/\omega_m$), i.e. for *large but finite* feedback gain [35,36,41]. This is consistent with the fact that stability imposes an upper bound to the feedback gain when κ and ω_{fb} are finite. The optimal cooling regime for cold damping is illustrated in Fig. 3a, where n is plotted versus the feedback gain g_{cd} and the input power P, at fixed $\kappa = 5\omega_m$ (bad-cavity condition) and $\omega_{fb} = 3.5\omega_m$. Fig. 3b instead explicitly shows the violation of the equipartition condition even in this regime close to ground state (the feedback gain is fixed at the value $g_{cd} = 1.2$): the resonator is in a position-squeezed thermal state corresponding to a very low effective temperature.

3.1.2 Generalized quadrature feedback

The above analysis shows that cold-damping feedback better cools the mechanical resonator when the feedback is not instantaneous and therefore the feedback force is not a simple viscous force. This suggests that one can further optimize feedback cooling by considering a *generalized* estimated quadrature which is a combination of phase and amplitude field quadratures. In fact one may expect that in the optimal regime, the information provided by the amplitude quadrature $X^{out}(t)$ is also useful.

Therefore, in order to optimize cooling via feedback, we apply a feedback force involving a generalized estimated quadrature

$$\delta Y_\theta^{est}(t) = \frac{Y^{out}(t)\cos\theta + X^{out}(t)\sin\theta}{\sqrt{2\kappa}}, \tag{48}$$

which is a linear combination of $Y^{out}(t)$ and $X^{out}(t)$ and where θ is a detection phase which has to be optimized. The adoption of the new estimated quadrature leads to three effects: i) a modification of the expression for $\chi_{eff}^{cd}(\omega)$ of Eq. (43) where $g(\omega)$ is replaced by $g(\omega)\cos\theta$; ii) a consequent reduction of the feedback-induced shot noise term $S_{fb}(\omega)$; iii) a reduction of radiation pressure noise. In fact, the radiation pressure and feedback-induced noise contributions become

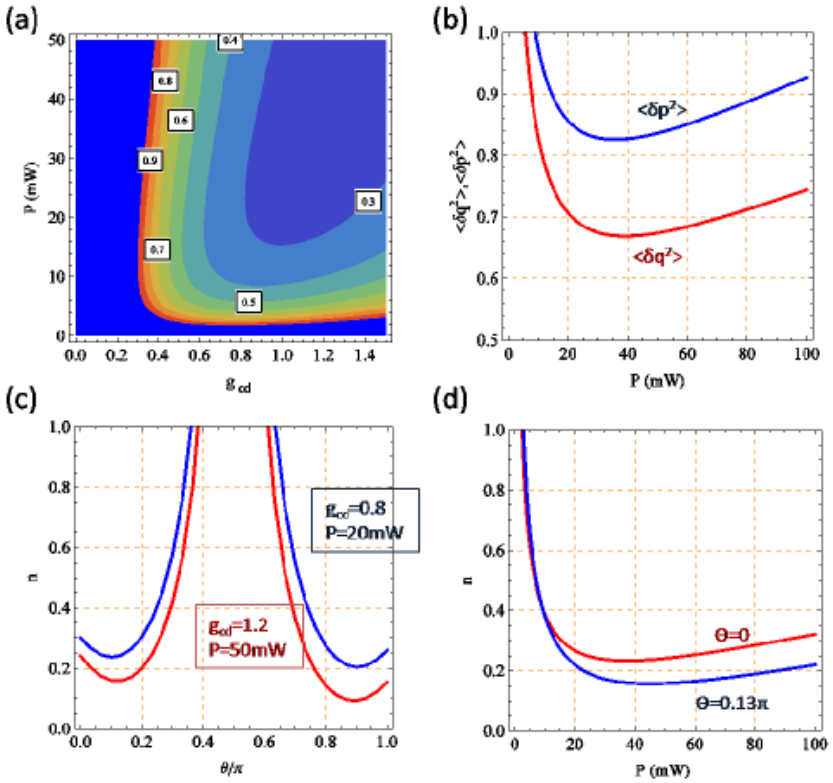

Fig. 3. Feedback cooling. (a) Contour plot of n as a function of $\mathcal{P}$ and g_{cd}. The parameters are p_0, $\kappa = 5\omega_m$ and $\omega_{fb} = 3.5\omega_m$. (b) Illustration of the violation of energy equipartition around the optimal cooling regime. Parameters as before with $g_{cd} = 1.2$. (c) n versus the phase of the generalized quadrature θ for two sets of g_{cd} and $\mathcal{P}$: the (upper) blue curve corresponds to $g_{cd} = 0.8$ and $\mathcal{P} = 20$ mW, while the (lower) red curve corresponds to $g_{cd} = 1.2$ and $\mathcal{P} = 50$ mW. (d) Comparison of n versus the input power $\mathcal{P}$ between the case of standard cold damping feedback $\theta = 0$ (upper red curve) and at a generalized detected quadrature with phase $\theta = 0.13\pi$ (lower blue curve). Parameters as before, with $g_{cd} = 1.2$.

$$S^{\theta}_{rp}(\omega) = \frac{G^2\kappa}{\kappa^2+\omega^2}\left|1 - \frac{g(\omega)\sin\theta}{2G\kappa}(\kappa + i\omega)\right|^2, \tag{49}$$

$$S^{\theta}_{fb}(\omega) = \frac{|g(\omega)|^2}{4\kappa}\cos^2\theta. \tag{50}$$

An improvement over the standard cold-damping feedback scheme can be obtained when the shot noise reduction effect predominates over the reduction of the effective damping due to feedback. This can be seen in Fig. (3c) where for two different choices for g_{cd} and $\mathcal{P}$, the occupancy n is plotted versus θ. For one of these optimal phases, $\theta_{opt} = 0.13\pi$, we plot in Fig. (3d) n as a function of $\mathcal{P}$ and compare it with the results of the standard phase quadrature feedback

to conclude that improvement via detection of a rotated output quadrature is indeed possible.

3.2 Back-action cooling

In analogy with well-known methods of atom and ion cooling [87,88], one can also think of cooling the mechanical resonator by exploiting its coherent coupling to a fast decaying system which provides an additional dissipation channel and thus cooling. In the present situation, radiation pressure couples the resonator with the cavity mode and the fast decaying channel is provided by the cavity photon loss rate κ. An equivalent description of the process can be given in terms of dynamical backaction [5,33]: the cavity reacts with a delay to the mirror motion and induces correlations between the radiation pressure force and the Brownian motion that lead to cooling or amplification, depending on the laser detuning. A quantitative description is provided by considering scattering of laser photons into the motional sidebands induced by the mirror motion (see Fig. 4) [39,40,41]. Stokes (red) and anti-Stokes (blue) sidebands are generated in the cavity at frequencies $\omega_l \pm \omega_m$. Laser photons are scattered by the moving oscillator into the two sidebands with rates

$$A_{\pm} = \frac{G^2\kappa}{2\left[\kappa^2 + (\Delta \pm \omega_m)^2\right]}, \tag{51}$$

simultaneously with the absorption (Stokes, A_+) or emission (anti-Stokes, A_-) of vibrational phonons. The inequality $A_- > A_+$ leads to a decrease in the oscillator phonon occupation number and thus to cooling. Eq. (51) shows that this occurs when $\Delta > 0$ and that an effective optical cooling rate,

$$\Gamma = A_- - A_+ = \frac{2G^2\Delta\omega_m\kappa}{[\kappa^2 + (\omega_m - \Delta)^2]\,[\kappa^2 + (\omega_m + \Delta)^2]}, \tag{52}$$

can be defined, providing a measure of the coupling rate of the resonator with the effective zero-temperature environment represented by the decaying cavity mode. Since the mechanical damping rate γ_m is the coupling rate with the thermal reservoir of the resonator, one can already estimate that, when $\Gamma \gg \gamma_m$, the mechanical oscillator is cooled at the new temperature $T \simeq (\gamma_m/\Gamma)\,T_0$.

One can perform a more precise and rigorous derivation of the cooling rate and steady state occupancy by using Eq. (33). The position and momentum variances can be in fact obtained by solving Eq. (29) or, equivalently, by solving the linearized QLE in the Fourier domain and integrating the resulting noise spectra. The result of these calculations, in the limit of large mechanical quality factor $\mathcal{Q}_m$, reads

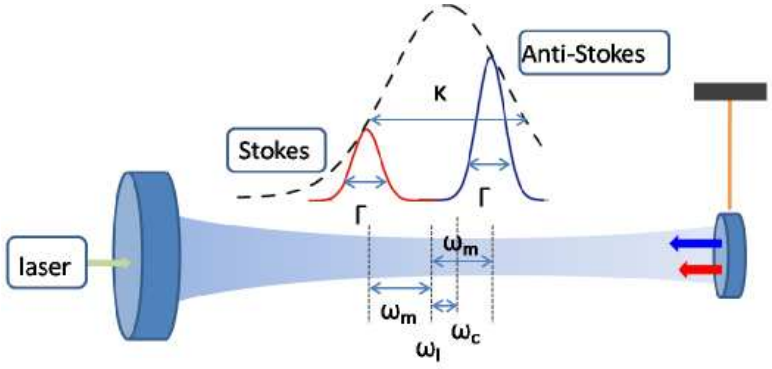

Fig. 4. Setup for cavity backaction cooling. Optical sidebands are scattered unevenly by the moving mirror. When the anti-Stokes sideband is resonant with the cavity ($\Delta = \omega_m$), an effective flow of energy from the mirror out of the cavity leads to an effective cooling.

$$\left\langle \delta p^2 \right\rangle = \frac{1}{\gamma_m + \Gamma} \left\{ \frac{A_+ + A_-}{2} + \gamma_m n_0 \left(1 + \frac{\Gamma}{2\kappa} \right) \right\}, \tag{53}$$

$$\left\langle \delta q^2 \right\rangle = \frac{1}{\gamma_m + \Gamma} \left\{ a \frac{A_+ + A_-}{2} + \frac{\gamma_m n_0}{\eta} \left(1 + \frac{\Gamma}{2\kappa} b \right) \right\}, \tag{54}$$

where η is given by Eq. (23),

$$a = \frac{\kappa^2 + \Delta^2 + \eta \omega_m^2}{\eta \left(\kappa^2 + \Delta^2 + \omega_m^2 \right)}, \tag{55}$$

$$b = \frac{2 \left(\Delta^2 - \kappa^2 \right) - \omega_m^2}{\kappa^2 + \Delta^2}. \tag{56}$$

In the perturbative limit $\omega_m \gg n_0 \gamma_m, G$ and $\kappa \gg \gamma_m, G$, Eqs. (53)-(54) simplify to $\langle \delta q^2 \rangle \simeq \langle \delta p^2 \rangle \simeq n + 1/2$, with $n \simeq \left[\gamma_m n_0 + A_+ \right] / \left[\gamma_m + \Gamma \right]$, which reproduces the result of [39,40]. This indicates that ground state cooling is reachable when $\gamma_m n_0 < \Gamma$ and provided that the radiation pressure noise contribution $A_+ / \Gamma \simeq \kappa^2 / \left(4 \omega_m^2 \right)$ is also small. The optical damping rate Γ can be increased by cranking up the input cavity power and thus G. However, when one considers the limitations imposed by the stability condition $\eta > 0$, one finds that there is an upper bound for G and consequently Γ. This is shown in Figs. 5a-5c, where one sees that for the chosen parameter regime p_0, optimal cooling is achieved for $\Delta \simeq \omega_m$ (when the anti-Stokes sideband is resonant with the cavity, as expected), and in a moderate good-cavity condition, $\kappa / \omega_m \simeq 0.2$. Fig. 5b shows that close to this optimal cooling condition, equipartition is soon violated when the input power (and therefore the effective coupling G) is further increased: the position variance becomes much larger than the momentum variance and it is divergent at the bistability threshold (see Eq. (54)).

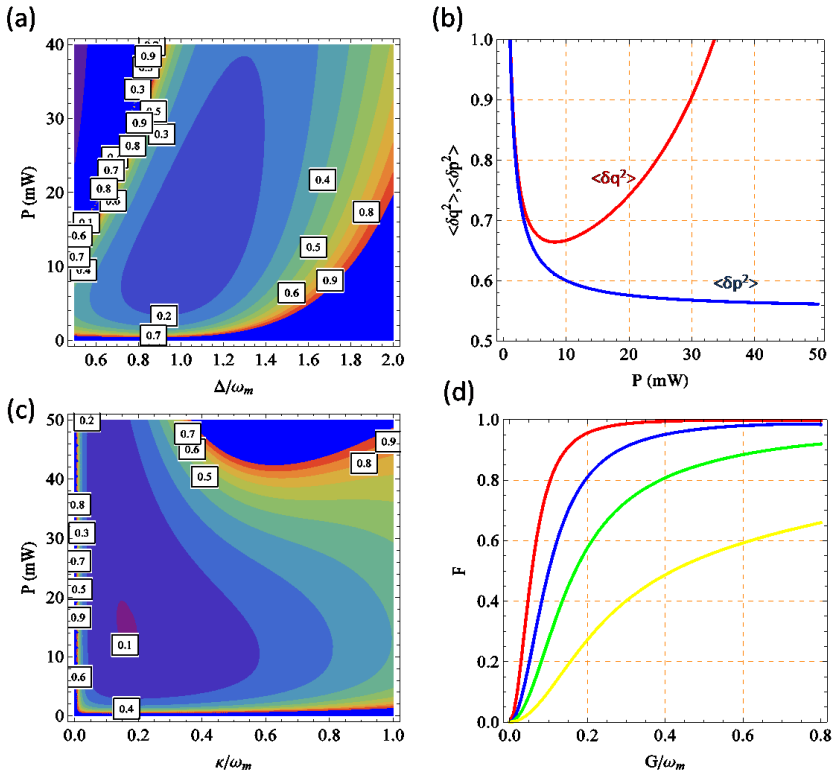

Fig. 5. Back action cooling. (a) Contour plot of n versus Δ/ω_m and $\mathcal{P}$. The parameters are p_0 and $\kappa = 0.37\omega_m$. Optimal cooling is seen to emerge around $\Delta = \omega_m$. (b) For large $\mathcal{P}$ extra shot-noise is fed-back into the position variance and the mirror thermalizes in a state where the equipartition theorem does not hold. (c) Contour plot of n vs. κ/ω_m and $\mathcal{P}$ for $\Delta = \omega_m$. Optimal cooling is achieved around $\kappa \simeq 0.2 \times \omega_m$. (d) Fidelity between the mirror and intracavity states in the cooling regime as a function of increasing intensity G/ω_m with different values of $\kappa/\omega_m = 0.2$ (red line), 0.5 (blue), 1 (green) and 2 (yellow).

3.3 Readout of the mechanical resonator state

Eq. (34) shows that the cavity output is sensitive to the resonator position. Therefore, after an appropriate calibration, the cavity output noise power spectrum provides a direct measurement of the position noise spectrum $S_q(\omega)$ which, when integrated over ω, yields the value of the position variance (see Eq. (38)). In many experiments [16,17,18,19,20,21,22,23,24,26], this value is employed to estimate the final effective temperature of the cooled resonator by assuming energy equipartition $\langle \delta p^2 \rangle \simeq \langle \delta q^2 \rangle$ so that $n \simeq \langle \delta q^2 \rangle - 1/2$. However, as we have seen above (see Eqs. (46), (47), (53), (54)), equipartition does not generally hold and one should rather estimate $\langle \delta p^2 \rangle$ from $S_q(\omega)$ using

Eq. (38), or directly measure independently the resonator momentum. A different and more direct way of measuring the resonator temperature, borrowed from trapped-ion experiments [88], has been demonstrated in [25]: if the two motional sidebands are well resolved and detected via heterodyne measurement, the height of the two sideband peaks is proportional to n and to $n+1$, so that one can directly measure the occupancy n from the comparison of the two peaks.

However, one should devise a scheme capable of reconstructing the *complete quantum state* of the resonator from the cavity output light, which is the only accessible degree of freedom carrying out information about it. In fact, the full reconstruction of the quantum state of the resonator is a necessary condition for the unambiguous demonstration of the quantum behavior of the mechanical resonator, as for example stationary entanglement, which will be discussed in the following. A scheme of this kind has been proposed in [64], based on the transfer of the resonator state onto the output field of an additional, fast-decaying, "probe" cavity mode. In fact, the annihilation operator of this probe cavity mode, a_p, obeys an equation analogous to the linearization of Eq. (14),

$$\delta\dot{a}_p = -(\kappa_p + i\Delta_p)\delta a_p + iG_p\alpha_p\delta q + \sqrt{2\kappa_2}a_p^{in}(t), \tag{57}$$

where κ_p, Δ_p, G_p, α_p, and $a_p^{in}(t)$ are respectively the decay rate, the effective detuning, the coupling, the intracavity field amplitude, and the input noise of the probe cavity mode. The presence of the probe mode affects the system dynamics, but if the driving of the probe mode is much weaker so that $|\alpha_p| \ll |\alpha_s|$, the back-action of the probe mode on the resonator can be neglected. If one chooses parameters so that $\Delta_p = \omega_m \gg k_p, G_p|\alpha_p|$, one can rewrite Eq. (57) in the frame rotating at $\Delta_p = \omega_m$ for the slow variables $\delta\tilde{o}(t) \equiv \delta o(t)\exp\{i\omega_m t\}$ and neglect fast oscillating terms, so to get

$$\delta\dot{\tilde{a}}_p = -\kappa_p\delta\tilde{a}_p + i\frac{G_p\alpha_p}{\sqrt{2}}\delta\tilde{b} + \sqrt{2\kappa_p}\tilde{a}_p^{in}(t), \tag{58}$$

where $\delta b = (i\delta p + \delta q)/\sqrt{2}$ is the mechanical annihilation operator. Finally, if $\kappa_p \gg G_p|\alpha_p|/\sqrt{2}$, the probe mode adiabatically follows the resonator dynamics and one has

$$\delta\tilde{a}_p \simeq i\frac{G_p\alpha_p}{\kappa_p\sqrt{2}}\delta\tilde{b} + \sqrt{\frac{2}{\kappa_p}}\tilde{a}_p^{in}(t). \tag{59}$$

The input-output relation $\tilde{a}_p^{out} = \sqrt{2\kappa_p}\delta\tilde{a}_p - \tilde{a}_p^{in}$ [79] implies

$$\tilde{a}_p^{out} = i\frac{G_p\alpha_p}{\sqrt{\kappa_p}}\delta\tilde{b} + \tilde{a}_p^{in}(t), \tag{60}$$

showing that, in the chosen parameter regime, the output light of the probe mode gives a direct measurement of the resonator dynamics. With an appropriate calibration and applying standard quantum tomographic techniques

[89] to this output field, one can therefore reconstruct the quantum state of the resonator.

An alternative way to detect the resonator state by means of state transfer onto an optical mode, which does not require an additional probe mode, can be devised by appropriately exploiting the strong coupling regime. In this second example state transfer is realized in a transient regime soon after the preparation of the desired resonator state. One sets the cavity onto resonance $\Delta = 0$ so that the system is always stable, and then strongly increases the input power in order to make the coupling G very large, $G \gg \kappa, n_0\gamma_m$. Under these conditions, coherent evolution driven by radiation pressure dominates and one has state swapping from the mechanical resonator onto the intracavity mode in a time $t_{swap} \simeq \pi/2G$ so that the cavity mode state reproduces the resonator state with a fidelity very close to unity. The fidelity of the swap can be computed and reads

$$F = \Big[\sqrt{\det\left(\mathcal{V}_1 + \mathcal{V}_2\right) + \left(\det \mathcal{V}_1 - 1/4\right)\left(\det \mathcal{V}_2 - 1/4\right)} - \sqrt{\left(\det \mathcal{V}_1 - 1/4\right)\left(\det \mathcal{V}_2 - 1/4\right)}\Big]^{-1}, \tag{61}$$

where $\mathcal{V}_1, \mathcal{V}_2$ are the block matrices in Eq. (32). The resulting fidelity under realistic conditions is plotted in Fig. (5d) as a function of G/ω_m for $\kappa/\omega_m = 0.2\,,\ 0.5,\ 1$ and 2. One can see that the fidelity is close to unity around the optimal cooling regime and that in this regime *both the mechanical resonator and intracavity field thermalize in the same state.* Under this condition one can reconstruct the quantum state of the mechanical mode from the detection of the cavity output.

4 Entanglement generation with a single driven cavity mode

As discussed in the introduction, a cavity coupled to a mechanical degree of freedom is capable of producing entanglement between the mechanical and the optical modes and also purely optical entanglement between the induced motional sidebands. In the following we elucidate the physical origins of this entanglement and analyze its magnitude and temperature robustness. Moreover, we analyze its use as a quantum-communication network resource in which the mechanical modes play the role of local nodes that store quantum information and optical modes carry this information among nodes. To this purpose we apply a multiplexing approach that allows one, by means of spectral filters, to select many traveling output modes originating from a single intracavity field.

Entanglement can be easily evaluated and quantified using the logarithmic negativity of Eq. (31), which requires the knowledge of the CM of the system of interest. For the steady state of the intracavity field-resonator system, the CM is determined in a straightforward way by the solution of Eq. (29). However, before discussing the general result we try to give an intuitive idea of how robust optomechanical entanglement can be generated, by using the sideband picture. Using the mechanical annihilation operator δb introduced in the above section, the linearized QLE of Eqs. (15)-(18) can be rewritten as

$$\delta\dot{\tilde{b}} = -\frac{\gamma_m}{2}\left(\delta\tilde{b} - \delta\tilde{b}^\dagger e^{2i\omega_m t}\right) + \sqrt{\gamma_m}b^{in} + i\frac{G}{2}\left(\delta\tilde{a}^\dagger e^{i(\Delta+\omega_m)t} + \delta\tilde{a}e^{i(\omega_m-\Delta)t}\right) \tag{62}$$

$$\delta\dot{\tilde{a}} = -\kappa\delta\tilde{a} + i\frac{G}{2}\left(\delta\tilde{b}^\dagger e^{i(\Delta+\omega_m)t} + \delta\tilde{b}e^{i(\Delta-\omega_m)t}\right) + \sqrt{2\kappa}\tilde{a}^{in}. \tag{63}$$

We have introduced the tilded slowly evolving operators $\delta\tilde{b}(t) = \delta b(t)e^{i\omega_m t}$, $\delta\tilde{a}(t) = \delta a(t)e^{i\Delta t}$, and the noises $\tilde{a}^{in}(t) = a^{in}(t)e^{i\Delta t}$ and $b^{in}(t) = \xi(t)e^{i\omega_m t}/\sqrt{2}$. The input noise $\tilde{a}^{in}(t)$ possesses the same correlation function as $a^{in}(t)$, while the Brownian noise $b^{in}(t)$ in the limit of large mechanical frequency ω_m acquires "optical-like" correlation functions $\langle b^{in,\dagger}(t)b^{in}(t')\rangle = n_0\delta(t-t')$ and $\langle b^{in}(t)b^{in,\dagger}(t')\rangle = [n_0+1]\,\delta(t-t')$ [90]. Eqs. (62)-(63) show that the cavity mode and mechanical resonator are coupled by radiation pressure via two kinds of interactions: i) a down-conversion process with interaction Hamiltonian $\delta\tilde{b}^\dagger\delta\tilde{a}^\dagger + \delta\tilde{a}\delta\tilde{b}$, which is modulated by a factor oscillating at $\omega_m + \Delta$; ii) a beam-splitter-like process with interaction Hamiltonian $\delta\tilde{b}^\dagger\delta\tilde{a} + \delta\tilde{a}^\dagger\delta\tilde{b}$, modulated by a factor oscillating at $\omega_m - \Delta$. Therefore, by tuning the cavity into resonance with either the Stokes sideband of the driving laser, $\Delta = -\omega_m$, or the anti-Stokes sideband of the driving laser, $\Delta = \omega_m$, one can resonantly enhance one of the two processes. In the rotating wave approximation (RWA), which is justified in the limit of $\omega_m \gg G, \kappa$, the off-resonant interaction oscillates very fast with respect to the timescales of interest and can be neglected. Therefore, in the RWA regime, when one chooses $\Delta = -\omega_m$, the radiation pressure induces a down-conversion process, which is known to generate bipartite CV entanglement. Instead when one chooses $\Delta = \omega_m$, the dominant process is the beam-splitter-like interaction, which is not able to generate optomechanical entanglement starting from classical input states [91], as in this case. This argument leads to the conclusion that, in the RWA limit $\omega_m \gg G, \kappa$, the best regime for optomechanical entanglement is when the laser is blue-detuned from the cavity resonance $\Delta = -\omega_m$ and down-conversion is enhanced. However, this argument is valid only in the RWA limit and it is strongly limited by the stability conditions, which rather force to work in the opposite regime of a red-detuned laser. In fact, the stability condition of Eq. (20) in the RWA limit $\Delta = -\omega_m \gg \kappa, \gamma_m$, simplifies to $G < \sqrt{2\kappa\gamma_m}$. Since one needs small mechani-

cal dissipation rate γ_m in order to see quantum effects, this means a very low maximum value for G. The logarithmic negativity $E_{\mathcal{N}}$ is an increasing function of the effective optomechanical coupling G (as expected) and therefore the stability condition puts a strong upper bound also on $E_{\mathcal{N}}$. It is possible to prove that the following bound on $E_{\mathcal{N}}$ exists [69]

$$E_{\mathcal{N}} \leq \ln\left[\frac{1+G/\sqrt{2\kappa\gamma_m}}{1+n_0}\right], \tag{64}$$

showing that $E_{\mathcal{N}} \leq \ln 2$ and above all that entanglement is extremely fragile with respect to temperature in the blue-detuned case because, due to the stability constraints, $E_{\mathcal{N}}$ vanishes as soon as $n_0 \geq 1$.

This suggests that, due to instability, one can find significant intracavity optomechanical entanglement, which is also robust against temperature, only far from the RWA regime, in the strong coupling regime in the region with positive Δ, because Eq. (22) allows for higher values of the coupling ($G < \sqrt{\kappa^2+\omega_m^2}$ when $\Delta = \omega_m$). This is confirmed by Fig. 6a, where the *exact* $E_{\mathcal{N}}$ calculated from the solution of Eq. (29) is plotted versus the normalized detuning Δ/ω_m and the normalized effective optomechanical coupling G/ω_m. One sees that $E_{\mathcal{N}}$ reaches significant values close to the bistability threshold; moreover it is possible to see that such intracavity entanglement is robust against thermal noise because it survives up to reservoir temperatures around 20 K [64]. It is also interesting to compare the conditions for optimal entanglement and cooling in this regime where the cavity is resonant with the anti-Stokes sideband. In Fig. 6b, n is plotted versus the same variables in the same parameter region. One can see that, while good entanglement is accompanied by good cooling, optimal entanglement is achieved for the largest possible coupling G allowed by the stability condition. This condition is far from the optimal cooling regime, which does not require very large G because otherwise the radiation pressure noise contribution and consequently the position variance become too large (see Eq. (54) and Fig. 5) [69].

4.2 Entanglement with output modes

Let us now define and evaluate the entanglement of the mechanical resonator with the fields at the cavity output, which may represent an essential tool for the future integration of micromechanical resonators as quantum memories within quantum information networks. The intracavity field $\delta a(t)$ and its output are related by the usual input-output relation [79]

$$a^{out}(t) = \sqrt{2\kappa}\delta a(t) - a^{in}(t), \tag{65}$$

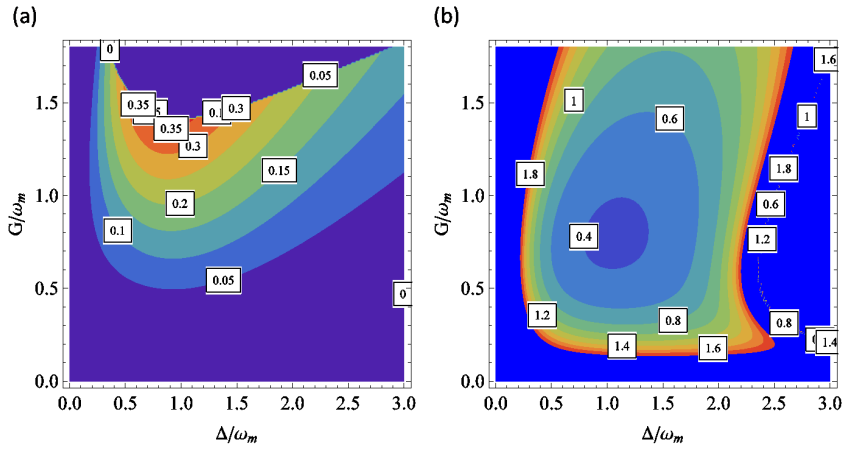

Fig. 6. Intracavity entanglement and cooling in the red-detuned regime. (a) Contour plot of logarithmic negativity of the field-mirror system at the steady state as a function of G/ω_m and Δ/ω_m for the parameters p_0 and $\kappa = \omega_m$. (b) n in the same parameter region: the plot shows that optimal cooling and optimal entanglement are both achieved close to $\Delta/\omega_m \simeq 1$. However, optimal cooling is obtained for smaller values of G/ω_m with respect to entanglement.

where the output field possesses the same correlation functions of the optical input field $a^{in}(t)$ and the same commutation relation, i.e., the only nonzero commutator is $\left[a^{out}(t), a^{out}(t')^\dagger\right] = \delta(t-t')$. From the continuous output field $a^{out}(t)$ one can extract many independent optical modes, by selecting different time intervals or equivalently, different frequency intervals (see e.g. [92]). One can define a generic set of N output modes by means of the corresponding annihilation operators

$$a_k^{out}(t) = \int_{-\infty}^{t} ds g_k(t-s) a^{out}(s), \quad k = 1, \dots N, \tag{66}$$

where $g_k(s)$ is the causal filter function defining the k-th output mode. These annihilation operators describe N independent optical modes when $\left[a_j^{out}(t), a_k^{out}(t)^\dagger\right] = \delta_{jk}$, which is verified when

$$\int_0^{\infty} ds g_j(s)^* g_k(s) = \delta_{jk}, \tag{67}$$

i.e., the N filter functions $g_k(t)$ form an orthonormal set of square-integrable functions in $[0, \infty)$. The situation can be equivalently described in the frequency domain: taking the Fourier transform of Eq. (66), one has

$$\tilde{a}_k^{out}(\omega) = \int_{-\infty}^{\infty} \frac{dt}{\sqrt{2\pi}} a_k^{out}(t) e^{i\omega t} = \sqrt{2\pi}\tilde{g}_k(\omega) a^{out}(\omega), \tag{68}$$

where $\tilde{g}_k(\omega)$ is the Fourier transform of the filter function. An explicit example of an orthonormal set of filter functions is given by

$$g_k(t) = \frac{\theta(t) - \theta(t-\tau)}{\sqrt{\tau}} e^{-i\Omega_k t}, \tag{69}$$

(θ denotes the Heavyside step function) provided that Ω_k and τ satisfy the condition

$$\Omega_j - \Omega_k = \frac{2\pi}{\tau} p, \quad \text{integer } \ p. \tag{70}$$

These functions describe a set of independent optical modes, each centered around the frequency Ω_k and with time duration τ, i.e., frequency bandwidth $\sim 1/\tau$, since

$$\tilde{g}_k(\omega) = \sqrt{\frac{\tau}{2\pi}} e^{i(\omega-\Omega_k)\tau/2} \frac{\sin\left[(\omega-\Omega_k)\tau/2\right]}{(\omega-\Omega_k)\tau/2}. \tag{71}$$

When the central frequencies differ by an integer multiple of $2\pi/\tau$, the corresponding modes are independent due to the destructive interference of the oscillating parts of the spectrum.

The entanglement between the output modes defined above and the mechanical mode is fully determined by the corresponding $(2N+2) \times (2N+2)$ CM, which is defined by

$$\mathcal{V}_{ij}^{out}(t) = \frac{1}{2} \left\langle u_i^{out}(t) u_j^{out}(t) + u_j^{out}(t) u_i^{out}(t) \right\rangle, \tag{72}$$

where

$$u^{out}(t) = \left(\delta q(t), \delta p(t), X_1^{out}(t), Y_1^{out}(t), \ldots, X_N^{out}(t), Y_N^{out}(t) \right)^T \tag{73}$$

is the vector formed by the mechanical position and momentum fluctuations and by the amplitude ($X_k^{out}(t) = \left[a_k^{out}(t) + a_k^{out}(t)^\dagger \right] / \sqrt{2}$), and phase ($Y_k^{out}(t) = \left[a_k^{out}(t) - a_k^{out}(t)^\dagger \right] / i\sqrt{2}$) quadratures of the N output modes. The vector $u^{out}(t)$ properly describes $N+1$ independent CV bosonic modes, and in particular the mechanical resonator is independent of (i.e., it commutes with) the N optical output modes because the latter depend upon the output field at former times only ($s < t$). From the intracavity CM and Eqs. (65),(66), and (72) one can determine the $(N+1) \times (N+1)$ CM matrix $\mathcal{V}^{out}$ at the steady state [69].

Let us first consider the case when we select and detect only one mode at the cavity output. Just to fix the ideas, we choose the mode specified by the filter function of Eqs. (69) and (71), with central frequency Ω and bandwidth τ^{-1}. Straightforward choices for this output mode are a mode centered either at the cavity frequency, $\Omega = \omega_c - \omega_l$, or at the driving laser frequency, $\Omega = 0$ (we are in the rotating frame and therefore all frequencies are referred to the laser frequency ω_l), and with a bandwidth of the order of the cavity bandwidth

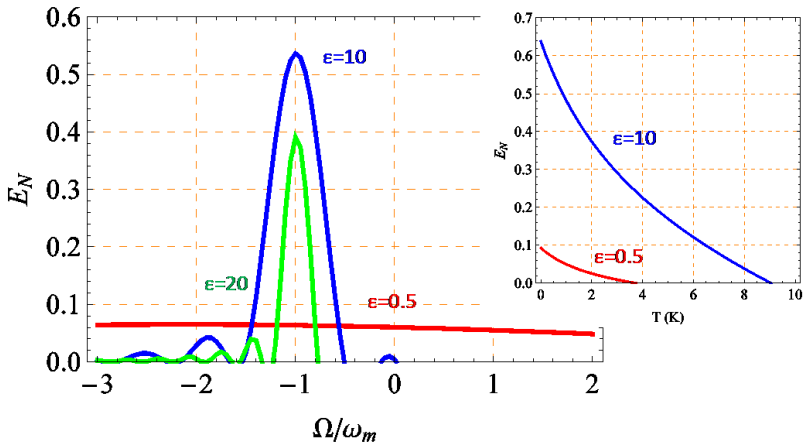

Fig. 7. Resonator-output field entanglement when the central frequency of the output mode is swept around the laser frequency. Parameters are p_0, $\Delta = \omega_m$, $G = \omega_m/2$ and $\kappa = \omega_m$. The entanglement is optimized when the output mode coincides with the Stokes sideband of the laser ($\Omega = -\omega_m$), with the appropriate bandwidth ($\epsilon \simeq 10$, corresponding to $\tau\gamma_m^{eff} \simeq 1$). For smaller ϵ, the selected output mode mixes Stokes and anti-Stokes photons and the entanglement is weak, while for larger ϵ only a fraction of the sideband is selected and part of the quantum correlations are lost. In the inset the robustness of Stokes-mirror $E_{\mathcal{N}}$ with respect to temperature is shown.

$\tau^{-1} \simeq \kappa$. However, as discussed above, the motion of the mechanical resonator generates Stokes and anti-Stokes motional sidebands, consequently modifying the cavity output spectrum.

In order to determine the output optical mode which is better entangled with the mechanical resonator, we study the logarithmic negativity $E_{\mathcal{N}}$ associated with the output CM $\mathcal{V}^{out}$ (for $N = 1$) as a function of the central frequency of the mode Ω and its bandwidth τ^{-1}, at the same parameter region considered in the previous subsection, p_0 and $\Delta = \omega_m$, where intracavity entanglement is optimal. The results are shown in Fig. 7, where $E_{\mathcal{N}}$ is plotted versus Ω/ω_m at different values of $\varepsilon = \tau\omega_m$. If $\varepsilon \lesssim 1$, i.e., the bandwidth of the detected mode is larger than ω_m, the detector does not resolve the motional sidebands, and $E_{\mathcal{N}}$ has a value (roughly equal to that of the intracavity case) which does not essentially depend upon the central frequency. For smaller bandwidths (larger ε), the sidebands are resolved by the detection and the role of the central frequency becomes important. In particular $E_{\mathcal{N}}$ becomes highly peaked around the *Stokes sideband* $\Omega = -\omega_m$, showing that the optomechanical entanglement generated within the cavity is mostly carried by this lower frequency sideband. What is relevant is that the optomechanical entanglement of the output mode is significantly larger than its intracavity counterpart and achieves its maximum value at the optimal value $\varepsilon \simeq 10$, i.e., a detection band-

width $\tau^{-1} \simeq \omega_m/10$. This means that in practice, by appropriately filtering the output light, one realizes an *effective entanglement distillation* because the selected output mode is more entangled with the mechanical resonator than the intracavity field.

The fact that the output mode which is most entangled with the mechanical resonator is the one centered around the Stokes sideband is also consistent with the physics of a previous model analyzed in [66]. In [66], a free-space optomechanical model is discussed, where the entanglement between a vibrational mode of a perfectly reflecting micro-mirror and the two first motional sidebands of an intense laser beam shined on the mirror is analyzed. Also in that case, the mechanical mode is entangled only with the Stokes mode and it is not entangled with the anti-Stokes sideband.

One can also understand why the output mode optimally entangled with the mechanical mode has a finite bandwidth $\tau^{-1} \simeq \omega_m/10$ (for the chosen operating point). In fact, the optimal situation is achieved when the detected output mode overlaps as best as possible with the Stokes peak in the spectrum, and therefore τ^{-1} coincides with the width of the Stokes peak. This width is determined by the effective damping rate of the mechanical resonator, $\gamma_m^{eff} = \gamma_m + \Gamma$, given by the sum of the intrinsic damping rate γ_m and the net laser cooling rate Γ of Eq. (52). It is possible to check that, with the chosen parameter values, the condition $\varepsilon = 10$ corresponds to $\tau^{-1} \simeq \gamma_m^{eff}$.

It is finally important to analyze the robustness of the present optomechanical entanglement with respect to temperature. As discussed above and shown in [64], the entanglement of the resonator with the intracavity mode is very robust. It is important to see if this robustness is kept also by the optomechanical entanglement of the output mode. This is shown also in the inset of Fig. 7, where the logarithmic negativity $E_{\mathcal{N}}$ of the output mode centered at the Stokes sideband $\Omega = -\omega_m$ is plotted versus the temperature of the reservoir at two different values of the bandwidth, the optimal one $\varepsilon = 10$, and at a larger bandwidth $\varepsilon = 0.5$. We see the expected decay of $E_{\mathcal{N}}$ for increasing temperature, but above all that also this output optomechanical entanglement is robust against temperature because it persists even above liquid He temperatures, at least in the case of the optimal detection bandwidth $\varepsilon = 10$.

4.3 Optical entanglement between sidebands

Let us now consider the case where we detect at the output two independent, well resolved, optical output modes. We use again the step-like filter functions of Eqs. (69) and (71), assuming the same bandwidth τ^{-1} for both modes and two different central frequencies, Ω_1 and Ω_2, satisfying the orthogonality

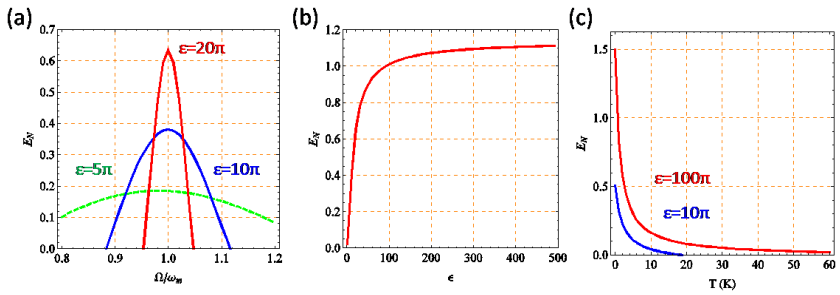

Fig. 8. Sideband-sideband entanglement. Parameters p_0, $\kappa = \omega_m$ and $G = \omega_m/2$. (a) Assuming one detection setup centered at the Stokes sideband and sweeping the second detection frequency around the anti-Stokes sideband at $\Omega = \omega_m$, the entanglement is clearly shown to be optimized when the anti-Stokes output field is detected. This entanglement is improving with smaller and smaller detection bandwidth ($\epsilon \to \infty$). (b) Logarithmic negativity increases asymptotically to a finite value with $\epsilon \to \infty$. (c) Temperature robustness for $\epsilon = 10\pi$ and $\epsilon = 100\pi$. The entanglement survives to very high temperatures.

condition of Eq. (70) $\Omega_1 - \Omega_2 = 2p\pi\tau^{-1}$ for some integer p, in order to have two independent optical modes. It is interesting to analyze the stationary state of the resulting tripartite CV system formed by the two output modes and the mechanical mode, in order to see if and when it is able to show purely optical bipartite entanglement between the two output modes.

The generation of two entangled light beams by means of the radiation pressure interaction of these fields with a mechanical element has been already considered in various configurations. In Ref. [93], and more recently in Ref. [63], two modes of a Fabry-Perot cavity system with a movable mirror, each driven by an intense laser, are entangled at the output due to their common ponderomotive interaction with the movable mirror (the scheme has been then generalized to many driven modes in [94]). In the single mirror free-space model of Ref. [66], the two first motional sidebands are also robustly entangled by the radiation pressure interaction as in a two-mode squeezed state produced by a non-degenerate parametric amplifier [95]. Robust two-mode squeezing of a bimodal cavity system can be similarly produced if the movable mirror is replaced by a single ion trapped within the cavity [96].

The situation considered here is significantly different from that of Refs. [63,93,94,96], which require many driven cavity modes, each associated with the corresponding output mode. In the present case instead, the different output modes *originate from the same single driven cavity mode*, and therefore it is simpler from an experimental point of view. The present scheme can be considered as a sort of "cavity version" of the free-space case of Ref. [66], where the reflecting mirror is driven by a single intense laser. Therefore, as in [66,95], one expects to find a parameter region where the two output modes centered

around the two motional sidebands of the laser are entangled. This expectation is clearly confirmed by Fig. 8a, where the logarithmic negativity $E_{\mathcal{N}}$ associated with the bipartite system formed by the output mode centered at the Stokes sideband ($\Omega_1 = -\omega_m$) and a second output mode with the same inverse bandwidth ($\varepsilon = \omega_m \tau = 10\pi$) and a variable central frequency Ω, is plotted versus Ω/ω_m. $E_{\mathcal{N}}$ is calculated from the CM $\mathcal{V}^{out}$ (for $N = 2$) eliminating the first two rows associated with the mechanical mode. One can clearly see that bipartite entanglement between the two cavity outputs exists only in a narrow frequency interval around the anti-Stokes sideband, $\Omega = \omega_m$, where $E_{\mathcal{N}}$ achieves its maximum. This shows that, as in [66,95], the two cavity output modes corresponding to the Stokes and anti-Stokes sidebands of the driving laser are significantly entangled by their common interaction with the mechanical resonator. The advantage of the present cavity scheme with respect to the free-space case of [66,95] is that the parameter regime for reaching radiation-pressure mediated optical entanglement is much more promising from an experimental point of view because it requires less input power and a not too large mechanical quality factor of the resonator. In Fig. 8b, the dependence of $E_{\mathcal{N}}$ of the two output modes centered at the two sidebands $\Omega = \pm\omega_m$ upon their inverse bandwidth ε is studied. We see that, differently from optomechanical entanglement of the former subsection, the logarithmic negativity of the two sidebands always increases for decreasing bandwidth, and it achieves a significant value, comparable to that achievable with parametric oscillators, for very narrow bandwidths. This fact can be understood from the fact that quantum correlations between the two sidebands are established by the coherent scattering of the cavity photons by the oscillator, and that the quantum coherence between the two scattering processes is maximal for output photons with frequencies $\omega_l \pm \omega_m$. Figs. 7 and 8 show that in the chosen parameter regime, the output mode centered around the Stokes sideband mode shows bipartite entanglement simultaneously with the mechanical mode and with the anti-Stokes sideband mode. This fact suggests that the CV tripartite system formed by the output Stokes and anti-Stokes sidebands and the mechanical resonator mode might be characterized by a fully tripartite-entangled stationary state. This is actually true and it can be checked by applying the classification criterion of Ref. [97], providing a necessary and sufficient criterion for the determination of the entanglement class in the case of tripartite CV Gaussian states, which is directly computable in terms of the eigenvalues of appropriate test matrices [97] (see Ref. [69]).

5 Entanglement generation with two driven cavity modes

We now generalize the system by considering the case when *two* cavity modes with different frequencies are intensely driven. We shall focus onto a param-

eter regime which will prove to be convenient for the generation of robust stationary CV entanglement between the resonator and the two cavity modes. A bichromatic driving of a cavity has been already experimentally considered in Refs. [21]. There however it was employed for cooling a macroscopically heavy ($m \simeq 1g$) movable mirror. One driven mode is used to "trap" the mirror, i.e., to induce a strong optical spring effect increasing by three orders of magnitude the oscillation frequency. The other driven mode is instead used to cool the mechanical resonator by increasing the effective mechanical damping, either via back-action, or via cold-damping feedback. The bichromatic driving configuration has been already considered for the generation of entanglement in various configurations in some theoretical proposals. In fact, in Ref. [93], and more recently in Ref. [63], two modes of a Fabry-Perot cavity system, each driven by an intense laser, are entangled at the output due to their common ponderomotive interaction with the movable mirror.

5.1 Quantum Langevin equations and stability conditions

We generalize the Hamiltonian of Eq. (1) by considering *two* cavity modes, with frequencies ω_{cA} and ω_{cB}, each driven by a laser with frequency ω_{0A} and ω_{0B}, and power $\mathcal{P}_A$ and $\mathcal{P}_B$, respectively. The resulting Hamiltonian is

$$H = \hbar\omega_{cA}\, a^\dagger a + \hbar\omega_{cB}\, b^\dagger b + \frac{1}{2}\hbar\omega_m(p^2+q^2) - \hbar(G_{0A}\, a^\dagger a + G_{0B}\, b^\dagger b)q$$
$$+i\hbar[E_A(a^\dagger e^{-i\omega_{0A}t} - a e^{i\omega_{0A}t}) + E_B(b^\dagger e^{-i\omega_{0B}t} - b e^{i\omega_{0B}t})], \tag{74}$$

where a and b now denote the annihilation operators of the two cavity modes, we have introduced the two coupling constants $G_{0x} = \sqrt{\hbar/m\omega_m}\,\omega_{cx}/L$, and the two driving rates $|E_x| = \sqrt{2P_x\kappa/\hbar\omega_{0x}}$, $x = A, B$. We have assumed for simplicity that the two modes have the same decay rate κ. We assume that scattering of photons of the driven modes into other cavity modes and also between the two chosen modes is negligible: this is verified when ω_m is much smaller then the free spectral range of the cavity.

Introducing again dissipation and noise terms as in Sec. 2, the system dynamics is described by the following set of nonlinear QLE, written in the interaction picture with respect to $\hbar\omega_{0A}a^\dagger a + \hbar\omega_{0B}b^\dagger b$,

$$\dot{q} = \omega_m p, \tag{75}$$
$$\dot{p} = -\omega_m q - \gamma_m p + G_{0A}a^\dagger a + G_{0B}b^\dagger b + \xi, \tag{76}$$
$$\dot{a} = -[\kappa + i(\Delta_{0A} - G_{0A}q)]a + E_A + \sqrt{2\kappa}a^{in}, \tag{77}$$
$$\dot{b} = -[\kappa + i(\Delta_{0B} - G_{0B}q)]b + E_B + \sqrt{2\kappa}b^{in}, \tag{78}$$

where $\Delta_{0x} \equiv \omega_{cx} - \omega_{0x}$ are the detunings of the two lasers, and we have introduced a vacuum input noise $b^{in}(t)$ for the cavity mode b, possessing the same correlations of Eqs. (7)-(8).

We assume again that both modes are intensely driven so that the system is characterized by a semiclassical steady state with large intracavity amplitudes for both modes and a modified cavity length. This classical steady state is determined by setting the time derivatives to zero, factorizing the averages and solving for the mean values $a_s = \langle a \rangle$, $b_s = \langle b \rangle$, $q_s = \langle q \rangle$, $p_s = \langle p \rangle$. One gets

$$a_s = \frac{E_A}{\kappa + i\Delta_A}, \tag{79}$$

$$b_s = \frac{E_B}{\kappa + i\Delta_B}, \tag{80}$$

$$q_s = \frac{G_{0A}|a_s|^2 + G_{0B}|b_s|^2}{\omega_m}, \tag{81}$$

$$p_s = 0, \tag{82}$$

where the effective detunings $\Delta_x \equiv \Delta_{0x} - (G_{0A}^2|a_s|^2 + G_{0B}^2|b_s|^2)/\omega_m$, $x = A, B$, have been defined, so that Eqs. (79)-(80) form actually a system of nonlinear equations, whose solution gives the stationary amplitudes a_s and b_s.

One then focuses onto the dynamics of the quantum fluctuations around this steady state, which are well described by linearizing the QLE of Eqs. (75)-(78) around the semiclassical steady state values, provided that $|a_s|, |b_s| \gg 1$. The linearized QLE for the resonator and for the amplitude and phase quadratures of the two modes, δX_A, δX_B, δY_A and δY_B, defined as in Sec. 2, can be written in compact form as

$$\dot{u}(t) = Au(t) + n(t),$$

where $u = (\delta q, \delta p, \delta X_A, \delta Y_A, \delta X_B, \delta Y_B)^T$ is the vector of quadrature fluctuations, and $n = (0, \xi, \sqrt{2\kappa}X_A^{in}, \sqrt{2\kappa}Y_A^{in}, \sqrt{2\kappa}X_B^{in}, \sqrt{2\kappa}Y_B^{in})^T$ is the corresponding vector of noises. The 6×6 matrix A is the drift matrix of the system, which reads

$$A = \begin{pmatrix} 0 & \omega_m & 0 & 0 & 0 & 0 \\ -\omega_m & \gamma_m & G_A & 0 & G_B & 0 \\ 0 & 0 & -\kappa & \Delta_A & 0 & 0 \\ G_A & 0 & -\Delta_A & -\kappa & 0 & 0 \\ 0 & 0 & 0 & 0 & -\kappa & \Delta_B \\ G_B & 0 & 0 & 0 & -\Delta_B & -\kappa \end{pmatrix}, \tag{83}$$

where we have chosen the phase reference of the two cavity modes so that a_s

and b_s are real and positive, and defined the effective couplings $G_A = G_{0A} a_s \sqrt{2}$ and $G_B = G_{0B} b_s \sqrt{2}$.

The steady state exists and it is stable if all the eigenvalues of the drift matrix A have negative real parts. The parameter region under which stability is verified can be obtained from the Routh-Hurwitz criteria [81], but the inequalities that come out in the present case are quite involved. One can have an idea of this fact from the expression of the characteristic polynomial of A, $P(\lambda) = \lambda^6 + c_1\lambda^5 + c_2\lambda^4 + c_3\lambda^3 + c_4\lambda^2 + c_5\lambda + c_6$, where

$$
\begin{aligned}
c_1 &= \gamma_m + 4\kappa, \\
c_2 &= \Delta_A^2 + \Delta_B^2 + 4\gamma_m\kappa + 6\kappa^2 + \omega_m^2, \\
c_3 &= \gamma_m(\Delta_A^2 + \Delta_B^2 + 6\kappa^2) + 2\kappa[\Delta_A^2 + \Delta_B^2 + 2(\kappa^2 + \Omega_m^2)], \\
c_4 &= \kappa^4 + 2\gamma_m\kappa(\Delta_B^2 + 2\kappa^2) + 6\kappa^2\omega_m^2 + \Delta_B^2(\kappa^2 + \omega_m^2) + \\
&\quad \Delta_A^2(\Delta_B^2 + 2\gamma_m\kappa + \kappa^2 + \omega_m^2) - \omega_m(G_A^2\Delta_A + G_B^2\Delta_B), \\
c_5 &= \gamma_m(\Delta_A^2 + \kappa^2)(\Delta_B^2 + \kappa^2) + 2\kappa\omega_m^2(\Delta_A^2 + \Delta^2 + 2\kappa^2) \\
&\quad -2\kappa\omega_m(G_A^2\Delta_A + G_B^2\Delta_B), \\
c_6 &= \omega_m^2(\Delta_A^2 + \kappa^2)(\Delta_B^2 + \kappa^2) - \omega_m[G_B^2\Delta_B(\Delta_A^2 + \kappa^2) \\
&\quad +G_A^2\Delta_A(\Delta_B^2 + \kappa^2)].
\end{aligned}
$$

We are considering here a bichromatic driving of the cavity in order to improve the size and the robustness of the generated entanglement. Entanglement monotonically increases with the optomechanical coupling but, as we have seen also in the previous sections, the stability conditions put a strict upper bound on the maximum achievable value of this coupling. Therefore it is interesting to find a regime in which the presence of the second driven mode makes the system always stable, so that the couplings can be made very large (for example by increasing the input power, the cavity finesse, or decreasing the cavity length) without entering the unstable regime. One then hopes that in this regime also entanglement can be made large and robust against temperature.

A simple way to have always a stable system is to find a particular relation between the parameters such that the characteristic polynomial of A does not depend upon G_A and G_B. In this case, the eigenvalues of A would be independent of the two couplings and stability would be guaranteed. The expressions above show that the eigenvalues of A are independent of G_A and G_B and the system is always stable if and only if

$$
|G_a| = |G_B| = G, \tag{84a}
$$

$$
\Delta_A = -\Delta_B = \Delta. \tag{84b}
$$

The condition described by Eqs. (84) represents a perfect balance between a

cooling cavity mode (which, without loss of generality, we can take as mode A, so that $\Delta_A > 0$) and a heating cavity mode, i.e., mode B with $\Delta_B < 0$. The fact that the eigenvalues of A do not depend upon the couplings means that the decay rates of both the resonator and the cavity modes are left unchanged and in this case radiation pressure mainly create quantum correlations, i.e., entanglement, between the modes. We shall assume conditions (84) from now on.

5.2 Entanglement of the output modes

We now calculate the entanglement properties of the steady state of the bichromatically driven cavity. However we shall not discuss here the intracavity entanglement, but only the entanglement properties of the optical *output modes*. In fact, as we have seen above in the case of a single driven mode, one can obtain a larger optomechanical entanglement with respect to the intracavity case by appropriately filtering the output modes. Moreover only the entanglement with output modes is relevant for any quantum communication application. We shall apply therefore the filter function formalism developed in Sec. 4.2, restricted however here to the simple case of *a single output mode* for each intracavity mode. In fact, we have now two driven cavity modes and considering the more general case of multiple output modes associated to each driven mode as in Sec. 4.2, would render the description much more involved without however gaining too much insight into the physics of the problem. The two output modes originate from two different cavity modes, and since the latter are not too close in frequency, they consequently describe two independent modes. Therefore we do not need orthogonal filter functions like those of Eq. (69) used for the single driven mode case, and we choose here a different filter function. We consider the two output modes with annihilation operators

$$a^{out}_{\Omega_x}(t) = \int_{-\infty}^{t} ds g_x(t-s) a^{out}_x(s) \quad x = A, B, \tag{85}$$

where $a^{out}_A(t)$ and $a^{out}_B(t)$ are the usual output fields associated with the two cavity modes and

$$g_x(t) = \sqrt{\frac{2}{\tau}} e^{-(1/\tau + i\Omega_x)t} \theta(t) \quad x = A, B \tag{86}$$

are the two filter functions, describing two output modes, both with bandwidth $1/\tau$ and with central frequencies, Ω_A and Ω_B, which are in general different from the cavity mode frequencies ω_{cA} and ω_{cB}.

The entanglement between the chosen output modes and the mechanical resonator mode is fully determined by the corresponding 6×6 CM, which is

defined as in Eq. (72)

$$\mathcal{V}_{ij}^{out}(t) = \frac{1}{2}\left\langle u_i^{out}(t)u_j^{out}(t) + u_j^{out}(t)u_i^{out}(t)\right\rangle, \tag{87}$$

where now

$$u^{out}(t) = \left[0, 0, \delta X_{\Omega_A}^{out}(t), \delta Y_{\Omega_A}^{out}(t), \delta X_{\Omega_B}^{out}(t), \delta Y_{\Omega_B}^{out}(t)\right]^T, \tag{88}$$

is the vector formed by the mechanical position and momentum fluctuations and by the amplitude and phase quadratures of the filtered modes. Using the various definitions, input-output relations and also the correlation function of the noise terms, one can derive an integral expression for the CM $\mathcal{V}^{out}$ of the system (see Ref. [69] for the details in a similar calculation), which is given by

$$\mathcal{V}^{out} = \int d\omega \tilde{T}(\omega)\left[\tilde{M}(\omega) + \frac{P_{out}}{2\kappa}\right] D(\omega)\left[\tilde{M}(\omega)^\dagger + \frac{P_{out}}{2\kappa}\right]\tilde{T}(\omega)^\dagger, \tag{89}$$

where $\tilde{T}(\omega)$ is the Fourier transform of

$$T(t) = \begin{pmatrix} \delta(t) & 0 & 0 & 0 & 0 & 0 \\ 0 & \delta(t) & 0 & 0 & 0 & 0 \\ 0 & 0 & \sqrt{2\kappa}\mathrm{Re}g_A(t) & -\sqrt{2\kappa}\mathrm{Im}g_A(t) & 0 & 0 \\ 0 & 0 & \sqrt{2\kappa}\mathrm{Im}g_A(t) & \sqrt{2\kappa}\mathrm{Re}g_A(t) & 0 & 0 \\ 0 & 0 & 0 & 0 & \sqrt{2\kappa}\mathrm{Re}g_B(t) & -\sqrt{2\kappa}\mathrm{Im}g_B(t) \\ 0 & 0 & 0 & 0 & \sqrt{2\kappa}\mathrm{Im}g_B(t) & \sqrt{2\kappa}\mathrm{Re}g_B(t) \end{pmatrix}, \tag{90}$$

,

$$\tilde{M}(\omega) = (i\omega + A)^{-1}, \tag{91}$$

$P_{out} = \mathrm{Diag}[0, 0, 1, 1, 1, 1]$ is the projector onto the optical quadratures, and $D(\omega)$ is the matrix associated with the Fourier transform of the noise correlation functions, given by

$$D(\omega) = \mathrm{Diag}[0, (\gamma_m\omega/\omega_m)\coth(\hbar\omega/2k_BT), \kappa, \kappa, \kappa, \kappa].$$

Using the CM $\mathcal{V}^{out}$ one can analyze the entanglement between the three different bipartitions of the system, when one of the three modes is traced out, and also tripartite entanglement.

5.2.1 Optomechanical entanglement

First of all we consider the entanglement between the output field of the "cooling mode" (A) (the one with $\Delta_A > 0$) and the mechanical resonator. We have seen in Sec. 4 that this configuration allows to achieve the maximum

optomechanical entanglement in the case of a single driven cavity mode. In fact, when $\Delta \simeq \omega_m$, G is large enough, and the selected output mode is centered around the Stokes sideband, the entanglement is optimized and it is also robust against temperature (see Fig. 7). Fig. 9 shows that the presence of the second "heating" mode B *disturbs* this optimal condition and that $E_{\mathcal{N}}$ is appreciably lower than the one with only one driven mode. In fact, we have considered here a similar parameter region, i.e. p_0, $\kappa = \omega_m$, $\Delta_A = \omega_m$, $\Delta_B = -\omega_m$, $G_a = 0.326\omega_m$, $G_b = 0.302\omega_m$. The qualitative behavior of $E_{\mathcal{N}}$ is identical to that of the corresponding Fig. 7, i.e., $E_{\mathcal{N}}$ is maximum when the output mode overlaps as best as possible with the Stokes sideband of the corresponding driving laser, which means centered around $-\omega_m$ and with an inverse bandwidth $\varepsilon = \omega_m\tau \simeq 10$. However the achievable values of $E_{\mathcal{N}}$ are significantly *lower*. Fig. 7b shows that, despite the lower values, entanglement is still quite robust against temperature.

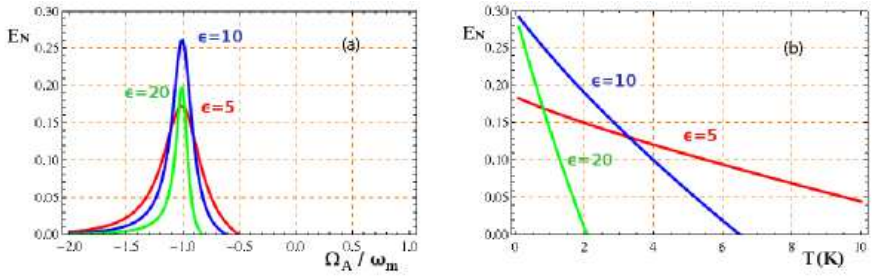

Fig. 9. Logarithmic negativity $E_{\mathcal{N}}$ of the bipartite system formed by the mechanical mode and the output of the "cooling" mode A. (a) $E_{\mathcal{N}}$ versus the center frequency of the output mode Ω_A/ω_m at three different values of the inverse detection bandwidth $\epsilon = \omega_m\tau$. As in the single driven mode case (see Fig. 7), entanglement is maximum when the output mode is centered around the the Stokes sideband $\Omega_A = -\omega_m$. The other parameters are p_0, $\kappa = \omega_m$, $\Delta_A = \omega_m$, $\Delta_B = -\omega_m$, $G_a = 0.326\omega_m$, $G_b = 0.302\omega_m$. (b) $E_{\mathcal{N}}$ versus the reservoir temperature T when the output mode is centered at the Stokes sideband ($\Omega_A = -\omega_m$) for the same three different values of ε.

The advantage of the bichromatic driving becomes instead apparent when one considers the bipartite system formed by the resonator and the output field of the "heating" mode (B), the one with $\Delta_B = -\omega_m$. The stationary optomechanical entanglement can achieve in this case significantly larger values. The results are shown in Fig. 10 which refers to the same parameters of Fig. 9 and shows the same qualitative behavior: $E_{\mathcal{N}}$ is optimized when the selected output mode well overlaps with the Stokes sideband of the driving laser $\Omega_B = -\omega_m$ and it persists up to reservoir temperatures of the order of 10 K. However, $E_{\mathcal{N}}$ is now roughly three times larger than the corresponding value for the "cooling" mode. This behavior is different from what is found in Sec. 4 for a single driven cavity mode, where we have seen that optomechanical entanglement in the "heating" regime of negative detunings is seriously

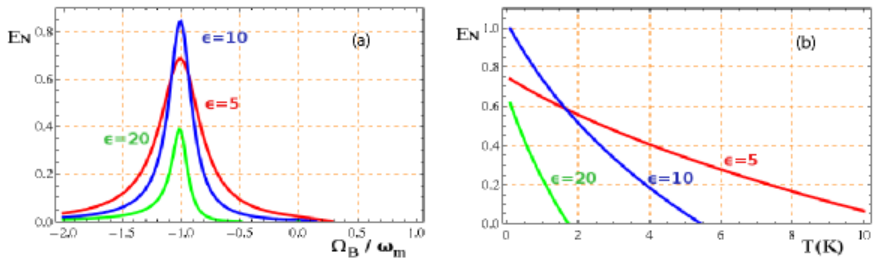

Fig. 10. Logarithmic negativity $E_{\mathcal{N}}$ of the bipartite system formed by the mechanical mode and the output of the "heating" mode B. (a) $E_{\mathcal{N}}$ versus the center frequency of the latter Ω_A/ω_m at three different values of the inverse detection bandwidth $\epsilon = \omega_m\tau$. As it happens for the "cooling" mode A, entanglement is maximum when the output mode is centered around the the Stokes sideband $\Omega_B = -\omega_m$. Parameters are as in Fig. 9. (b) $E_{\mathcal{N}}$ versus the reservoir temperature T when the output mode is centered at the Stokes sideband ($\Omega_B = -\omega_m$) for the same three different values of ε.

limited by stability conditions. Now, thanks to the combined action of the two driven modes and to the conditions (84), the system is always stable and the parametric-like process described in Sec. 4 is able to generate large and robust entanglement. Therefore we can say that in this bichromatic case, mode A helps to entangle in a robust way the output of the "heating" mode B, by counteracting its instability effect and making the system stable for any value of the couplings G_A and G_B. Notice that in this case, the Stokes sideband of the laser driving mode B is *resonant* with the cavity, because $\Delta_B = -\omega_m$ implies $\omega_{cB} = \omega_{0B} - \omega_m = \omega_{Stokes}$ and this provides a further reason why the optomechanical entanglement may become large.

5.2.2 Purely optical entanglement between output modes

Let us consider now the purely optical entanglement between the two output light beams. As discussed at the beginning of the section, the possibility to entangle two different output modes of a cavity by means of radiation pressure has been already suggested in different configurations [63,66,93,95]. We have also seen in Sec. 4 that this is possible even with a single driven mode. It is nonetheless interesting to compare the results of Sec. 4 with the present bichromatic driving case. The bichromatic case has been already studied in Ref. [63], which however restricted to the case of output modes with infinitely narrow bandwidth ($\tau = \infty$) and centered around the driving laser frequency ($\Omega_A = \Omega_B = 0$). The general filter function formalism instead allows us to consider generic values of τ, Ω_A, and Ω_B. By applying again Eq. (89) and tracing out now the mechanical mode, we get the results illustrated in Fig. 11. We have considered a slightly different parameter regime with respect to the previous subsection, by choosing slightly larger couplings, $G_a = 1.74\omega_m$, $G_b = 1.70\omega_m$,

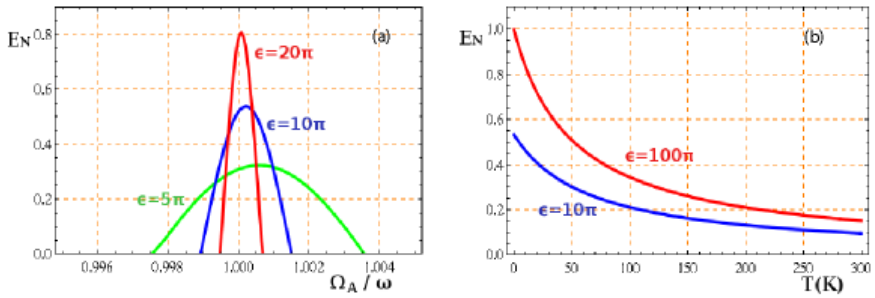

Fig. 11. Logarithmic negativity $E_{\mathcal{N}}$ of the bipartite system formed by the output modes associated with the two driven cavity modes. (a) $E_{\mathcal{N}}$ versus the center frequency of the "cooling" mode A Ω_A/ω_m for a center frequency of the "heating" mode fixed at $\Omega_B = -\omega_m$ (Stokes sideband), and at three different values of the inverse detection bandwidth $\epsilon = \omega_m\tau$. The other parameters are p_0, $\kappa = \omega_m$, $\Delta_A = \omega_m$, $\Delta_B = -\omega_m$, $G_a = 1.74\omega_m$, $G_b = 1.70\omega_m$. (b) $E_{\mathcal{N}}$ versus the reservoir temperature T when the output of the mode A is centered at the anti-Stokes sideband ($\Omega_A = \omega_m$) and the output of mode B is centered at the Stokes sideband ($\Omega_B = -\omega_m$), for two different values of ε.

i.e., larger input powers. Here, the oscillating mirror induces Stokes and anti-Stokes sidebands for *both* driving lasers and therefore it may be nontrivial to establish which are the most-entangled output modes. Fig. 11(a) shows that the largest all-optical entanglement is achieved between the *anti-Stokes sideband of the "cooling" mode and the Stokes sideband of the "heating" beam.* This is consistent with the results for a single cavity mode, because in both cases the motion of the resonator creates strong quantum correlations between the scattering of a Stokes and an anti-Stokes photon. Moreover this result can be understood from the fact that the two sidebands are those which are resonant with the corresponding cavity mode. Fig. 11(a) also shows that, as it happens in the single cavity mode case, and differently form the optomechanical entanglement, the all-optical $E_{\mathcal{N}}$ monotonically increases for decreasing detection bandwidths. This is reasonable because the two output modes are correlated as in two-mode squeezing which is based on the pairwise correlated production of photons from a pump laser beam via a parametric process. In this case the quantum correlations are optimally detected when only pairs of photons exactly satisfying the matching condition $\omega_s + \omega_{as} = \omega_{0A} + \omega_{0B}$ are detected, i.e., when $\tau = \infty$.

Fig. 11(b) instead shows the robustness of all-optical entanglement with respect to the reservoir temperature, which is extremely good: entanglement persists even at room temperature provided that one considers output modes with a sufficiently narrow bandwidth. In this respect, the bichromatic driving case proves to be more promising than the single driving mode case (compare Fig. 11(b) with Fig. 8(c)).

Combining all the results of this section, we see that the output modes associated with the two driven cavity modes and the mechanical mode form a tripartite system in which each bipartite subsystem is entangled. This suggests that a parameter region exists where this tripartite system is characterized by a fully tripartite-entangled stationary state. This is actually true and it can be checked by applying the classification criterion of Ref. [97], providing a necessary and sufficient criterion for the determination of the entanglement class in the case of tripartite CV Gaussian states, which is directly computable in terms of the eigenvalues of appropriate test matrices [97].

6 Cavity-mediated atom-mirror stationary entanglement

A final recent application of optomechanical systems, recently suggested by a number of papers (see Refs. [70,71]), is to couple them also to atomic ensembles in order to realize new and more flexible CV quantum interfaces. To be more specific, here we consider a hybrid system comprised of N_a two-level atoms of energy splitting $\hbar\omega_a$, coupled to an optical cavity, which is in turn coupled to a mechanical element by radiation pressure. We consider again the steady state of the system and choose a weak-coupling regime where the atoms and the cavity are far-off resonance (as illustrated by Fig. 12). The working point for the optomechanical system is the regime described in the previous section where red-detuned driving of the cavity ensures optimal entanglement between the Stokes sideband and the mechanical resonator. We show here that when the atoms are resonant with the Stokes sideband of the laser, a regime where both atoms-mirror bipartite CV entanglement and tripartite CV entanglement can be generated in the steady state, is achieved.

We start from the Hamiltonian of Eq. (1) to which we add the Tavis-Cummings atom-cavity field interaction

$$H_I = \hbar g \left(S_+ a + S_- a^\dagger \right),$$

where collective spin operators are defined as $S_{+,-,z} = \sum_{\{i\}} \sigma^{(i)}_{+,-,z}$ for $i = 1, N_a$ ($\sigma_{+,-,z}$ are the Pauli matrices) and satisfy the commutation relations $[S_+, S_-] = S_z$ and $[S_z, S_\pm] = \pm 2 S_\pm$. The atom-cavity coupling constant is given by $g = \mu\sqrt{\omega_c / 2\hbar\epsilon_0 V}$ where V is the cavity mode volume, μ is the dipole moment of the atomic transition, and ϵ_0 is the free space permittivity.

The dynamics of the tripartite system is fairly complicated. However, one can find a regime where a simpler dynamics of three coupled harmonics oscillators is a good approximation of the system dynamics. To this purpose, we assume that the atoms are initially prepared in their ground state, so that $S_z \simeq \langle S_z \rangle \simeq -N_a$ and this condition is not appreciably altered by the interaction

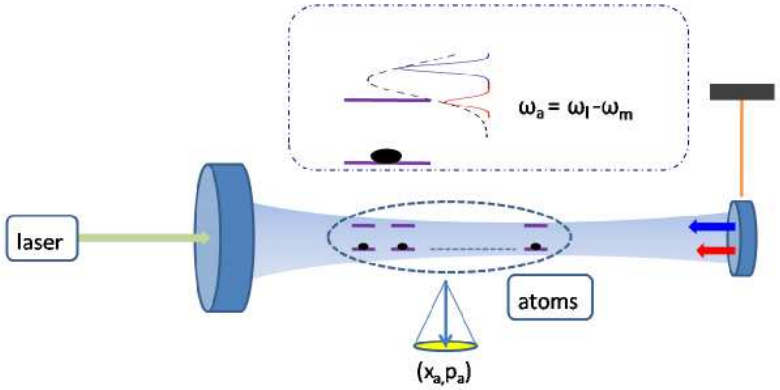

Fig. 12. Setup for tripartite hybrid entanglement. An atomic cloud of two-level atoms is placed inside a cavity driven by a laser. As seen in the inset, the atoms are resonant with the Stokes sideband of the laser. Since this latter sideband is the one carrying most of the optomechanical entanglement, also the atoms and movable mirror become entangled at the steady state.

with the cavity field. This is satisfied when the excitation probability of a single atom is small. In this limit the dynamics of the atomic polarization can be described in terms of bosonic operators: in fact if one defines the atomic annihilation operator $c = S_-/\sqrt{|\langle S_z \rangle|}$, one can see that it satisfies the usual bosonic commutation relation $[c, c^\dagger] = 1$ [98]. In the frame rotating at the laser frequency ω_l for the atom-cavity system, the quantum Langevin equations can then be written as

$$\dot{q} = \omega_m p, \tag{92}$$

$$\dot{p} = -\omega_m q - \gamma_m p + G_0 a^\dagger a + \xi, \tag{93}$$

$$\dot{a} = -(\kappa + i\Delta_0)a + iG_0 aq - iG_a c + \mathcal{E}_l + \sqrt{2\kappa}a_{in}, \tag{94}$$

$$\dot{c} = -(\gamma_a + i\Delta_a)\, c - iG_a a + \sqrt{2\gamma_a}F_c, \tag{95}$$

where $\Delta_0 = \omega_c - \omega_l$ and $\Delta_a = \omega_a - \omega_l$ are the cavity and atomic detuning with respect to the laser, $G_a = g\sqrt{N_a}$, and $2\gamma_a$ is the decay rate of the atomic excited level. The noise affecting the atoms has one non-vanishing correlation function $\langle F_c(t)\, F_c^\dagger(t')\rangle = \delta(t - t')$. We now assume that the cavity is intensely driven, so that at the steady state, the intracavity field has a large amplitude α_s, with $|\alpha_s| \gg 1$. However, the single-atom excitation probability is $g^2|\alpha_s|^2/(\Delta_a^2 + \gamma_a^2)$ and since this probability has to be much smaller than one for the validity of the bosonic description of the atomic polarization, this imposes an upper bound to $|\alpha_s|$. Therefore the two conditions are simultaneously satisfied only if the atoms are weakly coupled to the cavity, $g^2/[\Delta_a^2 + \gamma_a^2] \ll |\alpha_s|^{-2} \ll 1$.

If one is interested only in atoms-mirror entanglement, one could assume a bad cavity limit and adiabatically eliminate the cavity mode [71]. However, one

can have a more complete information by linearizing the Langevin equations Eqs. (92)-(95) around the semiclassical steady state and then solving for the exact solution of the 3-mode system steady state provided by the Lyapunov equation (29) [70]. In fact, owing to the Gaussian nature of the quantum noise terms ξ, a_{in} and F_c, and to the linearization of the dynamics, the steady state of the quantum fluctuations of the system is a CV tripartite Gaussian state, which is completely determined by its 6×6 correlation matrix (CM). The corresponding drift matrix after linearization is given by

$$A = \begin{pmatrix} 0 & \omega_m & 0 & 0 & 0 & 0 \\ -\omega_m & -\gamma_m & G & 0 & 0 & 0 \\ 0 & 0 & -\kappa & \Delta & 0 & G_a \\ G & 0 & -\Delta & -\kappa & -G_a & 0 \\ 0 & 0 & 0 & G_a & -\gamma_a & \Delta_a \\ 0 & 0 & -G_a & 0 & -\Delta_a & -\gamma_a \end{pmatrix}, \tag{96}$$

while the diffusion matrix is equal to $D =$diag$[0, \gamma_m (2n_0 + 1), \kappa, \kappa, \gamma_a, \gamma_a]$. We have solved Eq. (29) for the CM $\mathcal{V}$ in a wide range of the parameters G, G_a, Δ and Δ_a. We have studied first of all the stationary entanglement of the three possible bipartite subsystems, by quantifying it in terms of the logarithmic negativity of bimodal Gaussian states. We will denote the logarithmic negativities for the mirror-atom, atom-field and mirror-field bimodal partitions with E_{ma}, E_{af} and E_{mf}, respectively.

The results on the behavior of the bipartite entanglement E_{ma} are shown in Fig. 13a. Optimization requires, as expected that the atoms are resonant with the Stokes motional sideband. In Fig. 13b, the logarithmic negativity of the three bipartitions is plotted versus the normalized atomic detuning. It is evident that one has a sort of entanglement sharing: due to the presence of the atoms, the initial cavity-mirror entanglement (represented by the dashed line) is partially redistributed to the atom-mirror and atom-cavity subsystems and this effect is predominant when the atoms are resonant with the Stokes sideband ($\Delta_a = -\omega_m$). It is remarkable that, in the chosen parameter regime, the largest stationary entanglement is the one between atoms and mirror which are only indirectly coupled. Moreover, the nonzero atom-cavity entanglement appears only thanks to the effect of the mirror dynamics because in the bosonic approximation we are considering and with a fixed mirror, there would be no direct atom-cavity entanglement. We also notice that atom-mirror entanglement is instead not present at $\Delta_a = \omega_m$. This is due to the fact that the cavity-mirror entanglement is mostly carried by the Stokes sideband and that, when $\Delta_a = \omega_m$, mirror cavity-cooling is disturbed by the anti-Stokes photons being recycled in the cavity by the absorbing atoms.

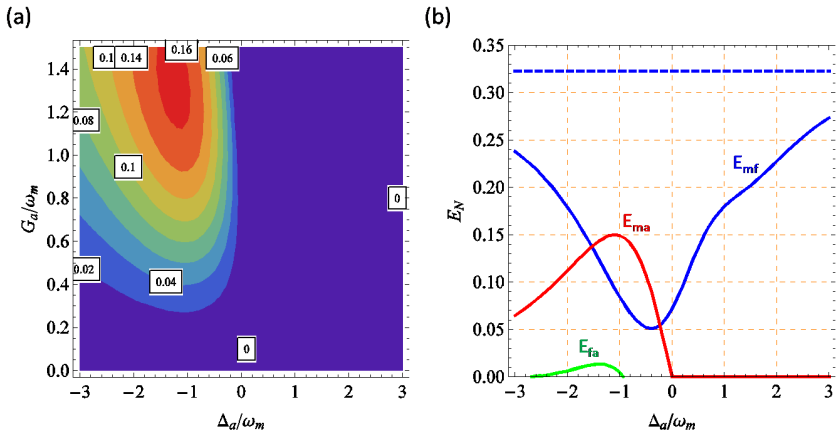

Fig. 13. Entanglement in the hybrid mirror-atom-field system. Parameters are p_0, $\kappa = \gamma_a = \omega_m$, $G = 1.3\omega_m$. (a) Contour plot of $E_{\mathcal{N}}$ between mirror and atoms as a function of G_a/ω_m and Δ_a/ω_m. The entanglement is optimized for $\Delta_a = -\omega_m$, i.e. when the atoms are resonant with the Stokes sideband of the laser. (b) The three bipartite entanglement versus the atomic detuning. The blue dashed line represents the mirror-field $E_{\mathcal{N}}$ in the absence of atom-field coupling. When the atoms are immersed in the mirror-field system, the entanglement is redistributed among the three sub-partitions, especially around the regime where $\Delta_a = -\omega_m$.

We notice that the chosen parameters correspond to a small cavity mode volume ($V \simeq 10^{-12}$ m^3), implying that for a dipole transition, g is not small. Therefore the assumed weak coupling condition $g^2/[\Delta_a^2 + \gamma_a^2] \ll |\alpha_s|^{-2} \ll 1$ can be satisfied only if g represents a much smaller, *time averaged*, coupling constant. This holds for example for an atomic vapor cell much larger than the cavity mode: if the (hot) atoms move in a cylindrical cell with axis orthogonal to the cavity axis, with diameter ~ 0.5 mm and height ~ 1 cm, they will roughly spend only one thousandth of their time within the cavity mode region. This yields an effective $g \sim 10^4$ Hz, so that the assumptions made here hold, and the chosen value $G_a/2\pi = 6 \times 10^6$ Hz can be obtained with $N_a \sim 10^7$. An alternative solution could be choosing a cold atomic ensemble and a dipole-forbidden transition.

The entanglement properties of the steady state of the tripartite system can be verified by experimentally measuring the corresponding CM. This can be done by combining existing experimental techniques. The cavity field quadratures can be measured directly by homodyning the cavity output, while the mechanical position and momentum can be measured with the schemes discussed in Sec. 3.3. Finally, the atomic polarization quadratures x and y (proportional to S_x and S_y) can be measured by adopting the same scheme of Ref. [99], i.e., by making a Stokes parameter measurement of a laser beam, shined transversal to the cavity and to the cell and off-resonantly tuned to another atomic transition.

7 Conclusions

The search for experimental demonstrations of the quantum behavior of macroscopic mechanical resonators is a fastly growing field of investigation. Recent experimental results [15,16,17,18,19,20,21,22,23,24,25,26,27,28,29,30,31] and theoretical predictions suggest that quantum states of resonators with a mass at the microgram scale will be generated and detected in the near future. In this chapter we have tried to give an overview of two relevant arguments of this research field: i) cooling to the motional ground state; ii) the generation of robust entangled steady states involving mechanical and optical degrees of freedom. The latter condition is the fundamental prerequisite for the eventual integration of micro- and nano-mechanical resonators serving as quantum memories and interfaces within quantum communication networks.

In the first part of the chapter we have described and compared the two main approaches for cooling micro-mechanical resonators via radiation pressure coupling to an optical cavity, cold-damping feedback [32,34,35,36,41], and back-action cooling [33,39,40,41,42,43]. We have adopted a general quantum Langevin treatment which is valid within the full parameter range of a stable cavity. Both back-action cooling and cold damping feedback are able to cool to the ground state, even though back-action cooling is preferable for a good cavity ($\kappa < \omega_m$), while cold damping is more convenient for a bad cavity ($\kappa > \omega_m$).

In the second part of the chapter we have analyzed the entanglement properties of the steady state of the system formed by the optical cavity coupled to a mechanical element. We have considered two different configurations, with either one or two intensely driven cavity modes. We have seen that the intracavity mode and the mechanical element can be entangled in a robust way against temperature, and that back-action cooling is *not* a necessary condition for achieving entanglement. In fact, entanglement is possible also in the opposite regime of a blue-detuned laser where the cavity mode *drives* and does not cool the resonator. More generally, the two phenomena are quite independent, and one is not necessarily accompanied by the other. Cooling is a classical process (even though it can ultimately lead to the quantum ground state), while entanglement is an intrinsically quantum phenomenon. Moreover, they are optimized in different parameter regimes. In fact, logarithmic negativity is maximized close to the stability threshold of the system, where instead the resonator is not cooled. We have then focused our study onto the entanglement properties of the cavity output field, which is the relevant one for quantum communication applications. We have developed a general theory showing how it is possible to define and evaluate the entanglement properties of the multipartite system formed by the mechanical resonator and N independent output modes of the cavity field. We have seen that the tripartite

system formed by the mechanical element and the two output modes centered at the first Stokes and anti-Stokes sideband of the driving laser (where the cavity output noise spectrum is concentrated) shows robust fully tripartite entanglement. In particular, the Stokes output mode is strongly entangled with the mechanical mode and shows a sort of entanglement distillation because its logarithmic negativity is significantly larger than the intracavity one when its bandwidth is appropriately chosen. In the same parameter regime, the Stokes and anti-Stokes sideband modes are robustly entangled, and the achievable entanglement in the limit of a very narrow detection bandwidth is comparable to that generated by a parametric oscillators. These results hold in both cases of single and bichromatic driving of the cavity. In this latter case, entanglement becomes larger and more robust against temperature under a particular parameter condition in which one mode is driven by a red-detuned laser and the other one by a blue-detuned laser. In fact, for equal optomechanical couplings and opposite detunings the system is always stable, even for large values of the intracavity power, and entanglement can persist also at higher temperatures.

Finally we have investigated a possible route for coupling optomechanical devices with atomic ensembles, by showing that if the atoms are placed inside the optical cavity and tuned into resonance with the Stokes sideband, optomechanical entanglement is optimally distributed also to the atomic ensemble [70]. Under these conditions one realizes a strongly coupled system showing robust tripartite entanglement which can be exploited for the realization of CV quantum interfaces [71].

8 Acknowledgements

This work has been supported by the European Commission (FP6 Integrated Project QAP, and FET-Open project MINOS), and by INFN (SQUALO project).

References

[1] M. P. Blencowe, Phys. Rep. **395**, 159 (2004).

[2] K. C. Schwab and M. L. Roukes, Phys. Today **58**, 36 (2005).

[3] T. J. Kippenberg and K. J. Vahala, Opt. Expr. **15**, 17172 (2007).

[4] M. Aspelmeyer and K. Schwab, New J. Phys. **10** 095001 (2008).

[5] V.B. Braginsky and F. Ya Khalili, *Quantum Measurements*, Cambridge University Press, Cambridge, (1992).

[6] B. Abbott *et al.*, Phys. Rev. D **69**, 122004 (2004); F. Acernese *et al.* Class. Quantum Grav. **22** S869 (2005).

[7] W. Marshall, C. Simon, R. Penrose, and D. Bouwmeester, Phys. Rev. Lett. **91**, 130401 (2003). W. H. Zurek, Rev. Mod. Phys. **75**, 715 (2003).

[8] A. J. Leggett, J. Phys. Cond. Mat., **14**, R415 (2002).

[9] L. Hackermüller, K. Hornberger, B. Brezger, A. Zeilinger, and M. Arndt, Nature (London) **427**, 711 (2004).

[10] B. Julsgaard, A. Kozhekin, E. S. Polzik, Nature (London) **413**, 400 (2001).

[11] A. J. Berkley, H. Xu, R. C. Ramos, M. A. Gubrud, F. W. Strauch, P. R. Johnson, J. R. Anderson, A. J. Dragt, C. J. Lobb, F. C. Wellstood, Science **300**, 1548 (2003).

[12] P. F. Cohadon, A. Heidmann, and M. Pinard, Phys. Rev. Lett. **83**, 3174 (1999).

[13] M. D. LaHaye, O. Buu, B. Camarota, and K. C. Schwab, Science **304**, 74 (2004).

[14] C. H. Metzger and K. Karrai, Nature (London), **432**, 1002 (2004).

[15] A. Naik, O. Buu, M. D. LaHaye, A. D. Armour, A. A. Clerk, M. P. Blencowe, and K. C. Schwab, Nature **443**, 193 (2006).

[16] O. Arcizet, P.-F. Cohadon, T. Briant, M. Pinard, and A. Heidmann, J. M. Mackowski, C. Michel, L. Pinard, O. Francais, L. Rousseau, Phys. Rev. Lett. **97**, 133601 (2006).

[17] S. Gigan, H. Böhm, M. Paternostro, F. Blaser, G. Langer, J. Hertzberg, K. Schwab, D. Bäuerle, M. Aspelmeyer, and A. Zeilinger, Nature (London) **444**, 67 (2006).

[18] O. Arcizet, P.-F. Cohadon, T. Briant, M. Pinard, and A. Heidmann, Nature (London) **444**, 71 (2006).

[19] D. Kleckner and D. Bouwmeester, Nature (London) **444**, 75 (2006).

[20] A. Schliesser, P. Del'Haye, N. Nooshi, K. J. Vahala, and T. J. Kippenberg, Phys. Rev. Lett. **97** 243905 (2006).

[21] T. Corbitt, Y. Chen, E. Innerhofer, H. Müller-Ebhardt, D. Ottaway, H. Rehbein, D. Sigg, S. Whitcomb, C. Wipf, and N. Mavalvala, Phys. Rev. Lett. **98**, 150802 (2007); T. Corbitt, C. Wipf, T. Bodiya, D. Ottaway, D. Sigg, N. Smith, S. Whitcomb, and N. Mavalvala, Phys. Rev. Lett. **99**, 160801 (2007).

[22] M. Poggio, C. L. Degen, H. J. Mamin, and D. Rugar, Phys. Rev. Lett. **99**, 017201 (2007).

[23] K. R. Brown, J. Britton, R. J. Epstein, J. Chiaverini, D. Leibfried, and D. J. Wineland, Phys. Rev. Lett. **99**, 137205 (2007).

[24] S. Groblacher, S. Gigan, H. R. Boehm, A. Zeilinger, M. Aspelmeyer, Europhys. Lett. **81**, 54003 (2008).

[25] A. Schliesser, R. Rivière, G. Anetsberger, O. Arcizet, and T. J. Kippenberg, Nat. Phys. **4**, 415 (2008).

[26] J. D. Thompson, B. M. Zwickl, A. M. Jayich, F. Marquardt, S. M. Girvin, and J. G. E. Harris, Nature (London) **452**, 72 (2008).

[27] C. A. Regal, J. D. Teufel, K. W. Lehnert, Nat. Phys. **4**, 555 (2008).

[28] A. Vinante *et al.*, Phys. Rev. Lett. **101**, 033601 (2008).

[29] J. D. Teufel, J. W. Harlow, C. A. Regal, and K. W. Lehnert, Phys. Rev. Lett. **101**, 197203 (2008).

[30] A. Schliesser, O. Arcizet, R. Rivière, T. J. Kippenberg, arXiv:0901.1456v1 [quant-ph].

[31] S. Groeblacher, J. B. Hertzberg, M. R. Vanner, S. Gigan, K. C. Schwab, M. Aspelmeyer, arXiv:0901.1801v1 [quant-ph].

[32] S. Mancini, D. Vitali, and P. Tombesi, Phys. Rev. Lett. **80**, 688 (1998).

[33] V. B. Braginsky, S. E. Strigin, and S. P. Vyatchanin, Phys. Lett. A **287**, 331 (2001).

[34] J.-M. Courty, A. Heidmann, and M. Pinard, Eur. Phys. J. D **17**, 399 (2001).

[35] D. Vitali, S. Mancini, and P Tombesi, Phys. Rev. A **64**, 051401(R) (2001).

[36] D. Vitali, S. Mancini, L. Ribichini, and P. Tombesi, Phys. Rev. A **65** 063803 (2002); **69**, 029901(E) (2004); J. Opt. Soc. Am. B **20**, 1054 (2003).

[37] I. Wilson-Rae, P. Zoller, and A. Imamoglu, Phys. Rev. Lett. **92**, 075507 (2004).

[38] I. Martin, A. Shnirman, L. Tian, and P. Zoller, Phys. Rev. B **69**, 125339 (2004)

[39] F. Marquardt, J. P. Chen, A. A. Clerk, and S. M. Girvin, Phys. Rev. Lett. **99**, 093902 (2007).

[40] I. Wilson-Rae, N. Nooshi, W. Zwerger, and T. J. Kippenberg, Phys. Rev. Lett. **99**, 093901 (2007).

[41] C. Genes, D. Vitali, P. Tombesi, S. Gigan, and M. Aspelmeyer, Phys. Rev. A **77**, 033804 (2008).

[42] A. Dantan, C. Genes, D. Vitali, and M. Pinard, Phys. Rev. A **77**, 011804(R) (2008).

[43] J. M. Dobrindt, I. Wilson-Rae, and T. J. Kippenberg, Phys. Rev. Lett. **101**, 263602 (2008).

[44] K. W. Murch, K. L. Moore, S. Gupta, and D. M. Stamper-Kurn, Nature Phys. **4**, 561 (2008); F. Brennecke, S. Ritter, T. Donner, T. Esslinger, Science **322**, 235 (2008).

[45] M. P. Blencowe and M. N. Wybourne, Physica B **280**, 555 (2000).

[46] P. Rabl, A. Shnirman and P. Zoller, Phys. Rev. B **70**, 205304 (2004); X. Zhou and A. Mizel, Phys. Rev. Lett. **97**, 267201 (2006); K. Jacobs, Phys. Rev. Lett. **99**, 117203 (2007); W. Y. Huo, G. L. Long, Appl. Phys. Lett. **92**, 133102 (2008).

[47] R. Ruskov, K. Schwab and A. N. Korotkov, Phys. Rev. B **71**, 235407 (2005); A. A. Clerk, F. Marquardt and K. Jacobs, New J. Phys. **10**, 095010 (2008); M. J. Woolley, A. C. Doherty, G. J. Milburn, K. C. Schwab, Phys. Rev. A **78**, 062303 (2008).

[48] J. S. Bell, Physics (N.Y.) **1**, 195 (1964).

[49] S. Mancini, V. Giovannetti, D. Vitali and P. Tombesi, Phys. Rev. Lett. **88**, 120401 (2002).

[50] A. D. Armour, M. P. Blencowe, K. C. Schwab, Phys. Rev. Lett. **88**, 148301 (2002).

[51] J. Eisert, M. B. Plenio, S. Bose, J. Hartley, Phys. Rev. Lett. **93**, 190402 (2004).

[52] X. Zou and W. Mathis, Phys. Lett. A **324**, 484-488 (2004).

[53] A. N. Cleland and M. R. Geller, Phys. Rev. Lett. **93**, 070501 (2004).

[54] L. Tian and P. Zoller, Phys. Rev. Lett. **93**, 266403 (2004).

[55] L. Tian, Phys. Rev. B **72**, 195411 (2005).

[56] F. Xue, Y. X. Liu, C. P. Sun, and F. Nori, Phys. Rev. B **76**, 064305 (2007).

[57] A. K. Ringsmuth and G. J. Milburn, J. Mod. Opt. **54** 2223 (2007).

[58] D. Vitali, P. Tombesi, M. J. Woolley, A. C. Doherty, G. J. Milburn, Phys. Rev. A **76**, 042336 (2007).

[59] J. Zhang, K. Peng, and S. L. Braunstein, Phys. Rev. A **68**, 013808 (2003).

[60] M. Pinard, A. Dantan, D. Vitali, O. Arcizet, T. Briant, A. Heidmann, Europhys. Lett. **72**, 747 (2005).

[61] M. Paternostro, D. Vitali, S. Gigan, M. S. Kim, C. Brukner, J. Eisert, and M. Aspelmeyer, Phys. Rev. Lett. **99**, 250401 (2007).

[62] M. Bhattacharya and P. Meystre, Phys. Rev. Lett. **99**, 073601 (2007); Phys. Rev. Lett. **99**, 153603 (2007); M. Bhattacharya, H. Uys, and P. Meystre, Phys. Rev. A **77**, 033819 (2008).

[63] C. Wipf, T. Corbitt, Y. Chen, N. Mavalvala, New J. Phys. **10**, 095017 (2008).

[64] D. Vitali, S. Gigan, A. Ferreira, H. R. Böhm, P. Tombesi, A. Guerreiro, V. Vedral, A. Zeilinger, and M. Aspelmeyer, Phys. Rev. Lett. **98**, 030405 (2007).

[65] D. Vitali, S. Mancini, and P. Tombesi, J. Phys. A: Math. Theor. **40**, 8055 (2007).

[66] S. Mancini, D. Vitali, and P. Tombesi, Phys. Rev. Lett. **90**, 137901 (2003); S. Pirandola, S. Mancini, D. Vitali, and P. Tombesi, Phys. Rev. A **68**, 062317 (2003).

[67] S. Pirandola S. Mancini, D. Vitali, and P. Tombesi, J. Mod. Opt. **51**, 901 (2004).

[68] S. Pirandola, D. Vitali, P. Tombesi, and S. Lloyd, Phys. Rev. Lett. **97**, 150403 (2006).

[69] C. Genes, A. Mari, P. Tombesi, and D. Vitali, Phys. Rev. A **78**, 032316 (2008).

[70] C. Genes, D. Vitali, and P. Tombesi, Phys. Rev. A **77**, 050307(R) (2008).

[71] H. Ian, Z. R. Gong, Yu-xi Liu, C. P. Sun, and F. Nori, Phys. Rev. A **78**, 013824 (2008); K. Hammerer, M. Aspelmeyer, E. S. Polzik, and P. Zoller, Phys. Rev. Lett. **102**, 020501 (2009).

[72] T. J. Kippenberg, H. Rokhsari, T. Carmon, A. Scherer, and K. J. Vahala,, Phys. Rev. Lett. **95** 033901 (2005).

[73] M. Pinard, Y. Hadjar, and A. Heidmann, Eur. Phys. J. D **7**, 107 (1999).

[74] C. Genes, D. Vitali, and P. Tombesi, New J. Phys. **10**, 095009 (2008).

[75] V. Giovannetti, D. Vitali, Phys. Rev. A **63**, 023812 (2001).

[76] C. K. Law, Phys. Rev. A **51**, 2537 (1995).

[77] L. Landau, E. Lifshitz, *Statistical Physics* (Pergamon, New York, 1958).

[78] R. Benguria, and M. Kac, Phys. Rev. Lett, **46**, 1 (1981).

[79] C. W. Gardiner and P. Zoller, *Quantum Noise*, (Springer, Berlin, 2000).

[80] S. Mancini and P. Tombesi, Phys. Rev. A **49**, 4055 (1994).

[81] I. S. Gradshteyn and I. M. Ryzhik, *Table of Integrals, Series and Products*, Academic Press, Orlando, 1980, pag. 1119.

[82] F. Marquardt, J. G. Harris, and S. M. Girvin , Phys. Rev. Lett. 96, 103901 (2006).

[83] A. Dorsel, J.D. McCullen, P. Meystre, E. Vignes, and H. Walther, Phys. Rev. Lett. **51**, 1550 (1983); A. Gozzini, F. Maccarone, F. Mango, I. Longo, and S. Barbarino, J. Opt. Soc. Am. B **2**, 1841 (1985).

[84] J. Eisert, Ph.D. thesis, University of Potsdam, 2001; G. Vidal and R. F. Werner, Phys. Rev. A **65**, 032314 (2002); G. Adesso *et al.*, Phys. Rev. A **70**, 022318 (2004).

[85] R. Simon, Phys. Rev. Lett. **84**, 2726 (2000).

[86] M. M. Wolf, G. Giedke and J. I. Cirac, Phys. Rev. Lett. **96**, 080502 (2006).

[87] S. Stenholm, Rev. Mod. Phys. **58**, 699 (1986).

[88] D. Leibfried, R. Blatt, C. Monroe, and D. Wineland, Rev. Mod. Phys. **75**, 281 (2003).

[89] G.M. DAriano, M. G. A. Paris, M. F. Sacchi, Adv. Imag. Electr. Phys. **128**, 205 (2003).

[90] C. W. Gardiner and P. Zoller, *Quantum Noise*, (Springer, Berlin, 2000), p. 71.

[91] M. S. Kim, W. Son, V. Bužek, and P. L. Knight, Phys. Rev. A **65**, 032323 (2002).

[92] S. J. van Enk and C. A. Fuchs, Phys. Rev. Lett. **88**, 027902 (2002); D. Vitali, P. Canizares, J. Eschner, and G. Morigi, New J. Phys. **10**, 033025 (2008).

[93] V. Giovannetti, S. Mancini, and P. Tombesi, Europhys. Lett. **54**, 559 (2001).

[94] S. Giannini, S. Mancini, and P. Tombesi, Quant. Inf. Comp. **3**, 265-279 (2003).

[95] S. Pirandola, S. Mancini, D. Vitali, P. Tombesi, J. Opt. B: Quantum Semiclass. Opt. **5**, S523-S529 (2003).

[96] G. Morigi, J. Eschner, S. Mancini, and D. Vitali, Phys. Rev. Lett. **96**, 023601 (2006); Phys. Rev. A **73**, 033822 (2006); D. Vitali, G. Morigi, and J. Eschner, Phys. Rev. A **74**, 053814 (2006).

[97] G. Giedke, B. Kraus, M. Lewenstein, and J. I. Cirac, Phys. Rev. A **64**, 052303 (2001).

[98] T. Holstein, and H. Primakoff, Phys. Rev. **58**, 1098 (1940).

[99] J. Sherson, H. Krauter, R. K. Olsson, B. Julsgaard, K. Hammerer, I. Cirac, E. S. Polzik, Nature **443**, 557 (2006).

Chapter 4

Gently modulating optomechanical systems

Gently Modulating Optomechanical Systems

A. Mari and J. Eisert

Institute of Physics and Astronomy, University of Potsdam, D-14476 Potsdam, Germany
Institute for Advanced Study Berlin, D-14193 Berlin, Germany

(Received 4 July 2009; published 18 November 2009)

We introduce a framework of optomechanical systems that are driven with a mildly amplitude-modulated light field, but that are not subject to classical feedback or squeezed input light. We find that in such a system one can achieve large degrees of squeezing of a mechanical micromirror—signifying quantum properties of optomechanical systems—without the need of any feedback and control, and within parameters reasonable in experimental settings. Entanglement dynamics is shown of states following classical quasiperiodic orbits in their first moments. We discuss the complex time dependence of the modes of a cavity-light field and a mechanical mode in phase space. Such settings give rise to certifiable quantum properties within experimental conditions feasible with present technology.

DOI: 10.1103/PhysRevLett.103.213603 PACS numbers: 42.50.Dv, 03.67.Bg, 42.50.Lc, 85.85.+j

Periodically driven quantum systems exhibit a rich behavior and display nonequilibrium properties that are absent in their static counterparts. By appropriately exploiting time-periodic driving, strongly correlated Bose-Hubbard-type models can be dynamically driven to quantum phase transitions [1], systems can be dynamically decoupled from their environments to avoid decoherence in quantum information science [2], and quite intriguing dynamics of Rydberg atoms strongly driven by microwaves [3] can arise. It has also been muted that such time-dependent settings may give rise to entanglement dynamics in oscillating molecules [4]. A framework of such periodically driven systems is provided by the theory of linear differential equations with periodic coefficients or inhomogeneities, including Floquet's theorem [5].

In this Letter, we aim at transferring such ideas to describe a new and in fact quite simple regime of optomechanical systems, of micromirrors as part of a Fabry-Perot cavity [6–9], and also to one of the settings [10–14] that are the most promising candidates in the race of exploring certifiable quantum effects involving macroscopic mechanical modes. This is an instance of a regime of driving with mildly amplitude-modulated light. We find that in this regime, high degrees of squeezing below the vacuum noise level can be reached, signifying genuine quantum dynamics. More specifically, in contrast to earlier descriptions of optomechanical systems with a periodic time dependence in some aspect of the description, we will not rely on classical feedback based on processing of measurement-outcomes—a promising idea in its own right in a continuous-measurement perspective [15,16]—or resort to driving with squeezed light. Instead, we will consider the plain setting of a time-periodic amplitude modulation of an input light. The picture developed here, based in the theory of differential equations, gives rise to a framework of describing such situations. We find that large degrees of squeezing can be reached (complementing other very recent nonperiodic approaches based on cavity-assisted squeezing using an additional squeezed light beam [17]). It is the practical appeal of this work that such quantum signatures can be reached without the necessity of any feedback, no driving with additional fields, and no squeezed light input (the scheme by far outperforms direct driving with a single squeezed light mode): in a nutshell, one has to simply gently shake the system in time with the right frequency to have the mechanical and optical modes rotate appropriately around each other, reminiscent of parametric amplification, and to so directly certify quantum features of such a system.

Time-dependent picture of system.—Before we discuss the actual time dependence of the driven system, setting the stage, we start our description with the familiar Hamiltonian of a system of a Fabry-Perot cavity of length L and finesse F being formed on one end by a moving micromirror,

$$H = \hbar\omega_c a^\dagger a + \frac{1}{2}\hbar\omega_m(p^2+q^2) - \hbar G_0 a^\dagger a q + i\hbar\sum_{n=-\infty}^{\infty}(E_n e^{-i(\omega_0+n\Omega)t}a^\dagger - E_n^* e^{i(\omega_0+n\Omega)t}a). \quad (1)$$

Here, ω_m is the frequency of the mechanical mode with quadratures q and p satisfying the usual commutation relations of canonical coordinates, while the bosonic operators a and $a^\dagger$ are associated to the cavity mode with frequency ω_c and decay rate $\kappa = \pi c/(2FL)$. $G_0 = \sqrt{\hbar/(m\omega_m)}\omega_c/L$ is the coupling coefficient of the radiation pressure, where m is the effective mass of the mode of the mirror being used. Importantly, we allow for any periodically modulated driving at this point, which can be expressed in such a Fourier series, where $\Omega = 2\pi/\tau$ and $\tau > 0$ is the modulation period. The main frequency of the driving field is ω_0 while the modulation coefficients $\{E_n\}$ are related to the power of the associated sidebands $\{P_n\}$ by $|E_n|^2 = 2\kappa P_n/(\hbar\omega_0)$. The resulting dynamics under this Hamiltonian together with an unavoidable coupling of the

mechanical mode to a thermal reservoir and cavity losses gives rise to the quantum Langevin equation in the reference frame rotating with frequency ω_0, $\dot{q} = \omega_m p$, and

$$\begin{aligned} \dot{p} &= -\omega_m q - \gamma_m p + G_0 a^\dagger a + \xi, \\ \dot{a} &= -(\kappa + i\Delta_0)a + iG_0 aq \\ &\quad + \sum_{n=-\infty}^{\infty} E_n e^{-in\Omega t} + \sqrt{2\kappa}a^{\mathrm{in}}, \end{aligned} \tag{2}$$

where $\Delta_0 = \omega_c - \omega_0$ is the cavity detuning. γ_m is here an effective damping rate related to the oscillator quality factor Q by $\gamma_m = \omega_m/Q$. The mechanical (ξ) and the optical (a^{in}) noise operators have zero mean values and are characterized by their auto correlation functions which, in the Markovian approximation, are $\langle \xi(t)\xi(t') + \xi(t')\xi(t)\rangle/2 = \gamma_m(2\bar{n}+1)\delta(t-t')$ and $\langle a^{\mathrm{in}}(t)a^{\mathrm{in}\dagger}(t')\rangle = \delta(t-t')$, where $\bar{n} = [\exp(\frac{\hbar\omega_m}{k_B T}) - 1]^{-1}$ is the mean thermal phonon number. Here, we have implicitly assumed that such an effective damping model holds [18], which is a reasonable assumption in a wide range of parameters including the current experimental regime.

Semiclassical phase space orbits.—Our strategy of a solution will be as follows: we will first investigate the classical phase space orbits of the first moments of quadratures. We then consider the quantum fluctuations around the asymptotic quasiperiodic orbits, by implementing the usual linearization of the Heisenberg equations of motion [11,12] (excluding the very weak driving regime). Exploiting results from the theory of linear differential equations with periodic coefficients, we can then proceed to describe the dynamics of fluctuations and find an analytical solution for the second moments.

If we average the Langevin equations (2), assuming $\langle a^\dagger a\rangle \simeq |\langle a\rangle|^2$, $\langle aq\rangle \simeq \langle a\rangle\langle q\rangle$ (true in the semiclassical driving regime we are interested in), we have a nonlinear differential equation for the first moments. Far away from instabilities and multistabilities, a power series ansatz in the coupling G_0 $\langle O\rangle(t) = \sum_{j=0}^{\infty} O_j(t) G_0^j$ is justified, where $O = a,\ p,\ q$. If we substitute this expression into the averaged Langevin equation (2), we get a set of recursive differential equation for the variables $O_j(.)$. The only two nonlinear terms in Eq. (2) are both proportional to G_0, therefore, for each j, the differential equation for the set of unknown variables $O_j(.)$ is a *linear* inhomogeneous system with constant coefficients and τ-periodic driving. Then, after an exponentially decaying initial transient (of the order of $1/\gamma_m$), the asymptotic solutions O_j will have the same periodicity of the modulation [5], justifying the Fourier expansion

$$\langle O\rangle(t) = \sum_{j=0}^{\infty}\sum_{n=-\infty}^{\infty} O_{n,j} e^{in\Omega t} G_0^j. \tag{3}$$

Substituting this in Eq. (2), we find the following recursive formulas for the time independent coefficients $O_{n,j}$, $q_{n,0} = p_{n,0} = 0$, $a_{n,0} = E_{-n}/(\kappa + i(\Delta_0 + n\Omega))$, corresponding to the zero coupling $G_0 = 0$, while for $j \geq 1$, we have

$$\begin{aligned} q_{n,j} &= \omega_m \sum_{k=0}^{j-1}\sum_{m=-\infty}^{\infty} \frac{a^*_{m,k} a_{n+m,j-k-1}}{\omega_m^2 - n\Omega^2 + i\gamma_m n\Omega}, \\ p_{n,j} &= \frac{in\Omega}{\omega_m} q_{n,j}, \quad a_{n,j} = i\sum_{k=0}^{j-1}\sum_{m=-\infty}^{\infty} \frac{a_{m,k} q_{n-m,j-k-1}}{\kappa + i(\Delta_0 + n\Omega)}, \end{aligned} \tag{4}$$

Within the typical parameter space, considering only the first terms in the double expansion (3), corresponding to the first sidebands, leads to a good analytical approximation of the classical periodic orbits, see Fig. 1. On physical grounds, this is expected to be a good approximation, since $G_0 \ll \omega_m$, and because high sidebands fall outside the cavity bandwidth, $n\Omega > 2\kappa$. What is more, the decay behavior of E_n related to the smoothness of the drive inherits a good approximation in terms of few sidebands.

Quantum fluctuations around the classical orbits.—We will now turn to the actual quantum dynamics taking first moments into account separately when writing any operator as $O(t) = \langle O\rangle(t) + \delta O(t)$. The frame will hence be provided by the motion of the first moments. In this reference frame, as long as $|\langle a\rangle| \gg 1$, the usual linearization approximation to (2) can be implemented. In what follows, we will also use the quadratures $\delta x = (\delta a + \delta a^\dagger)/\sqrt{2}$ and $\delta y = -i(\delta a - \delta a^\dagger)/\sqrt{2}$, and the analogous input noise quadratures x^{in} and y^{in}. For the vector of all quadratures we will write $u = (\delta q, \delta p, \delta x, \delta y)^T$, with $n = (0, \xi, \sqrt{2\kappa}x^{\mathrm{in}}, \sqrt{2\kappa}y^{\mathrm{in}})^T$ being the noise vector [11,18]. Then the time-dependent inhomogeneous equations of motion arise as $\dot{u}(t) = A(t)u(t) + n(t)$, with

$$A(t) = \begin{bmatrix} 0 & \omega_m & 0 & 0 \\ -\omega_m & -\gamma_m & G_x(t) & G_y(t) \\ -G_y(t) & 0 & -\kappa & \Delta(t) \\ G_x(t) & 0 & -\Delta(t) & -\kappa \end{bmatrix}, \tag{5}$$

where the real $A(t)$ contains the time-modulated coupling constants and the detuning as $G(t) = G_x(t) + iG_y(t)$,

$$G(t) = \sqrt{2}\langle a(t)\rangle G_0, \qquad \Delta(t) = \Delta_0 - G_0\langle q(t)\rangle. \tag{6}$$

From now on we will consider quasiperiodic orbits only, so the long-time dynamics following the initial one, when the first moments follow a motion that is τ periodic. Then, A is

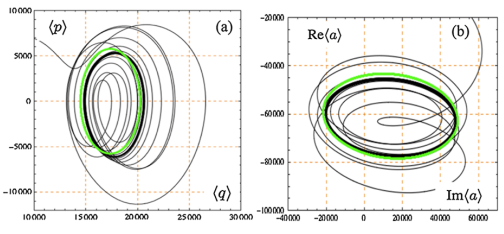

FIG. 1 (color online). Phase space trajectories of the first moments of the mirror (a) and light (b) modes. Numerical simulations for $t \in [0, 50\tau]$ (black) and analytical approximations of the asymptotic orbits (green or light gray).

τ periodic, and hence $A(t) = A(t+\tau) = \sum_{n=-\infty}^{\infty} A_n e^{i\Omega n t}$. In turn, if all eigenvalues of $A(.)$ having negative real parts for all $t \in [0, \tau]$ is a sufficient condition for stability. From the Markovian assumption, we have $\langle n_i(t) n_j(t') + n_j(t') n_i(t)\rangle/2 = \delta(t-t') D_{i,j}$, where $D = \mathrm{diag}(0, \gamma_m(2\bar{n}+1), \kappa, \kappa)$. The formal solution of Eq. (5) is [5]

$$u(t) = U(t, t_0) u(t_0) + \int_{t_0}^{t} U(t, s) n(s) ds, \tag{7}$$

where $U(t, t_0)$ is the principal matrix solution of the homogeneous system satisfying $\dot{U}(t, t_0) = A(t) U(t, t_0)$ and $U(t_0, t_0) = \mathbb{1}$. From Eqs. (5) and (7), we have as an equation of motion of the covariance matrix (CM)

$$\dot{V}(t) = A(t) V(t) + V(t) A^T(t) + D. \tag{8}$$

Here, the CM $V(.)$ is the 4×4 matrix with components $V_{i,j} = \langle u_i u_j + u_j u_i\rangle/2$, collecting the second moments of the quadratures. This is again an inhomogeneous differential equation for the second moments which can readily be solved using quadrature methods, providing numerical solutions that will be used to test and justify analytical approximate results in important regimes. Moreover, now the coefficients and not the inhomogeneity are τ periodic, $A(t) = A(t+\tau)$. Again, we can invoke results from the theory of linear differential equations to Eq. (8) [5]: we find that in the long time limit, the CM is periodic and can be written as $V(t) = \sum_n V_n e^{in\Omega t}$. An analytical solution for $V(.)$, is most convenient in the Fourier domain, $\tilde{f}(\omega) = \int_{-\infty}^{+\infty} e^{-i\omega t} f(t) dt$, giving rise to

$$-i\omega \tilde{u}(\omega) + \sum_{n=-\infty}^{\infty} A_n \tilde{u}(\omega - n\Omega) = -\tilde{n}(\omega). \tag{9}$$

If $A_{n\neq 0} = 0$, corresponding to no modulation, we are in the usual regime where the spectra are centered around $\pm\omega_m$ for the mechanical oscillator and around $\pm\Delta$ for the optical mode. The modulation introduces sidebands shifted by $\pm n\Omega$. If the modulation is weak, only the first two sidebands at $\pm\Omega$ significantly contribute. For strong modulation also further sidebands play a role: Disregarding higher sidebands means truncating the summation to $\pm N$ [valid if $u(\omega \pm N\Omega) \simeq 0$]. Then Eq. (9) can be written as $\bar{A}(\omega)\bar{u}(\omega) = \bar{n}(\omega)$, where $\bar{u}^T(\omega) = (\tilde{u}^T(\omega - N\Omega), \ldots, \tilde{u}^T(\omega), \ldots, \tilde{u}^T(\omega + N\Omega))$ and $\bar{n}^T(\omega) = (\tilde{n}^T(\omega - N\Omega), \ldots, \tilde{n}^T(\omega), \ldots, \tilde{n}^T(\omega + N\Omega))$ are $4 \times (2N+1)$ vectors, while, in terms of 4×4 blocks,

$$\bar{A}(\omega) = \begin{bmatrix} B_{-N} & A_{-1} & A_{-2} & \cdots & A_{-2N} \\ A_1 & B_{-(N-1)} & A_{-1} & & \vdots \\ A_2 & A_1 & B_{-(N-2)} & & \\ \vdots & & & & \\ \vdots & & & & \vdots \\ A_{2N} & \cdots & & A_1 & B_N \end{bmatrix} \tag{10}$$

with $B_k = A_0 - i(\omega + k\Omega)$.

We have that $\phi_{i,j}(\omega, \omega') = \langle \bar{n}_i(\omega)\bar{n}_j^*(\omega') + \bar{n}_j^*(\omega')\bar{n}_i(\omega)\rangle/2 = \sum_{n=-2N}^{2N} \delta(\omega - \omega' - n\Omega) D_n$, where $D_0 = \mathrm{diag}(D, D, \ldots, D)$, then D_1 is the matrix that has D on all first right off diagonal blocks, D_2 on the second off diagonals, with D_n analogously defined, and $D_{-n} = D_n^T$. We now define the two frequency correlation function as $\bar{V}_{i,j}(\omega, \omega') = \langle \bar{u}_i(\omega)\bar{u}_j^*(\omega') + \bar{u}_j^*(\omega')\bar{u}_i(\omega)\rangle/2$. We have $\bar{V}(\omega, \omega') = \bar{A}^{-1}(\omega)\phi(\omega, \omega')[\bar{A}^{-1}(\omega')]^\dagger$. We are interested only on the central 4×4 block of $\bar{V}$ which we call $\tilde{V}(\omega, \omega') = [\bar{V}(\omega, \omega')]_4$. We find $\tilde{V}(\omega, \omega') = \sum_{n=-2N}^{2N} \tilde{V}_n(\omega)\delta(\omega - \omega' - n\Omega)$, where $\tilde{V}_n(\omega) = [\bar{A}^{-1}(\omega) D_n [\bar{A}^{-1}(\omega - n\Omega)]^\dagger]_4$. This means that the driving modulation correlates different frequencies, but only if they are separated by a multiple of the modulation frequency Ω. By inverse Fourier transforms we recover the time-periodic expression for the CM, where the components V_n are given by the integral of their noise spectra, i.e.,

$$V_n = \frac{1}{2\pi} \int_{-\infty}^{+\infty} \tilde{V}_n(\omega) d\omega. \tag{11}$$

Squeezing and entanglement modulation.—We will now see that the mild amplitude-modulated driving in the cooling regime is exactly the tool that we need in order to arrive at strong degrees of squeezing, in the absence of feedback or squeezed light. We will apply the previous general theory to setting of an optomechanical system that is experimentally feasible with present technology. In fact, all values that we assume have been achieved already and reported on in publications with the exception of assuming a relatively good mechanical Q factor. The reasonable set of experimental parameters [9] that we assume is $L = 25$ mm, $F = 1.4 \times 10^4$, $\omega_m = 2\pi$ MHz, $Q = 10^6$, $m = 150$ ng, $T = 0.1$ K. We then consider the—in the meantime well known—self-cooling regime [7] in which a cavity eigenmode is driven with a red detuned laser $\Delta_0 \simeq \omega_m$ (with wavelength $\lambda = 1064$ nm), but we also add a small sinusoidal modulation to the input amplitude with a frequency $\Omega = 2\omega_m$, so twice the mechanical frequency. To be more precise we choose the power of the carrier component equal to $P_0 = 10$ mW, and the power of the two modulation sidebands equal to $P_{\pm 1} = 2$ mW.

We approximate the asymptotic classical mean values in Eq. (3) by truncating the series only to the first terms with indexes $j = 0, \ldots, 3$ and $n = -1, 0, 1$. Figure 1 shows that, after less than 50 modulation periods, the first moments reach quasiperiodic orbits which are well approximated by our analytical results.

In order to calculate the variances of the quantum fluctuations around the classical orbits, we truncate the sum in Eq. (9) to $N = 2$ and we apply all the previous theory to find the covariance matrix V. In Fig. 2 we compare two regimes: with or without ($P_{\pm 1} = 0$) modulation (computed analytically and numerically). We see that the modulation of the driving field causes the emergence of significant true quantum squeezing below the Heisenberg limit of the mechanical oscillator state and also the interesting phenomenon of light-mirror entanglement oscillations. This dynamics reminds of the effect of parametric amplification [13,16], as if the spring constant of the mechanical motion

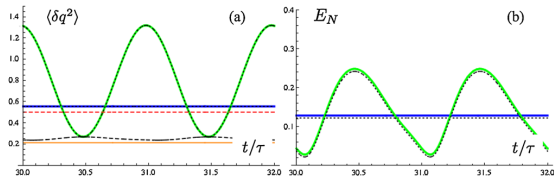

FIG. 2 (color online). (a) Variance of the mirror position and (b) light-mirror entanglement E_N as functions of time. In both (a) and (b) the nonmodulated driving regime (blue or dark gray), the modulated driving regime (green or gray), and the numerical solutions (black dash-dotted) are plotted. (a) also shows the standard quantum limit (red or gray dashed) at $1/2$, the minimum eigenvalue of the mirror covariance matrix (black dashed) and its analytical estimation (12) in the RWA (orange or light gray).

was varied in time with just twice the frequency of the mechanical motion, leading to the squeezing of the mechanical mode. For related ideas of reservoir engineering, making use of bichromatic microwave coupling to a charge qubit of nanomechanical oscillators, see Refs. [20]. Here, it is a more complicated joint dynamics of the cavity field and the mechanical mode—where the dynamics of the first and the second moments can be separated—which for large times yet yields a similar effect. Indeed, this squeezing can directly be measured when considering the output power spectrum, following Ref. [21], and no additional laser light is needed for the readout, giving hence rise to a relatively simple certification of the squeezing. Entanglement here refers to genuine quantum correlations between the mirror and the field mode, as being quantified by the logarithmic negativity defined as $E_N(\rho) = \log\|\rho^\Gamma\|_1$, essentially the trace norm of the partial transpose [22,23]. The minimum eigenvalue of the mirror covariance matrix—the logarithm thereof typically referred to as single mode squeezing parameter—is almost constant and this means that the state is always squeezed but that the squeezing direction continuously rotates in phase space with the same period of the modulation. Calling this rotating squeezed quadrature δx_R, a rough estimate of its variance can be calculated in the rotating-wave approximation (RWA, compare, e.g., Ref. [24]),

$$\langle \delta x_R^2 \rangle = \frac{1}{2} + \bar{n} - \frac{2\kappa(G_0 - G_{-1})(G_0\bar{n} + G_{-1}(\bar{n}+1))}{(\gamma_m + 2\kappa)(G_0^2 - G_{-1}^2 + 2\gamma_m\kappa)}, \quad (12)$$

with $\{G_n\}$ being defined as $G(t) = \sum_{n=-\infty}^{\infty} G_n e^{in\Omega t}$.

Conclusions and outlook.—In this Letter we have introduced a framework of describing periodically amplitude-modulated optomechanical systems. Interestingly, such a surprisingly simple setting feasible with present technology [9] leads to a setting showing high degrees of mechanical squeezing, with no feedback or additional fields needed. We hope that such ideas contribute to experimental studies finally certifying first quantum mechanical effects in macroscopic mechanical systems, constituting quite an intriguing perspective.

This work has been supported by the EU (MINOS, COMPAS, QAP), and EURYI.

[1] A. Eckardt, C. Weiss, and M. Holthaus, Phys. Rev. Lett. **95**, 260404 (2005); E. Kierig *et al.*, arXiv:0803.1406.
[2] L. Viola, E. Knill, and S. Lloyd, Phys. Rev. Lett. **82**, 2417 (1999); S. Kohler, T. Dittrich, and P. Hänggi, Phys. Rev. E **55**, 300 (1997).
[3] H. P. Breuer, M. Holthaus, and K. Dietz, Z. Phys. D **8**, 349 (1988).
[4] H. J. Briegel and S. Popescu, arXiv:0806.4552.
[5] G. Teschl, Ordinary Differential Equations and Dynamical Systems, http://www.mat.univie.ac.at/~gerald.
[6] C. H. Metzker and K. Karrai, Nature (London) **432**, 1002 (2004).
[7] S. Gigan *et al.*, Nature (London) **444**, 67 (2006); O. Arcizet *et al.*, *ibid.* **444**, 71 (2006); D. Kleckner and D. Bouwmeester, *ibid.* **444**, 75 (2006).
[8] A. Schliesser *et al.*, Nature Phys. **4**, 415 (2008).
[9] S. Groeblacher *et al.*, Nature Phys. **5**, 485 (2009).
[10] M. D. LaHaye, O. Buu, B. Camarota, and K. C. Schwab, Science **304**, 74 (2004).
[11] D. Vitali, S. Mancini, L. Ribichini, and P. Tombesi, Phys. Rev. A **65**, 063803 (2002).
[12] A. Ferreira, A. Guerreiro, and V. Vedral, Phys. Rev. Lett. **96**, 060407 (2006); D. Vitali *et al.*, *ibid.* **98**, 030405 (2007); M. Paternostro *et al.*, *ibid.* **99**, 250401 (2007); C. Genes *et al.*, Phys. Rev. A **78**, 032316 (2008).
[13] F. Marquardt and S. M. Girvin, Physics **2**, 40 (2009).
[14] J. Eisert, M. B. Plenio, S. Bose, and J. Hartley, Phys. Rev. Lett. **93**, 190402 (2004); I. Wilson-Rae, P. Zoller, and A. Imamoglu, *ibid.* **92**, 075507 (2004).
[15] A. A. Clerk, F. Marquardt, and K. Jacobs, New J. Phys. **10**, 095010 (2008).
[16] M. J. Woolley, A. C. Doherty, G. J. Milburn, and K. C. Schwab, Phys. Rev. A **78**, 062303 (2008); A. Serafini, A. Retzker, and M. B. Plenio, arXiv:0904.4258.
[17] K. Jaehne *et al.*, Phys. Rev. A **79**, 063819 (2009).
[18] Pedantically speaking—unless one is in the limit of very weak coupling compared to the free evolution (''quantum optical Markovian limit'')—this requires an Ohmic spectral density of the heat bath and a high temperature (''quantum Brownian motion limit''), see, e.g., Ref. [19]. For the considered system, the Markovian approximation is typically a very good one.
[19] H. P. Breuer and F. Petruccione, *Open Quantum Systems* (Cambridge University Press, Cambridge, U.K., 2002).
[20] P. Rabl, A. Shnirman, and P. Zoller, Phys. Rev. B **70**, 205304 (2004); J. F. Poyatos, J. I. Cirac, and P. Zoller, Phys. Rev. Lett. **77**, 4728 (1996).
[21] M. Paternostro *et al.*, New J. Phys. **8**, 107 (2006).
[22] J. Eisert, Ph.D. thesis Potsdam, 2001; G. Vidal and R. F. Werner, Phys. Rev. A **65**, 032314 (2002); M. B. Plenio, Phys. Rev. Lett. **95**, 090503 (2005).
[23] $E_N(\rho) = -\sum_{i=1}^{2} \min(0, \log(c_i))$, where $c_{1,2}$ are the eigenvalues of $2|V^{1/2} i S V^{1/2}|$, where S is the 4×4-matrix with $S_{1,2} = S_{4,3} = 1$, $S_{2,1} = S_{3,4} = -1$ and zero otherwise.
[24] D. Vitali *et al.*, Phys. Rev. A **76**, 042336 (2007).

Chapter 5

Directly estimating non-classicality

Directly Estimating Nonclassicality

A. Mari,[1] K. Kieling,[1] B. Melholt Nielsen,[2] E. S. Polzik,[2] and J. Eisert[1,3]
[1]*Institute of Physics and Astronomy, University of Potsdam, 14476 Potsdam, Germany*
[2]*Niels Bohr Institute, Danish National Research Foundation Center for Quantum Optics, DK-2100 Copenhagen, Denmark*
[3]*Institute for Advanced Study Berlin, 14193 Berlin, Germany*
(Received 1 June 2010; published 7 January 2011)

We establish a method of directly measuring and estimating nonclassicality—operationally defined in terms of the distinguishability of a given state from one with a positive Wigner function. It allows us to certify nonclassicality, based on possibly much fewer measurement settings than necessary for obtaining complete tomographic knowledge, and is at the same time equipped with a full certificate. We find that even from measuring two conjugate variables alone, one may infer the nonclassicality of quantum mechanical modes. This method also provides a practical tool to eventually certify such features in mechanical degrees of freedom in opto-mechanics. The proof of the result is based on Bochner's theorem characterizing classical and quantum characteristic functions and on semidefinite programming. In this joint theoretical-experimental work we present data from experimental optical Fock state preparation.

DOI: 10.1103/PhysRevLett.106.010403 PACS numbers: 03.65.Ta, 03.67.Mn, 42.50.−p

Where is the "boundary" between classical and quantum physics? Unsurprisingly, acknowledging that quantum mechanics is the fundamental theory from which classical properties should emerge in one way or the other, instances of this question have a long tradition in physics. Possibly the most conservative and stringent criterion for nonclassicality of a quantum state of bosonic modes is that the Wigner function—the closest analogue to a classical probability distribution in phase space—is negative, and can hence no longer be interpreted as a classical probability distribution [1–3]. From this, negativity of other quasiprobability distributions, familiar in quantum optics, such as the P-function [1,4] follows. In fact, a lot of experimental progress was made in recent years on preparing quantum states of light modes that exhibit such nonclassical features, when preparing number states, photon subtracted states, or small Schrödinger cat states [5–8]. At the same time, a lot of effort is being made of driving mesoscopic mechanical degrees of freedom into quantum states eventually showing such nonclassical features [9]. All this poses the question, needless to say, of how to best and most accurately certify and measure such features.

In this work, (i) we demonstrate that, quite remarkably, nonclassicality in the above sense can be detected from mere measurements of two conjugate variables. For a single mode, this amounts to position and momentum detection, as can be routinely done by homodyne measurements in optical systems. (ii) What is more, using such data (or also data that are tomographically complete) one can get a direct and rigorous lower bound to the probability of operationally distinguishing this quantum state from one with a positive Wigner function—including a full certificate. Such a bound uses information from possibly much fewer measurement settings than needed for full quantum state tomography. At the same time, quantum state tomography using Radon transforms for quantum modes is overburdened with problems of ill-conditioning.

The method introduced here, in contrast, is a *direct method* giving rise to a *certified bound* which arises from conditions all classical and quantum characteristic functions have to satisfy as being grasped by the classical and quantum Bochner's theorem [10]. Hence, we ask: "What is the smallest nonclassicality consistent with the data"? Intuitively speaking, the proof circles around the deviation of a quantum characteristic function as the Fourier transform of the Wigner function from a classical characteristic function. This deviation can then be formulated in terms of a semidefinite program—so a well-behaved convex optimization problem—giving rise to certifiable bounds. The same technique can also be applied to notions of entanglement, and indeed, the rigor applied here reminds of applying quantitative entanglement witnesses [11,12]. What is more, the criterion evaluation procedure is efficient. At present, such techniques should be most applicable to systems in quantum optics, and we indeed implement this idea in a quantum optical experiment preparing a field mode in a nonclassical state. Yet, they should be expected to be helpful when eventually certifying that a mesoscopic mechanical system has eventually reached quantum properties [9], where "having achieved a nonclassical state", with careful error analysis, will constitute an important benchmark.

Measure of nonclassicality.—Nonclassicality is most reasonably quantified in terms of the possibility of operationally distinguishing a given state from a state that one would conceive as being classical. That is to say, the meaningful notion of distinguishing a state from a classical one is as follows.

Definition 1: (Measure of nonclassicality).—Nonclassicality is measured in terms of the operational

distinguishability of a given state from a state having a positive Wigner function,

$$\eta(\rho) = \min_{\omega \in \mathcal{C}} \|\rho - \omega\|_1, \tag{1}$$

where $\mathcal{C}$ denotes the set of all quantum states with positive Wigner function and $\|\cdot\|_1$ is the trace norm.

This measure is indeed *the* operational definition of a nonclassical state—as long as one accepts the negativity of the Wigner function as the figure of merit of nonclassicality. Needless to say, the operational distinguishability with respect to other properties would also be quantified by trace-distances, and naturally several quantities of such a type can be found in the literature (see, e.g., Ref. [13] for a similar notion of nonclassicality and Ref. [14] for a related idea to quantify entanglement). It has the following natural properties: It is (a) invariant under passive and active linear transformations, and (b) nonincreasing under Gaussian channels, and in fact under any operation that cannot map a state with a positive Wigner function onto a negative one. The latter property is an immediate consequence of the trace norm being contractive under completely positive maps. Moreover, since Gaussian states are positive this measure of negativity gives a direct lower bound to the non-Gaussianity of the same state—quantified again in terms of the distance to the set of Gaussian states. Such a notion of non-Gaussianity (see, e.g., Refs. [15]), just as the negativity of the Wigner function as such, can be viewed as quantifying a *resource* in quantum information processing. Similar to entanglement measures being monotones under local operations with classical communication, these measures are monotones under Gaussian operations. What is more, the negativity of the Wigner function may also be seen as quantifying the potential of violating a Bell inequality based on homodyning [16].

Characteristic functions and Bochner's theorems.—We consider physical systems of n bosonic modes, associated with canonical coordinates $R = (q_1, \ldots, q_n, p_1, \ldots, p_n)$, of "position" and "momentum", or some quadratures. In the center of the analysis will be quantum characteristic functions [2,17], for n modes as a function χ: $\mathbb{R}^{2n} \to \mathbb{C}$ defined as $\chi(\xi) = \mathrm{tr}[\rho D(\xi)]$, $D(\xi) = e^{i\xi\cdot\sigma R}$, so as the expectation value of the *Weyl* or *displacement operator* [18]. This characteristic function is nothing but the Fourier transform of the familiar *Wigner function* W: $\mathbb{R}^{2n} \to \mathbb{R}$,

$$W(z) = \frac{1}{(2\pi)^{2n}} \int \chi(\xi) e^{-i\xi\cdot\sigma z} d\xi. \tag{2}$$

A key tool will be the notion of λ *positivity* [10]:

Definition 2: (λ positivity).—A function χ: $\mathbb{R}^{2n} \to \mathbb{C}$ is λ-positive definite for $\lambda \in \mathbb{R}$ if for every $m \in \mathbb{N}$ and for every set of real vectors $T = (\xi_1, \xi_2, \ldots, \xi_m)$ the $m \times m$ matrix $M^{(\lambda)}(\chi, T)$ is non-negative, $M^{(\lambda)}(\chi, T) \geq 0$, with

$$(M^{(\lambda)}(\chi, T))_{k,l} = \chi(\xi_k - \xi_l) e^{i\lambda \xi_k \cdot \sigma \xi_l/2}. \tag{3}$$

Conversely, one can ask for a classification of all functions that can be characteristic functions of a quantum state, or some classical probability distribution. Such a characterization is captured in the quantum and classical Bochner's theorems [10]. (i) Every characteristic function of a quantum state must be *1-positive definite*. (ii) Every characteristic function of a quantum state with a positive Wigner function must be at the same time *1-positive definite* and *0-positive definite*.

Measuring nonclassicality.—Data are naturally taken as slices in phase space, resulting from measurements of some linear combinations of the canonical coordinates, as they would be obtained from a phase sensitive measurement such as homodyning in quantum optics. One collects data from measuring observables $u_k R$ for some collection of $u_k \in \mathbb{R}^{2n}$ with $\|u_k\| = 1$. E.g., in the simplest case of one mode one could measure only q and p or, if the state is phase invariant, one could average over all the possible directions. With repeated measurements one can estimate the associated probability distributions P_k: $\mathbb{R} \to \mathbb{R}^+$, related to slices of the characteristic functions by a simple Fourier transform $\int P_k(s) e^{i\omega s} ds = \chi(\omega \sigma u_k)$. Actually, in a real experiment one can build only a statistical histogram rather than a continuous probability distribution. Hence, measurements of values of the characteristic function must be equipped with error bars [19]

$$\delta(\omega) = |\omega| h + n/\sqrt{N}, \tag{4}$$

where $2h$ is the width of each bin of the histogram, N is the number of measurements and n is the number of standard deviations that one should consider depending on the desired level of confidence [20]. This kind of measurements can be performed also in *optomechanical systems* where a particular quadrature of a mechanical oscillator can be measured *a posteriori* by appropriately homodyning a light mode coupled to it [21]. A different idea has recently been proposed for directly pointwise measuring the characteristic function of a mechanical mode coupled to a two-level system [22]. In both cases the method that we are going to describe can be easily applied. Restricted measurements also arise in the context of *bright beams* [23], where Mach-Zehnder interferometers have to replace homodyning. In the study of states of *macroscopic atomic ensembles* [24] similar issues arise.

Bounds to the nonclassicality from convex optimization.—We assume that we estimate the values of the characteristic function $\chi(\bar{\xi}_j) \simeq c_j$ for a given set of points $\bar{\xi}_j$, $j = 1, \ldots, p$, within a given error $\delta_j \geq 0$ [20], so that $|\chi(\bar{\xi}_j) - c_j| \leq \delta_j$. Now pick a set of suitable test vectors $T = (\xi_1, \ldots, \xi_m)$, the differences $\xi_j - \xi_k$ of which at least contain the data points $\bar{\xi}_1, \ldots, \bar{\xi}_p$. Based on this, we define the following convex optimization problem as over χ, x,

$$\text{minimize } x, \tag{5}$$

such that

$$|\mathrm{Re}(\chi(\bar{\xi}_j)) - \mathrm{Re}(c_j)| \leq \delta_j, \qquad j = 1, \ldots, p, \tag{6}$$

$$|\mathrm{Im}(\chi(\bar{\xi}_j)) - \mathrm{Im}(c_j)| \leq \delta_j, \qquad j = 1, \ldots, p, \tag{7}$$

$$M^{(0)}(\chi, T) + xm\mathbb{1} \geq 0, \qquad M^{(1)}(\chi, T) \geq 0, \tag{8}$$

where $M^{(0)}(\chi, T)$ and $M^{(1)}(\chi, T)$ are the Hermitian matrices (3) associated with the λ positivity, based on the test points $\xi_1, \ldots, \xi_m$ as being specified in Def. 2. The minimization is in principle performed over all functions χ: $\mathbb{R}^{2n} \to \mathbb{C}$ such that $\chi(-\xi) = \chi(\xi)^*$, where $\chi(\bar{\xi}_l)$ is constrained by the data and $M^{(0/1)}(\chi, T)$ depend on the test points. Since we take only a finite number of points of χ, yet, the above problem gives rise to a *semidefinite problem (SDP)* [25]. This can be efficiently solved with standard numerical algorithms. By means of the notion of Lagrange duality, one readily gives *analytical certifiable bounds*: Every solution for the dual problem will give a proven lower bound to the primal problem [25], and hence a lower bound to the measure of nonclassicality itself. The entire procedure hence amounts to an arbitrarily tight *convex relaxation* of the Bochner constraints. We can now formulate the main result: Eq. (5) gives rise to a lower bound for the nonclassicality: Given the data (and errors), one can find good and robust bounds to the smallest nonclassicality that is consistent with the data.

Theorem 3: (Estimating nonclassicality).—The output x' of Eq. (5) is a lower bound for the nonclassicality, $\eta(\rho) \geq x'$. The proof proceeds by constructing a *witness operator*

$$F = \frac{1}{m} \sum_{k,l=1}^{m} v_k^* v_l D(\xi_k - \xi_l), \tag{9}$$

where $\xi_1, \ldots, \xi_m \in \mathbb{R}^{2n}$ are the test vectors from Bochner's theorem used in the SDP and v is the normalized eigenvector associated with the minimum eigenvalue of $M^{(0)}(\chi', T)$, where χ' is the optimal solution for χ. For a given state ρ, this operator F has the following properties:

(i) $F = F^\dagger$, (ii) $|\mathrm{tr}(F\omega)| \leq 1$ for all quantum states ω. (iii) $\mathrm{tr}(F\omega) \geq 0$ for all quantum states $\omega \in \mathcal{C}$. (4) If $x' \geq 0$ is the optimal solution, then $\mathrm{tr}(F\rho) \leq -x'$. These properties will be proven to be valid in the Supplementary material [19], involving some technicalities. They suggest that F is actually a *witness observable* able to distinguish a subset of nonclassical states from the convex set of classical states. Formally, from the variational definition of the trace norm, we have the lower bound to be shown [26],

$$\eta(\rho) = \min_{\omega \in \mathcal{C}} \|\rho - \omega\|_1 \geq \min_{\omega \in \mathcal{C}} \mathrm{tr}(\omega F) - \mathrm{tr}(F\rho) \geq x'. \tag{10}$$

An example: Schrödinger cat state.—As an example we consider a quantum superposition of two coherent states, so $|\psi\rangle \sim (|\alpha\rangle + |-\alpha\rangle)$ with $\alpha = 1.77$. We assume to measure only the probability distributions of position and momentum [Fig. 1(a)]: $P_1(q) = |\langle q|\psi\rangle|^2$ and $P_2(p) = |\langle p|\psi\rangle|^2$, i.e., the data is collected from a mere *pair of canonical operators*. This amount of information is of course not sufficient for tomographically reconstructing the state since it corresponds to just two orthogonal slices of the characteristic function. In order to define the SDP we consider a 25×25 square lattice centered at the origin of the domain of the characteristic function, optimizing over the values of χ at the lattice points. Position and momentum measurements define the constraints (6) and (7) for only two slices of the lattice (assuming an error of $\delta_j = 10^{-3}$ for each point). We generate 100 random test vectors and we construct the associated λ-positivity constraints (8). The output of the SDP is $x' \simeq 0.05 > 0$ which is a certified lower bound for the nonclassicality of the state.

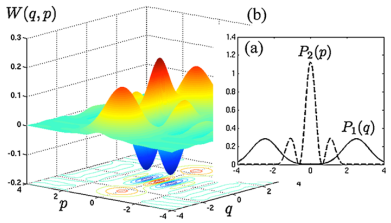

FIG. 1 (color online). (a) Position and momentum distributions for an exact cat state. (b) Wigner function based on the SDP.

Experimentally detecting nonclassicality.—Finally, to certify the functioning of the idea in a quantum optical context, we apply our method to experimental data. We consider data from a heralded single-photon source based on parametric down-conversion (cf. Ref. [8]). Here, an optical parametric oscillator (OPO), pumped continuous-wave and far below threshold, delivers the down-converted photon pair at frequencies $\omega_\pm$. The pair is separated using an optical cavity; the transmitted photon ω_- is frequency filtered by additional cavities before impinging an avalanche photodiode (APD) giving the heralding event for homodyne measurement of the reflected twin photon ω_+. On every event the homodyne current is sampled around the heralding time and postprocessed into one quadrature value using an appropriate mode function [27]. In total, quadrature values from 180 000 events are accumulated [Fig. 2(a)]. Data is phase randomized meaning that we can use the same probability distribution for every phase space direction, the phase being unavailable in the experiment. Since our nonclassicality measure is convex, averaging over phase space directions is an operation which can only decrease the negativity of the state. This means

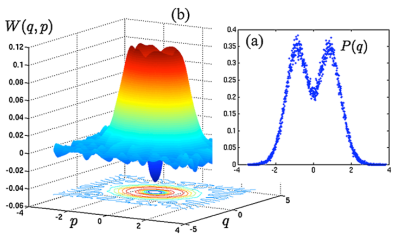

FIG. 2 (color online). (a) Raw measured quadrature distribution from the experiment. (b) Wigner function based on the output of the SDP.

that a lower bound to the nonclassicality of the phase randomized state will be valid for the original state.

In order to apply our algorithm we use the measured data to constrain all the points of the characteristic function on a 37×37 lattice. Error bars are estimated using Eq. (6) with $n = 5$ standard deviations. This means that the probability that all the points of the lattice lie inside the error bars is larger than 99.9%. The lower bound for the nonclassicality coming out from the SDP (200 random test vectors) is $x' \simeq 0.0028$, meaning that the Wigner function of the state cannot be a positive probability distribution. The Wigner function reconstructed from the optimal solution of the SDP [Fig. 2(b)] is clearly negative even if we asked for the most positive one consistent with measured data.

Extensions of this approach.—Needless to say, this approach can be extended in several ways. Indeed, the method can readily be generalized to produce lower bounds for *entanglement measures* [11] in the multimode setting. Also, this idea can be applied to the situation when not slices are measured, but *points in phase space*, such as when using a detector-atom that is simultaneously coupled to a cantilever [22]. It also constitutes an interesting perspective to apply the present ideas to certify deviations from *stabilizer states* for spin systems (as those states having a positive discrete Wigner function [28]).

Summary.—We have introduced a method to directly measure the nonclassicality of quantum mechanical modes, requiring less information than tomographic knowledge, but at the same time in a certified fashion. These ideas are further advocating the paradigm of ''learning much from little''—getting much certified information from few measurements—complementing methods of *witnessing entanglement* [11,12], ideas of *compressed sensing* [29] or *matrix-product based* [30] approaches to quantum state tomography, *detector tomography* [31], or the direct estimation of *Markovianity* [32].

This work has been supported by the EU (MINOS, COMPAS, QESSENCE), and the EURYI.

[1] E. P. Wigner, Phys. Rev. **40**, 749 (1932); R. J. Glauber, Phys. Rev. **131**, 2766 (1963).
[2] U. Leonhardt, *Measuring the Quantum State of Light* (Cambridge University Press, Cambridge, England, 1997); W. Schleich, *Quantum Optics in Phase Space* (Wiley VCH, Weinheim, 2000).
[3] A. Kenfack and K. Zyczkowski, J. Opt. B **6**, 396 (2004); K. Kim, J. Kim, and J. Bae, Phys. Rev. A **82**, 042105 (2010).
[4] J. Sperling and W. Vogel, arXiv:1004.1944; Th. Richter and W. Vogel, Phys. Rev. Lett. **89**, 283601 (2002); D. T. Smithey, M. Beck, M. G. Raymer, and A. Faridani, *ibid.* **70**, 1244 (1993); T. Kiesel *et al.*, Phys. Rev. A **79**, 022122 (2009).
[5] G. Nogues *et al.*, Phys. Rev. A **62**, 054101 (2000).
[6] A. Ourjoumtsev, R. Tualle-Brouri, J. Laurat, and P. Grangier, Science **312**, 83 (2006); A. Ourjoumtsev, A. Dantan, R. Tualle-Brouri, and P. Grangier, Phys. Rev. Lett. **98**, 030502 (2007).
[7] J. S. Neergaard-Nielsen *et al.*, Phys. Rev. Lett. **97**, 083604 (2006).
[8] J. S. Neergaard-Nielsen *et al.*, Opt. Express **15**, 7940 (2007); B. Melholt Nielsen, J. S. Neergaard-Nielsen, and E. S. Polzik, Opt. Lett. **34**, 3872 (2009).
[9] S. Gigan *et al.*, Nature (London) **444**, 67 (2006); O. Arcizet *et al.*, Nature (London) **444**, 71 (2006); D. Kleckner and D. Bouwmeester, Nature (London) **444**, 75 (2006).
[10] C. D. Cushen and R. L. Hudson, J. Appl. Probab. **8**, 454 (1971); S. Bochner, Math. Ann. **108**, 378 (1933).
[11] J. Eisert, F. G. S. L. Brandão, and K. M. R. Audenaert, New J. Phys. **9**, 46 (2007); K. M. R. Audenaert and M. B. Plenio, *ibid.* **8**, 266 (2006); O. Gühne, M. Reimpell, and R. F. Werner, Phys. Rev. Lett. **98**, 110502 (2007).
[12] B. M. Terhal, Phys. Lett. A **271**, 319 (2000); O. Gühne and G. Toth, Phys. Rep. **474**, 1 (2009).
[13] M. Hillery, Phys. Rev. A **35**, 725 (1987).
[14] V. Vedral and M. B. Plenio, Phys. Rev. A **57**, 1619 (1998).
[15] F. DellAnno, S. De Siena, and F. Illuminati, Phys. Rev. A **81**, 012333 (2010); M. Ohliger, K. Kieling, and J. Eisert, *ibid.* **82**, 042336 (2010).
[16] R. Garcia-Patron *et al.*, Phys. Rev. Lett. **93**, 130409 (2004).
[17] J. Eisert and M. B. Plenio, Int. J. Quantum. Inform. **1**, 479 (2003); S. L. Braunstein and P. van Loock, Rev. Mod. Phys. **77**, 513 (2005).
[18] $$\sigma = \begin{bmatrix} 0 & \mathbb{1}_n \\ -\mathbb{1}_n & 0 \end{bmatrix}$$ reflects the commutation relations.
[19] See supplementary material at http://link.aps.org/supplemental/10.1103/PhysRevLett.106.010403.
[20] Since the error follows a Gaussian distribution, the probability P_{out} that the actual value of the characteristic function lies outside the error bar is never zero but it is exponentially suppressed for increasing n. E.g., for $n = 3$ one has $P_{\text{out}} < 2.7 \times 10^{-3}$, for $n = 5$ one has $P_{\text{out}} < 6 \times 10^{-7}$, etc..
[21] H. Miao *et al.*, Phys. Rev. A **81**, 012114 (2010).
[22] S. Singh and P. Meystre, Phys. Rev. A **81**, 041804(R) (2010).
[23] Ch. Silberhorn *et al.*, Phys. Rev. Lett. **86**, 4267 (2001).
[24] T. Fernholz *et al.*, Phys. Rev. Lett. **101**, 073601 (2008); B. Brask *et al.*, Phys. Rev. Lett. **105**, 160501 (2010).
[25] S. Boyd and L. Vandenberghe, *Convex Optimization* (Cambridge University Press, Cambridge, 2004).
[26] Note that the approach followed here is general enough to accommodate further additional constraints, as long as they can be captured in terms of an SDP based on values of the characteristic function. In this way, one can also add specific figures of merit related to actual target states.
[27] A. E. B. Nielsen and K. Mølmer, Phys. Rev. A **75**, 023806 (2007).
[28] D. Gross, J. Math. Phys. (N.Y.) **47**, 122107 (2006).
[29] D. Gross, Y.-K. Liu, S. T. Flammia, S. Becker, and J. Eisert, Phys. Rev. Lett. **105**, 150401 (2010); A. Shabani, R. L. Kosut, and H. Rabitz, arXiv:0910.5498.
[30] S. T. Flammia, D. Gross, S. D. Bartlett, and R. Somma, arXiv:1002.3839; M. Cramer and M. B. Plenio, arXiv:1002.3780.
[31] J. S. Lundeen *et al.*, Nature Phys. **5**, 27 (2008).
[32] M. M. Wolf, J. Eisert, T. S. Cubitt, and J. I. Cirac, Phys. Rev. Lett. **101**, 150402 (2008).

Chapter 6

Cooling by heating

Cooling by heating

A. Mari[1,2] and J. Eisert[1,2]

[1]*Institute for Physics and Astronomy, University of Potsdam, 14476 Potsdam, Germany*
[2]*Dahlem Center for Complex Quantum Systems, Freie Universität Berlin, 14195 Berlin, Germany*

We introduce the idea of actually cooling quantum systems by means of incoherent thermal light, hence giving rise to a counter-intuitive mechanism of "cooling by heating". In this effect, the mere incoherent occupation of a quantum mechanical mode serves as a trigger to enhance the coupling between other modes. This notion of effectively rendering states more coherent by driving with incoherent thermal quantum noise is applied here to the opto-mechanical setting, where this effect occurs most naturally. We discuss two ways of describing this situation, one of them making use of stochastic sampling of Gaussian quantum states with respect to stationary classical stochastic processes. The potential of experimentally demonstrating this counter-intuitive effect in opto-mechanical systems with present technology is sketched.

Cooling in quantum physics is usually achieved in just the same way as it occurs in classical physics or in common everyday situations: One brings a given system into contact with a colder bath. Coherent driving of quantum systems can effectively achieve the same aim, most prominently in instances of laser cooling of ions or in its opto-mechanical variant, cooling mechanical degrees of freedom using the radiation pressure of light. The coherence then serves a purpose of, in a way, rendering the state of the system "more quantum". In any case, in these situations, the interacting body should first and foremost be cold or coherent.

In this work, we introduce a paradigm in which thermal hot states of light can be used to significantly cool down a quantum system. To be specific, we will focus on an opto-mechanical [1–6] implementation of this idea: This type of system seems to be an ideal candidate to demonstrate this effect with present technology; it should however be clear that several other natural instances can well be conceived. Intuitively speaking, it is demonstrated that due to the driving with thermal noise, the interaction of other modes can be effectively enhanced, giving rise to a "transistor-like" effect [8]. We flesh out this effect at hand of two approaches following different approximation schemes. The first approach is essentially a weak coupling master equation, while the second approach makes use of stochastic samplings with respect to colored classical stochastic processes [10], which constitutes an interesting and practical tool to study such quantum optical systems of several modes in its own right.

The observation made here adds to the insight that appears to be appreciated only fairly recently, in that quantum noise does not necessarily only give rise to heating, decoherence, and dissipation, providing in particular a challenge in applications in quantum metrology and in quantum information science. When suitably used, quantum noise can also assist in processes thought to be necessarily of coherent nature, in noise-driven quantum phase transitions [11], quantum criticality [12], in entanglement distillation [13] or in quantum computation [14]. It turns out that thermal noise, when appropriately used, can also assist in cooling. Alas, this counter-intuitive effect is not in contradiction to the laws of thermodynamics, as is plausible when viewing this set-up as a thermal machine or heat engine [15] operating in the quantum regime.

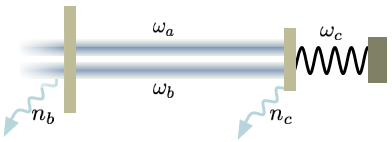

FIG. 1. The opto-mechanical setup primarily being considered in this work, involving two optical modes and a mechanical one.

The system under consideration. We consider a system of two optical modes at frequencies ω_a and ω_b, respectively, that are coupled to a mechanical degree of freedom at frequency ω_c. The Hamiltonian of the entire system is assumed to be well-approximated by $H = H_0 + H_1$, where the free part is given by $H_0 = \hbar\omega_a a^\dagger a + \hbar\omega_b b^\dagger b + \hbar\omega_c c^\dagger c$, and the interaction can be cast into the form

$$H_1 = \hbar g(a+b)^\dagger(a+b)(c+c^\dagger). \tag{1}$$

It is convenient to move to a rotating interaction picture with respect to $\hbar\omega_b(a^\dagger a + b^\dagger b)$. The radiation pressure interaction is invariant under this transformation, while H_0 simplifies to

$$H_0' = \hbar\Delta a^\dagger a + \hbar\omega_c c^\dagger c,$$

where $\Delta = \omega_a - \omega_b$. For most of what follows, the frequencies are chosen such that $\Delta = \omega_c$, as we will see is the optimal resonance for cooling the mechanical resonator. This can be realized by tuning the mechanical degree of freedom or the cavity mode splitting. In fact, this is exactly the setting proposed in Ref. [16] as a feasible three-mode optoacoustic interaction, in an idea that can be traced back to studies of parametric oscillatory instability in Fabry-Perot interferometers [17]. Similarly, with systems of high-finesse optical cavities coupled to thin semi-transparent membranes [18], of double-microdisk whispering-gallery resonators [19] or of opto-mechanical crystals [20] such a situation can be achieved. Surely numerous other architectures are well conceivable.

In addition to this coherent dynamics, the system is assumed to undergo natural damping and decoherence – un-

avoidable in the opto-mechanical context. The quantum master equation governing the dynamics of the entire system embodying the two optical modes and the mechanical degree of freedom is given by

$$\dot{\rho} = \mathcal{L}\rho = -\frac{i}{\hbar}[H,\rho] + (\mathcal{L}_a + \mathcal{L}_b + \mathcal{L}_c)\rho, \tag{2}$$

with the generators being defined by $\mathcal{L}_a = \kappa D_a$ and

$$\mathcal{L}_b = (1+n_b)\kappa D_b + n_b \kappa D_{b^\dagger}, \tag{3}$$
$$\mathcal{L}_c = (1+n_c)\gamma D_c + n_c \gamma D_{c^\dagger}, \tag{4}$$

making use of the notation for a generator in Lindblad form

$$D_x(\rho) = 2x\rho x^\dagger - \{x^\dagger x, \rho\}. \tag{5}$$

Here, we allow the optical bath of mode b to be in a Gibbs or thermal state having an arbitrary temperature.

This type of damping reflects the plausible mechanism of loss. For the mechanical motion, we are primarily interested in the regime where $\omega_m \gg \gamma$, such that the damping mechanism of quantum Brownian motion based on some spectral density is virtually indistinguishable from the quantum optical Markovian damping as for an optical mode [21]. For that reason, for coherence of presentation, the same type of dissipative dynamics has been chosen for the optical and mechanical modes.

We will now discuss this given situation in two different pictures. The first one is a weak coupling approach leading to approximate analytical expressions. The second one involves sampling over colored classical stochastic processes. These methods are further discussed in the range of their validity in the EPAPS, where they are also compared with exact diagonalization methods for small photon numbers [23].

Description 1: Weak coupling approximation as an analytical approach. In this approach, a picture is developed grasping the physical situation well for small couplings g. In addition to the actual physical baths of the three modes a, b, and c giving rise to dissipative dynamics, we also consider mode b as a further external "bath" and derive an effective master equation for modes a and c only. This is a good approximation if the back action on mode b is negligible and up to second order in the coupling constant g. Having this picture in mind, the Liouvillian in Eq. (2) can be decomposed as $\mathcal{L} = \mathcal{L}_{\rm sys} + \mathcal{L}_{\rm int} + \mathcal{L}_{\rm bath}$, where $\mathcal{L}_{\rm bath} = \mathcal{L}_b$ and

$$\mathcal{L}_{\rm sys} = -\frac{i}{\hbar}[H_0', \cdot] + \mathcal{L}_a + \mathcal{L}_c, \quad \mathcal{L}_{\rm int} = -\frac{i}{\hbar}[H_1, \cdot]. \tag{6}$$

Using projection operators techniques [22], one can derive a master equation for the reduced system $\rho_{a,c} = {\rm tr}_b[\rho]$

$$\dot{\rho}_{a,c}(t) = \mathcal{L}_{\rm sys}\rho_{a,c}(t) + {\rm tr}_b \mathcal{L}_{\rm int} \int_0^\infty ds\, e^{\mathcal{L}_r s} \mathcal{L}_{\rm int} \rho_{a,c}(t-s) \otimes \rho_b.$$

Here $\mathcal{L}_r = \mathcal{L}_{\rm sys} + \mathcal{L}_{\rm bath}$. Making use of the explicit expression (6) for $\mathcal{L}_{\rm int}$, we have

$$\dot{\rho}_{a,c}(t) = \mathcal{L}_{\rm sys}\rho_{a,c}(t) - \frac{1}{\hbar^2}{\rm tr}_b[H_1, \int_0^\infty ds e^{\mathcal{L}_r s}[H_1, \rho_{a,c}(t-s)\otimes\rho_b]] \tag{7}$$

In what follows, we will make a sequential approximation of the interaction Hamiltonian H_1 and the damping mechanism. In order to be as transparent as possible, we mark each of the steps with a roman letter.

Eq. (7) – up to second order expansion in the coupling g, which constitutes the first approximation step (a) – can also be written as

$$\dot{\rho}_{a,c}(t) = \mathcal{L}_{\rm sys}\rho_{a,c}(t) - \frac{1}{\hbar^2}{\rm tr}_b[H_1, \int_0^\infty ds[e^{\mathcal{L}_r^\dagger s}(H_1), \rho_{a,c}(t)\otimes\rho_b]], \tag{8}$$

where $\mathcal{L}_r^\dagger$ acts only on the Hamiltonian H_1, corresponding to a "dissipative interaction picture" with respect to $\mathcal{L}_r$.

We start from Eq. (1) and (b) neglect the term proportional to $a^\dagger a$ because we assume mode a to be weakly perturbed from its ground state. In contrast, we allow the physical optical bath of mode b to have an arbitrary temperature and therefore we cannot neglect the term proportional to $b^\dagger b$. We rewrite the approximated H_1 as

$$H_1' = \hbar g(a^\dagger b + b^\dagger a + \delta)(c + c^\dagger), \tag{9}$$

where the operator $\delta = b^\dagger b - n_b$ represents the intensity fluctuations of mode b. In order to have vanishing first moments with respect to mode b, the mean force proportional to $\langle b^\dagger b\rangle$ has been subtracted, which is responsible of merely shifting the resonator equilibrium position. Since $\omega_a - \omega_b = \omega_c$, the (c) rotating wave approximation (RWA) of Eq. (9) is

$$H_1'' = \hbar g(a^\dagger b c + a b^\dagger c^\dagger) + \hbar g \delta(c + c^\dagger). \tag{10}$$

As will be explained later in more details, the first term of the Hamiltonian is responsible for the *cooling* of the mechanical resonator, while the second term corresponds to an additional *heating* noise.

In order to compute the partial trace in Eq. (8), we need the two-time correlation functions of the thermal light in mode b,

$$\langle b e^{\mathcal{L}_r^\dagger s} b^\dagger\rangle = e^{-\kappa s} n_b, \quad \langle \delta e^{\mathcal{L}_r^\dagger s}\delta\rangle = e^{-2\kappa s}(n_b^2 + n_b). \tag{11}$$

The exponential functions in Eqs. (11) determine the time scale of the integral kernel in Eq. (8), which will be of the order of κ^{-1}. Within this time scale (d) we can neglect the effect of the mechanical reservoir ($\gamma \ll \kappa$), and the action of the map $e^{\mathcal{L}_r^\dagger s}$ on the system operators will be

$$e^{\mathcal{L}_r^\dagger s} a = e^{-(\kappa + i\Delta)s} a = e^{-(\kappa + i\omega_c)s} a,$$
$$e^{\mathcal{L}_r^\dagger s} c = e^{-(\gamma + i\omega_c)s} c \simeq e^{-i\omega_c s} c.$$

We can finally perform the integral in Eq. (8), and since all the odd moments of ρ_b vanish, the *cooling* and *heating* terms in Eq. (10) generate two independent contributions to the master equation, respectively

$$\mathcal{L}_{\rm cool} = \frac{g^2}{2\kappa}\left((1+n_b)D_{ac^\dagger} + n_b D_{a^\dagger c}\right), \tag{12}$$

$$\mathcal{L}_{\rm heat} = \frac{2\kappa g^2(n_b^2 + n_b)}{4\kappa^2 + \omega_c^2}\left(D_{c^\dagger} + D_c\right), \tag{13}$$

where in calculating $\mathcal{L}_{\rm heat}$ we (e) kept only the counter-rotating terms. The effect of $\mathcal{L}_{\rm heat}$ is simply a renormalization of the mean occupation number of the mechanical bath

$$n_c \mapsto \tilde{n}_c = n_c + \frac{2\kappa g^2(n_b^2+n_b)}{\gamma(4\kappa^2+\omega_c^2)},$$

always increasing, as expected, the effective temperature of the environment. Denoting with $\tilde{\mathcal{L}}_{\rm sys}$ the corresponding renormalized Liouvillian, the master equation can be written as

$$\dot{\rho}_{a,c} = (\tilde{\mathcal{L}}_{\rm sys} + \mathcal{L}_{\rm cool})\rho_{a,c}. \tag{14}$$

With respect to Eq. (2), Eq. (14) can be numerically solved with much less computational resources but we have to remind ourselves that this approach is valid only within the RWA and for weak coupling: $\gamma, g \ll \omega_c$. Another advantage of Eq. (14) is that the corresponding adjoint equations for the number operators $n_a = a^\dagger a$ and $n_c = b^\dagger b$ are closed with respect to these operators, that is

$$\dot{n}_a = -2\kappa n_a - \frac{g^2}{\kappa}\left((n_b+1)n_a - n_b n_c - n_a n_c\right),$$
$$\dot{n}_c = -2\kappa n_c - \frac{g^2}{\kappa}\left(n_b n_c - (n_b+1)n_a - n_a n_c\right) + 2\gamma\tilde{n}_c.$$

Assuming (f) that the factorization property $\langle n_a n_c\rangle \simeq \langle n_a\rangle\langle n_c\rangle$ holds – which is essentially a mean-field approach which is expected to be good in case of small correlations, or, again as assumed, for small values of g – we can find analytical expressions for the steady state expectation values:

$$\langle n_c\rangle = \frac{\tilde{n}_c-\eta}{2} + \left(\frac{(\tilde{n}_c+\eta)^2}{4} - \frac{\kappa n_b \tilde{n}_c}{\gamma}\right)^{1/2},$$
$$\langle n_a\rangle = \frac{(\tilde{n}_c - \langle n_c\rangle)\gamma}{\kappa},$$

where $\eta = 1 + n_b(1+\kappa/\gamma) + 2\kappa^2/g^2$.

Description 2: Sampling with respect to colored stationary classical stochastic processes. In this approach, we start from the exact dynamics Eq. (2) but treat mode b as a classical thermal field and neglect any feed-back from the resonator. We substitute the bosonic operator with a complex amplitude $b(t) \mapsto \beta_t$, giving rise to a semi-classical picture. The parameter β_t can be described as a classical stochastic process defined by the stochastic differential equation (SDE)

$$d\beta_t = -\kappa\beta_t dt + \sqrt{\kappa n_b}(dW^{(x)} + i dW^{(y)}), \tag{15}$$

with independent Wiener increments [10] obeying the Itō rules $dW^{(a)}dW^{(b)} = \delta_{a,b}dt$, $dW^{(a,b)}dt = 0$. The dynamics of the remaining modes a and c instead, can be efficiently treated quantum mechanically; this is true, since for every single realization of the process (15), the evolution defines a Gaussian completely positive map and therefore the corresponding Gaussian state $\rho_{a,c}^{(\beta_t)}(t) = \mathcal{E}_t^{(\beta_t)}(\rho_{a,c})$ can be described entirely in terms of first and second moments. The actual quantum state of the system will in general not be exactly Gaussian, it can nonetheless be simulated by sampling over many Gaussian states associated with different realizations of β_t: Only the respective weight in the convex combinations are such that the resulting state can be non-Gaussian. The resulting state $\rho_{a,c}(t) = \mathbb{E}\rho_{a,c}^{(\beta_t)}(t)$ will be our semi-classical description of the system.

It is convenient to introduce a vector of quadratures operators $u = [x_c, y_c, x_a, y_a]$, where $x_j = (j + j^\dagger)/\sqrt{2}$, $y_j = i(j^\dagger - j)/\sqrt{2}$ and $j = a, c$. From Eq. (2), we get a SDE for the first moments

$$\frac{d\langle u\rangle_t}{dt} = A_t\langle u\rangle_t + f_t, \tag{16}$$

where

$$A_t = \begin{bmatrix} -\gamma & \omega_c & 0 & 0 \\ -\omega_c & -\gamma & g\beta_t^{(x)} & g\beta_t^{(y)} \\ -g\beta_t^{(y)} & 0 & -\kappa & \Delta \\ g\beta_t^{(x)} & 0 & -\Delta & -\kappa \end{bmatrix}, f_t = \begin{bmatrix} 0 \\ g|\beta_t|^2 \\ 0 \\ 0 \end{bmatrix} \tag{17}$$

$\beta_t^{(x)} = (\beta_t + \beta_t^*)$, $\beta_t^{(y)} = i(\beta_t^* - \beta_t)$. The second moments can be arranged in the matrix $V_t = \mathrm{Re}\langle uu^\dagger\rangle_t$, satisfying the SDE

$$\frac{dV_t}{dt} = A_t V_t + V_t A_t^T + D + F_t, \tag{18}$$

where $D = \mathrm{diag}[\gamma(2n_c+1), \gamma(2n_c+1), \kappa, \kappa]$, and $F_t = f_t\langle u\rangle_t^T + \langle u\rangle_t f_t^T$. The statistical average over many realization of V_t will be an estimator for the second moments of the quantum state $V(t) = \mathbb{E}(V_t)$. In particular, the first two diagonal elements give the effective phonon number of the mechanical oscillator, since $\langle n_c\rangle(t) = (V_{1,1}(t) + V_{2,2}(t) - 1)/2$. The three stochastic differential equations (15,16,18) can be numerically integrated in sequential order. In our simulations, see Fig. 2, we used the Euler method, for each time step dt sampling the associated Wiener increments in Eq. (15) with normal distributions of variance $\sigma^2 = dt$.

Intuitive explanation of the effect of cooling by heating. This effect can be intuitively explained at hand of Eq. (10) in Description 1: Two competing processes play here an important role: The first term appears like a beam splitter interaction between the modes a and c with a "reflectivity" given by the thermal fluctuations of the amplitude of mode b. This is responsible for the cooling of the mirror. That is to say, the occupation of mode b takes the role resembling the "basis of a transistor": A high occupation renders the interaction between a and c stronger, hence triggering the cooling effect. For this effect to be relevant, the coherence or purity of the state of b does not play a dominant role, and hence even thermal noise can give rise to cooling. This is referred to as "good noise". The second term corresponds to the fluctuations of the radiation pressure of mode b and it is a source of "bad" noise which heats the mechanical mode.

Similarly, this effect can be studied at hand of the stochastic picture of Description 2, when observing Eq. (18). In addition to the intrinsic quantum noise described by D, stochastic fluctuations of β_t generate an additional heating noise given by

the matrix F_t. However, the same process β_t is also contained in the matrix A_t and corresponds to a cooling noise, up to the approximations identical to the above "good noise". The reason is quite evident from Eq. (17), where we observe that the coupling between the hot mechanical oscillator and the cold optical mode is mediated by the thermal fluctuations of β_t. This opto-mechanical coupling, which would be zero without noise, leads to a sympathetic cooling of the mechanical mode.

Example. We will now discuss the effect of cooling by heating at hand of an example using realistic parameters in an opto-mechanical setting. Fig. 2 shows the effective temperature of the mechanical mode as a function of the number of photons in mode b: Here, effective temperature is defined as the temperature T of a Gibbs state

$$\rho_c(T) = \frac{e^{-\hbar\omega_c c^\dagger c/(kT)}}{\mathrm{tr}(e^{-\hbar\omega_c c^\dagger c/(kT)})}$$

such that $\langle n_c\rangle = \mathrm{tr}(\rho_c(T)c^\dagger c)$. One quite impressively encounters the effect of cooling by heating, for increasing photon number and hence effective temperature of this optical mode. For very large values of the photon number, the "bad noise" eventually becomes dominant, resulting again in a heating up of the mechanical mode. Note that needless to say, the effective temperature of the optical mode b is usually larger than the mechanical one by many orders of magnitude (approximately 10^{10}K for reasonable parameters).

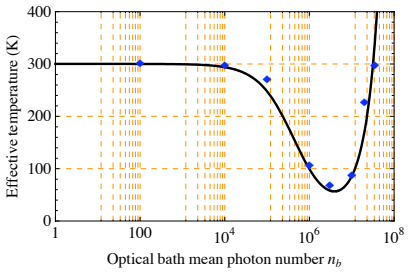

FIG. 2. Room temperature cooling with parameters reminding of those typical in realistic experiments [3]: $\omega_c = 2\pi$MHz, $\kappa = 0.2\omega_c$, $g = 0.3\times10^{-5}\omega_c$, and $\gamma = 10^{-3}\omega_c$. The black line shows the predictions of the steady state using Description 1, the dots are a result from stochastic sampling using Description 2 (with 100 realizations), which qualitatively coincide well. One clearly finds that an increased population of mode b leads to a significant cooling of the mechanical mode – up to a point when eventually the "bad noise" becomes dominant.

Summary. In this work, we have established the notion of cooling by heating, which means that cooling processes can be assisted by means of incoherent hot thermal light. We focused on an opto-mechanical implementation of this paradigm. We also introduced new theoretical tools to grasp the situation of driving by quantum noise, including sampling techniques over stochastic processes. To experimentally demonstrate this counterintuitive effect should be exciting in its own right. Putting things upside down, one could also conceive settings similar to the one discussed here as demonstrators of small heat engines [15] operating at the quantum mechanical level, where b takes the role of an "engine" and mode a of a "condenser". To fully explore these implications for feasibly realizing quantum thermal machines constitutes an exciting perspective. It would also be interesting to fully flesh out the potential for the effect to assist in generating non-classical states [24]. Finally, quite intriguingly, this work may open up ways to think of optically cooling mechanical systems without using lasers at all, but rather with basic, cheap LEDs emitting incoherent light.

Acknowledgements. We would like to thank the EU (Minos, Compas, Qessence), the EURYI, and QuOReP for support.

[1] S. Gigan et al., Nature **444**, 67 (2006); O. Arcizet et al., ibid. **444**, 71 (2006); D. Kleckner and D. Bouwmeester, ibid. **444**, 75 (2006).
[2] A. Schliesser et al., Nature Physics **4**, 415 (2008).
[3] S. Groeblacher et al., Nature Phys. **5**, 485 (2009); Nature **460**, 724 (2009).
[4] D. Vitali, S. Mancini, L. Ribichini, and P. Tombesi, Phys. Rev. A **65**, 063803 (2002).
[5] A. Ferreira, A. Guerreiro, and V. Vedral, Phys. Rev. Lett. **96**, 060407 (2006); M. Paternostro et al., ibid. **99**, 250401 (2007); D. Vitali et al., ibid. **98**, 030405 (2007); C. Genes et al., Phys. Rev. A **78**, 032316 (2008).
[6] F. Marquardt and S. M. Girvin, Physics **2**, 40 (2009).
[7] J. Eisert, M. B. Plenio, S. Bose, and J. Hartley, Phys. Rev. Lett. **93**, 190402 (2004); I. Wilson-Rae, P. Zoller, and A. Imamoglu, ibid. **92**, 075507 (2004).
[8] This cooling is not due to some energy minimum being favored, with a transition facilitated by small amounts of quantum noise, reminding of quantum versions of stochastic resonance [9].
[9] M. B. Plenio and S. F. Huelga, Phys. Rev. Lett. **88**, 197901 (2002); I. Goychuk and P. Hänggi, ibid. **91**, 070601 (2003).
[10] N.G. van Kampen, *Stochastic processes in physics and chemistry* (Elsevier, 2007).
[11] S. Diehl, A. Micheli, A. Kantian, B. Kraus, H. P. Büchler, and P. Zoller, Nat. Phys. **4**, 878 (2008).
[12] J. Eisert and T. Prosen, arXiv:1012.5013.
[13] K. G. H. Vollbrecht, C. A. Muschik, and J. I. Cirac, arXiv:1011.4115.
[14] F. Verstraete, M. M. Wolf, and J. I. Cirac, Nat. Phys. **5**, 633 (2009).
[15] N. Linden, S. Popescu, and P. Skrzypczyk, Phys. Rev. Lett. **105**, 130401 (2010); S. Popescu, arXiv:1009.2536.
[16] Z.-Q. Yin, Phys. Rev. A **80**, 033821 (2009); H. Miao et al., Phys. Rev. A **78**, 063809 (2008); C. Zhao et al., Phys. Rev. Lett. **102**, 243902 (2009).
[17] V. B. Braginsky, S. E. Strigin and S. P. Vyatchanin, Phys. Lett. A **287**, 331 (2001).
[18] C. Biancofiore et al., arXiv:1102.2210.
[19] Q. Lin et al., arXiv:0908.1128.
[20] T. P. Mayer Alegre, A. Safavi-Naeini, M. Winger, and O. Painter, Opt. Exp. **19**, 5658 (2011).
[21] A picture of quantum Brownian motion has also been compared to this quantum optical Markovian limit, with no notable differ-

ences in any predictions within the parameters that are of interest in this work.
[22] C. W. Gardiner and P. Zoller, *Quantum noise* (Springer, 2004).
[23] See EPAPS.
[24] A. Mari and J. Eisert, Phys. Rev. Lett. **103**, 213603 (2009); K. Jaehne, C. Genes, K. Hammerer, M. Wallquist, E. S. Polzik, and P. Zoller, Phys. Rev. **79**, 063819 (2009); A. A. Clerk, F. Marquardt, and K. Jacobs, New J. Phys. **10**, 095010 (2008).

SUPPLEMENTARY MATERIAL

In this supplementary material, we compare the methods of Description 1 and 2 of the main text with an exact simulation of the master equation (2) in a truncated, finite-dimensional Hilbert space of the three involved modes, $\mathcal{H} = \mathbb{C}^{N_a} \otimes \mathbb{C}^{N_b} \otimes \mathbb{C}^{N_c}$. The unique stationary state of Eq. (2) can easily be found numerically; a dimension $d = N_a N_b N_c$ of the total Hilbert space of, say, $d \lesssim 400$, is well feasible. This is obviously an essentially exact method for small occupation numbers in each of the three modes, and the error made can easily be estimated. This analysis, see Fig. 3, together with analogous ones in similar regimes, shows that the methods used here are also suitable in the deep quantum regime.

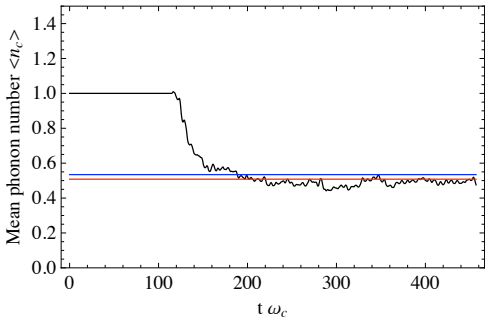

FIG. 3. Stochastic simulation – introduced in Description 2 – of the mean number of phonons as a function of time (black line), compared with the exact steady state (blue line) and with the analytical approximation given in Description 1 (red line). Parameters: $n_b = n_c = 1$, $\kappa = 0.1\omega_c$, $\gamma = 0.01\omega_c$, $g = 0.006\omega_c$.

Chapter 7

Opto and electro-mechanical entanglement improved by modulation

Opto- and electro-mechanical entanglement improved by modulation

A. Mari[1,2] and J. Eisert[1,2]
[1] *Dahlem Center for Complex Quantum Systems, Freie Universität Berlin, 14195 Berlin, Germany and*
[2] *Institute of Physics and Astronomy, University of Potsdam, D-14476 Potsdam, Germany*

One of the main milestones in the study of opto- and electro-mechanical systems is to certify entanglement between a mechanical resonator and an optical or microwave mode of a cavity field. In this work, we show how a suitable time-periodic modulation can help to achieve large degrees of entanglement, building upon the framework introduced in [Phys. Rev. Lett. **103**, 213603 (2009)]. It is demonstrated that with suitable driving, the maximum degree of entanglement can be significantly enhanced, in a way exhibiting a non-trivial dependence on the specifics of the modulation. Such time-dependent driving might help experimentally achieving entangled mechanical systems also in situations when quantum correlations are otherwise suppressed by thermal noise.

INTRODUCTION

Opto-mechanical [1–7] and electro-mechanical systems [8–13] are promising candidates for realizing architectures exhibiting quantum behavior in macroscopic structures. Once the quantum regime is reached, exciting applications in quantum technologies such as realizing precise force sensors are conceivable [15, 16]. One of the requirements to render such an approach feasible, needless to say, is to be able to certify that a mechanical degree of freedom is deeply in the quantum regime [16–20]. The detection of entanglement arguably constitutes the ultimate benchmark in this respect. While effective ground state cooling has indeed been experimentally closely approached [6, 10] and achieved [7, 9, 13], the detection of entanglement is still awaiting.

In this work, we emphasize that a mere suitable time-modulation of the driving field may significantly help to achieve entanglement between a mechanical mode and a radiation mode of the system. We extend the idea of Ref. [21], putting emphasis on the improvement of entanglement by means of suitable modulations [21–23]. The method used here is not a direct modulation of the frequencies of the two modes (parametric amplification), but the system is instead externally driven with a modulated field. This time dependence of the driving indirectly affects the effective radiation pressure coupling between the two modes and generates non-trivial entanglement resonances. In this way, with the appropriate choice of the modulation pattern, large degrees of two-mode squeezing can be reached.

MODULATED OPTO- AND ELECTRO-MECHANICAL SYSTEMS

We consider the simplest scenario of a mechanical resonator of frequency ω_m coupled to a single mode of the electromagnetic field of frequency ω_a. This radiation field could be an optical mode of a Fabry-Perot cavity [1–7, 18, 19, 24] or a microwave mode of a superconductive circuit [8–10, 14]. It can be shown that the Hamiltonians associated to this two experimental settings are formally equivalent [14, 19] and therefore the theory that we are going to introduce is general enough to describe both types of systems.

We assume that the radiation mode is driven by a coherent field with a time dependent amplitude $E(t)$ and frequency ω_l. The particular choice of the time dependence is left unspecified but we impose the structure of a periodic modulation such that $E(t+\tau) = E(t)$ for some $\tau > 0$ of the order of ω_m^{-1}. In this sense, the driving regime that we are going to study is intermediate between the two opposite extremes of constant amplitude and short pulses. The Hamiltonian of the system is

$$H = \hbar\omega_a a^\dagger a + \frac{1}{2}\hbar\omega_m(p^2+q^2) - \hbar g a^\dagger a q \\ +i\hbar[E(t)e^{-i\omega_l t}a^\dagger - E^*(t)e^{i\omega_l t}a], \quad (1)$$

where the mechanical mode is described in terms of dimensionless position and momentum operators satisfying $[q,p] = i$, while the radiation mode is captured by creation and annihilation operators obeying the bosonic commutation rule $[a,a^\dagger] = 1$. The two modes interact via a radiation pressure potential with a strength given by the coupling parameter g.

In addition to this coherent dynamics, the mechanical mode will be unavoidably damped at a rate γ_m, while the optical/microwave mode will decay at a rate κ. These dissipative processes and the associated fluctuations can be taken into account in the Heisenberg picture by the following set of quantum Langevin equations [14, 17–19],

$$\begin{aligned} \dot{q} &= \omega_m p, \quad (2)\\ \dot{p} &= -\omega_m q - \gamma_m p + g a^\dagger a + \xi, \\ \dot{a} &= -(\kappa + i\Delta)a + igaq + E(t) + \sqrt{2\kappa}a^{\rm in}. \end{aligned}$$

In this set of equations a convenient rotating frame has be chosen $a \mapsto a e^{-i\omega_l t}$, such that the detuning parameter is $\Delta = \omega_a - \omega_l$. The operators ξ and $a^{\rm in}$ represent the mechanical and optical bath operators respectively, and their correlation functions are well approximated by delta functions

$$\begin{aligned} \langle \xi(t)\xi(t') + \xi(t')\xi(t)\rangle/2 &= \gamma_m(2n_m+1)\delta(t-t'), \quad (3)\\ \langle a^{\rm in}(t)a^{\rm in\dagger}(t')\rangle &= (n_a+1)\delta(t-t'), \\ \langle a^{\rm in\dagger}(t)a^{\rm in}(t')\rangle &= n_a\delta(t-t'), \end{aligned}$$

where $n_x = (\exp(\hbar\omega_x/(k_B T)) - 1)^{-1}$, is the bosonic mean occupation number at temperature T.

CLASSICAL PERIODIC ORBITS: FIRST MOMENTS

We are interested in the coherent strong driving regime when $\langle a\rangle \gg 1$. In this limit, the semiclassical approximations $\langle a^\dagger a\rangle \simeq |\langle a\rangle|^2$ and $\langle aq\rangle \simeq \langle a\rangle\langle q\rangle$ are good approximations. Within this approximation, one can average both sides of Eq. (2) and get a differential equation for the first moments of the canonical coordinates

$$\begin{aligned}\langle\dot{q}\rangle &= \omega_m\langle p\rangle, \\ \langle\dot{p}\rangle &= -\omega_m\langle q\rangle - \gamma_m\langle p\rangle + g|\langle a\rangle|^2, \\ \langle\dot{a}\rangle &= -(\kappa+i\Delta)\langle a\rangle + ig\langle a\rangle\langle q\rangle + E(t).\end{aligned} \tag{4}$$

Far away from the well known opto- and electromechanical instabilities, asymptotic τ-periodic solutions can be used as ansatz for Eqs. (4) (see the Appendix for a more detailed analysis). These solutions represent periodic orbits in phase space and are usually called limit cycles. These cycles are induced by the modulation and should not be confused with the limit cycles emerging in the strong driving regime due to the non-linearity of the system. Because of the asymptotic periodicity of the solutions, one can define the fundamental modulation frequency as $\Omega = 2\pi/\tau$, such that each periodic solution can be expanded in the following Fourier series

$$\langle O(t)\rangle = \sum_{n=-\infty}^{\infty} O_n e^{in\Omega t}, \quad O = q, p, a. \tag{5}$$

The Fourier coefficients $\{O_n\}$ appearing in Eq. (5) can be analytically estimated as shown in Appendix and they completely characterize the classical asymptotic dynamics of the system.

Finally we notice that the classical evolution of the dynamical variables will shift the detuning to the effective value of $\tilde{\Delta}(t) = \Delta - g\langle q(t)\rangle$. For the same reason, it is also convenient to introduce an effective coupling constant defined as

$$\tilde{g}(t) = ig\langle a(t)\rangle/\sqrt{2}. \tag{6}$$

QUANTUM CORRELATIONS: SECOND MOMENTS

The classical limit cycles are given by the asymptotic solutions of Eqs. (4). In order to capture the quantum fluctuations around the classical orbits, we introduce a column vector of new quadrature operators $u = [\delta q, \delta p, \delta x, \delta y]^T$ defined as:

$$\begin{aligned}\delta q &= q - \langle q(t)\rangle, \\ \delta p &= p - \langle p(t)\rangle, \\ \delta x &= \left[(a - \langle a(t)\rangle) + (a - \langle a(t)\rangle)^\dagger\right]/\sqrt{2}, \\ \delta y &= -i\left[(a - \langle a(t)\rangle) - (a - \langle a(t)\rangle)^\dagger\right]/\sqrt{2}.\end{aligned} \tag{7}$$

This set of canonical coordinates can be viewed as describing a time-dependent reference frame co-moving with the classical orbits. The corresponding vector of noise operators will be

$$n = [0, \xi, (a^{\rm in} + a^{\rm in\dagger})/\sqrt{2}, -i(a^{\rm in} - a^{\rm in\dagger})/\sqrt{2}]^T. \tag{8}$$

Since we are in the limit in which classical orbits emerge ($\langle a\rangle \gg 1$), it is a reasonable approximation to express the previous set of Langevin equations (2) in terms of the new fluctuation operators (7) and neglect all quadratic powers of them. The resulting linearized system can be written as a matrix equation [21],

$$\dot{u} = A(t)u + n(t), \tag{9}$$

where,

$$A(t) = \begin{bmatrix} 0 & \omega_m & 0 & 0 \\ -\omega_m & -\gamma_m & \Re\tilde{g}(t) & \Im\tilde{g}(t) \\ -\Im\tilde{g}(t) & 0 & -\kappa & \tilde{\Delta}(t) \\ \Re\tilde{g}(t) & 0 & -\tilde{\Delta}(t) & -\kappa \end{bmatrix} \tag{10}$$

is a real time-dependent matrix.

If the system is stable, and as long as the linearization is valid, the quantum state of the system will converge to a Gaussian state with time dependent first and second moments. The first moments of the state correspond to the classical limit cycles introduced in the previous section. The second moments can be expressed in terms of the covariance matrix $V(t)$ with entries

$$V_{k,l}(t) = \langle u_k(t)u_l^\dagger(t) + u_l^\dagger(t)u_k(t)\rangle/2. \tag{11}$$

One can also define a diffusion matrix D as

$$\delta(t-t')D_{k,l} = \langle n_k(t)n_l^\dagger(t') + n_l^\dagger(t')n_k(t)\rangle/2, \tag{12}$$

which, from the properties of the bath operators (3), is diagonal and equal to

$$D = \mathrm{diag}[0, \gamma(2n_m+1), \kappa(2n_a+1), \kappa(2n_a+1)]. \tag{13}$$

From Eqs. (9) and (12), one can easily derive a linear differential equation for the correlation matrix,

$$\frac{d}{dt}V(t) = A(t)V(t) + V(t)A^T(t) + D. \tag{14}$$

Since the first and the second moments are specified, Eqs. (4) and (14) provide a complete description of the asymptotic dynamics of the system. Apart from the linearization around classical cycles, no further approximation has been done: Neither a weak coupling, adiabatic or rotating-wave approximation. Numerical solutions of both equations (4) and (14) can be straightforwardly found. These solutions will be used to calculate the exact amount opto- and electro-mechanical entanglement present in the system.

The asymptotic periodicity of the classical solutions (Eq. (5)) implies that, in the long time limit, $A(t+\tau) = A(t)$. This means that Eq. (14) is a linear differential equation with periodic coefficients and then all the machinery of Floquet theory is in principle applicable. Here, however, since we are only interested on asymptotic solutions, we are not going to study all the Floquet exponents of the system. The only property

that we need is that, in the long time limit, stable solutions will acquire the same periodicity of the coefficients:

$$V(t+\tau) = V(t). \tag{15}$$

This is a simple corollary of Floquet's theorem. In the subsequent sections we will apply the previous theory to some particular experimental setting and show how a simple modulation of the driving field can significantly improve the amount of opto- and electro-mechanical entanglement.

ENTANGLEMENT RESONANCES

In this section we are going to study what kind of amplitude modulation is optimal for generating entanglement between the radiation and mechanical modes. As a measure of entanglement we use the logarithmic negativity E_N which, since the state is Gaussian, can be easily computed directly from the correlation matrix $V(t)$ [26–28]. We have also seen that the correlation matrix is, in the long time limit, τ-periodic. This suggests that it is sufficient to study the variation of entanglement in a finite interval of time $[t, t+\tau]$ for large times t. One can then define the maximum amount of achievable entanglement as

$$\hat{E}_N = \lim_{t\to\infty} \max_{h\in[t,t+\tau]} E_N(h). \tag{16}$$

This will be the quantity that we are going to optimize.

We first study a very simple set of parameters (see caption of Figure 1) in order to understand what the optimal choice is for the modulation frequency. For this purpose we impose the effective coupling to have this simple structure

$$\tilde{g}(t) = \tilde{g}_0 + \tilde{g}_\Omega\, e^{-i\Omega t}, \tag{17}$$

where $\tilde{g}_0$ is associated to the main driving field with detuning Δ, while $\tilde{g}_\Omega$ is the amplitude of a further sideband shifted by a frequency Ω from the main carrier. Without loss of generality we will assume $\tilde{g}_0$ and $\tilde{g}_\Omega$ to be positive reals. This kind of driving is a natural one and has been chosen for reasons that will become clear later. From now on we set the detuning of the carrier frequency to be equal to the mechanical frequency $\Delta = \omega_m$. This choice of the detuning corresponds to the well known sideband cooling setting [17, 24] and it has been shown to be also optimal for maximizing opto-mechanical entanglement with a non-modulated driving [19]. Fig. 1 shows the maximum entanglement $\hat{E}_N$ between the mechanical and the radiation modes as a function of the modulation frequency Ω and for different values of the driving amplitude $\tilde{g}_0$. This maximum degree of entanglement has been calculated for $t > 200/\kappa$ when the system has well reached its periodic steady state.

We observe that in Fig. 1 there are two main resonant peaks at the modulation frequencies

$$\Omega \simeq 2\omega_m \pm \tilde{g}_0. \tag{18}$$

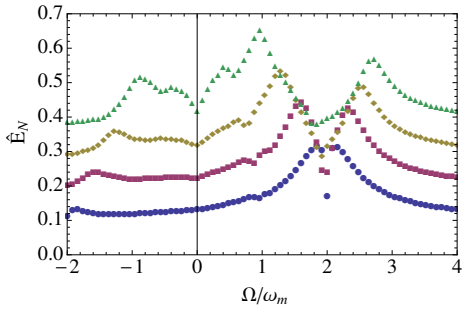

FIG. 1. Maximum entanglement $\hat{E}_N$ as a function of the modulation frequency Ω and for different values of the driving strength $\tilde{g}_0$. The chosen parameters in units of ω_m are: $\kappa = 0.2$, $\gamma_m = 10^{-6}$, $\bar{\Delta} = 1$, $n_m = n_a = 0$, $\tilde{g}_\Omega = 0.1$, $\tilde{g}_0 = 0.2$ (circles), 0.4 (squares), 0.6 (diamonds), 0.8 (triangles).

We will now provide some intuition why one should expect the main resonances at the locations where they are observed. First assume that $\tilde{g}_0 = 0$. Then, for $\Delta = \omega_m$, the linearized Hamiltonian in the interaction picture is

$$H_{\rm int} = -\hbar\tilde{g}_\Omega \left(e^{i(\omega_m-\Omega)}\delta a^\dagger + e^{-i(\omega_m-\Omega)}\delta a\right) \left(e^{i\omega_m}\delta b^\dagger + \delta b e^{-i\omega_m}\right)/2, \tag{19}$$

where the bosonic operators are defined as $\delta a = (\delta x + i\delta y)/\sqrt{2}$, $\delta b = (\delta q + i\delta p)/\sqrt{2}$. From Eq. (19), it is clear that for $\Omega = 2\omega_m$, neglecting all rotating terms, we get the well known two-mode squeezing generator

$$H_{\rm int} \simeq -\hbar\tilde{g}_\Omega \left(\delta a^\dagger \delta b^\dagger + \delta a \delta b\right)/2. \tag{20}$$

So, in the case of $\tilde{g}_0 = 0$, a modulation of $\Omega = 2\omega_m$ would be the most reasonable choice in order to generate entanglement. However, this regime is well known to be highly unstable and, in practice, it cannot be used for preparing entangled steady states [14].

This is why we need to consider a modulated coupling of the form given in Eq. (17) – or a similar type of modulation sharing these features. We now allow for $\tilde{g}_0$ being different from zero, giving rise to a situation which can be assessed in a very similar way as above (only that the rotation terms will take a more involved form). The main amplitude $\tilde{g}_0$ then takes the role of cooling and stabilizing the system while the modulation amplitude $\tilde{g}_\Omega$ is used to generate entanglement. At the same time however, as shown in Refs. [5, 25], for $\tilde{g}_0 > \kappa/\sqrt{2}$ the system hybridizes in two normal modes of frequencies

$$\omega_\pm \simeq \omega_m \pm \tilde{g}_0/2. \tag{21}$$

As a consequence, this will affect the modulation frequency Ω that one has to choose in order to achieve the two-mode squeezing interaction given in Eq. (20). This is the reason for the presence of two resonant peaks in Fig. 1 and for the resonance condition given in Eq. (18).

Note also that the choices of modulations that give rise to the optimal local single-mode squeezing [21] of the mechanical mode and the degree of entanglement are not identical. This is rooted in the "monogamous nature" of squeezing: For a fixed spectrum of the covariance matrix, one can either have large local or two-mode squeezing. This effect is observed when considering the modulation frequencies that achieve maximum single- and two-mode squeezing.

We finally observe that the height of the two peaks, due to the cavity filtering, is not equal: the first resonance at $\Omega = 2\omega_m - \tilde{g}_0$ is better for the amount of steady state entanglement. One could also ask what the behavior of entanglement is when we change the amplitude of the modulation. Fig. 2 shows the amount of entanglement $\hat{E}_N$ as a function of $\tilde{g}_\Omega$ and for different choices of $\tilde{g}_0$. We observe that entanglement is monotonically increasing in $\tilde{g}_\Omega$ up to a threshold where the system becomes unstable.

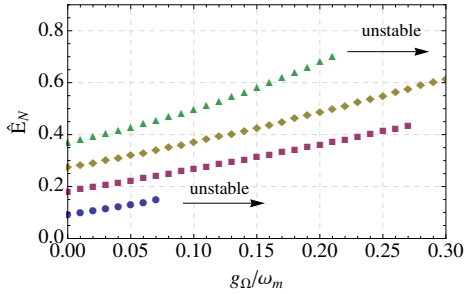

FIG. 2. Maximum entanglement $\hat{E}_N$ as a function of the modulation amplitude $\tilde{g}_\Omega$ and for different values of the driving strength $\tilde{g}_0$. The chosen parameters in units of ω_m are: $\kappa = 0.2, \gamma_m = 10^{-6}, \Delta = 1$, $n_m = n_a = 0$, $\Omega = 2\omega_m - \tilde{g}_0$, $\tilde{g}_0 = 0.2$ (circles), 0.4 (squares), 0.6 (diamonds), 0.8 (triangles).

OPTO- AND ELECTRO-MECHANICAL ENTANGLEMENT IN REALISTIC SETTINGS

We have seen that an effective coupling of the form $\tilde{g}(t) = \tilde{g}_0 + \tilde{g}_\Omega\, e^{-i(2\omega_m - \tilde{g}_0)t}$ is optimal for the generation of entanglement within the considered class of drivings. However, the parameter $\tilde{g}(t)$ depends on the average amplitude $\langle a(t)\rangle$ and assuming such a simple structure may seem somewhat artificial. In this section, we show how the desired time-dependent coupling can indirectly result from the classical limit cycles of the system (see insets of Figs. 3 and 4) and we also take into account the effect of a temperature of the order of $T \simeq 100$ mK. The natural "educated guess" for the structure of the driving field will be

$$E(t) = E_0 + E_\Omega E e^{-i(2\omega_m - \tilde{g}_0)t}. \qquad (22)$$

For the choice of the other parameters, we focus on two set of parameters corresponding to two completely different systems: an optical cavity with a moving mirror and a superconducting wave guide coupled to a mechanical resonator. The parameters are chosen according to realistic experimental settings, see, e.g., Ref. [5] (opto-mechanical system) and Ref. [9] (electro-mechanical system). Fig. 3 and Fig. 4 show that, in both experimental scenarios, entanglement can significantly be increased by an appropriate modulation of the driving field.

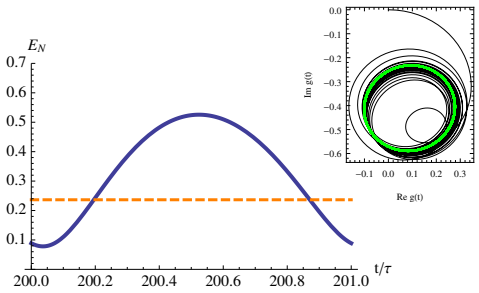

FIG. 3. (Optical cavity). The degree of entanglement, measured in terms of the logarithmic negativity, as a function of time. The full line refers to a modulated driving ($\Omega = 1.4\omega_m$) while the dotted line corresponds to a non-modulated driving ($\Omega = 0$). The chosen parameters in units of ω_m are: $\kappa = 0.2$, $\gamma_m = 10^{-6}$, $\Delta = 1$, $n_m = 2\times10^3$, $n_a = 0$, $g_0 = 4 \times 10^{-6}$, $E_0 = 7 \times 10^4$, $E_\Omega = 2.5 \times 10^4$. The inset shows the trajectory of the effective coupling $\tilde{g}(t) = \sqrt{2}g\langle a(t)\rangle$ in the complex plane due to the time evolution of the optical amplitude. The phase space orbit (black line) is numerically simulated from Eq. (4), while the limit cycle (green line) is an analytical approximation (see Appendix for more details).

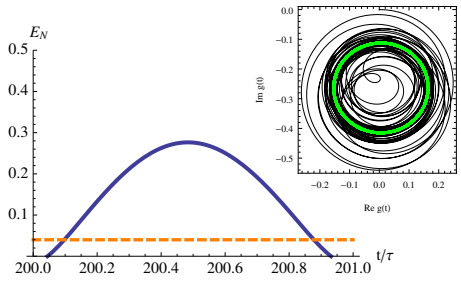

FIG. 4. (Microwave cavity). Entanglement log-negativity as a function of time. The full line refers to a modulated driving ($\Omega = 1.3\omega_m$) while the dotted line corresponds to a non-modulated driving ($\Omega = 0$). The chosen parameters in units of ω_m are: $\kappa = 0.02$, $\gamma_m = 3 \times 10^{-6}$, $\Delta = 1$, $n_m = 200$, $n_a = 0.03$, $g_0 = 2 \times 10^{-5}$, $E_0 = 9 \times 10^3$, $E_\Omega = 1.3 \times 10^3$. The inset depicts the trajectory of the effective coupling $\tilde{g}(t) = \sqrt{2}g\langle a(t)\rangle$ in the complex plane due to the time evolution of the microwave amplitude. The phase space orbit (black line) is numerically simulated from Eq. (4), while the limit cycle (green line) is an analytical approximation (see Appendix for more details).

SUMMARY

In this work, we have shown how time-modulation can significantly enhance the maximum degree of entanglement. Triggered by the time-modulated driving, the mode of the electromechanical field as well as the mechanical mode start "rotating around each other" in a complex fashion, giving rise to increased degrees of entanglement. The dependence on the frequencies of the additional modulation is intricate, with resonances highly improving the amount of entanglement that can be reached. The ideas presented here could be particularly beneficial to prepare systems in entangled states in the first place, in scenarios where the parameters are such that the states prepared are close to the boundary to entangled states, but where this boundary is otherwise not yet quite reachable with present technology. At the same time, such ideas are expected to be useful in metrological applications whenever high degrees of entanglement are needed.

APPENDIX

In this appendix we derive analytical formulas for the asymptotic solutions of the classical system of dynamical equations (4). A crucial assumption for the following procedure is that it is possible to expand the solutions in powers of the the coupling constant g_0

$$\langle O\rangle(t) = \sum_{j=0}^{\infty} O_j(t) g_0^j, \tag{23}$$

where $O = a, p, q$. This is justified only if the system is far away from multi-stabilities and the radiation pressure coupling can be treated in a perturbative way. A very important feature of the set of equations (4) is that they contain only two non linear terms and those terms are proportional to the coupling parameter g_0. This implies that, if we use the ansatz (23), each function O_j will be a solution of *linear* differential equation with time dependent parameters depending on the previous solution $O_{j-1}(t)$. Since $E(t) = E(t+\tau)$, from a recursive application of Floquet's theorem, follows that stable solutions will converge to periodic limit cycles having the same periodicity of the driving: $\langle O(t)\rangle = \langle O(t+\tau)\rangle$. One can exploit this property and perform a double expansion in powers of g_0 and in terms of Fourier components

$$\langle O\rangle(t) = \sum_{j=0}^{\infty}\sum_{n=-\infty}^{\infty} O_{n,j} e^{in\Omega t} g_0^j, \tag{24}$$

where n are integers and $\Omega = 2\pi/\tau$. A similar Fourier series can be written for the periodic driving field,

$$E(t) = \sum_{n=-\infty}^{\infty} E_n e^{in\Omega t}. \tag{25}$$

The coefficients $O_{n,j}$ can be found by direct substitution in Eq. (4). They are completely determined by the following set of recursive relations:

$$q_{n,0} = p_{n,0} = 0, \qquad a_{n,0} = \frac{E_{-n}}{\kappa + i(\Delta_0 + n\Omega)}, \tag{26}$$

corresponding to the 0-order perturbation with respect to G_0, and

$$p_{n,j} = \frac{in\Omega}{\omega_m} q_{n,j}, \tag{27}$$

$$q_{n,j} = \omega_m \sum_{k=0}^{j-1}\sum_{m=-\infty}^{\infty} \frac{a^*_{m,k}\, a_{n+m,j-k-1}}{\omega_m^2 - n\Omega^2 + i\gamma_m n\Omega}, \tag{28}$$

$$a_{n,j} = i \sum_{k=0}^{j-1}\sum_{m=-\infty}^{\infty} \frac{a_{m,k} q_{n-m,j-k-1}}{\kappa + i(\Delta_0 + n\Omega)}, \tag{29}$$

giving all the j-order coefficients in a recursive way. For all the examples analyzed in this paper we truncated the analytical solutions up to $j \leq 3$ and $|n| \leq 2$. This level of approximation is already high enough to well reproduce the exact numerical solutions.

ACKNOWLEDGEMENTS

We would like to thank the EU (MINOS, COMPAS, QESSENCE) and the BMBF (QuOReP) for support.

[1] S. Gigan, H. R. Böhm, M. Paternostro, F. Blaser, G. Langer, J. B. Hertzberg, K. Schwab, D. Baeuerle, M. Aspelmeyer, and A. Zeilinger, Nature **444**, 67 (2006).
[2] O. Arcizet, P.-F. Cohadon, T. Briant, M. Pinard, and A. Heidmann, Nature **444**, 71 (2006).
[3] D. Kleckner and D. Bouwmeester, Nature **444**, 75 (2006).
[4] A. Schliesser, P. DelHaye, N. Nooshi, K. J. Vahala, and T. J. Kippenberg, Phys. Rev. Lett. **97**, 243905 (2006).
[5] S. Gröblacher, K. Hammerer, M. R. Vanner, and M. Aspelmeyer, Nature **460**, 724 (2009).
[6] R. Riviere, S. Deleglise, S. Weis, E. Gavartin, O. Arcizet, A. Schliesser, T. J. Kippenberg, Phys. Rev. A **83**, 063835 (2011).
[7] J. Chan, T. P. Mayer Alegre, A. H. Safavi-Naeini, J. T. Hill, A. Krause, S. Groeblacher, M. Aspelmeyer, and O. Painter, Nature **478**, 89 (2011).
[8] J. D. Teufel, J. W. Harlow, C. A. Regal, and K. W. Lehnert, Phys. Rev. Lett. **101**, 197203 (2008).
[9] J. D. Teufel, T. Donner, D. Li, J. H. Harlow, M. S. Allman, K. Cicak, A. J. Sirois, J. D. Whittaker, K. W. Lehnert, and R. W. Simmonds, Nature **475**, 359 (2011).
[10] T. Rocheleau, T. Ndukum, C. Macklin, J. B. Hertzberg, A. A. Clerk, and K. C. Schwab, Nature **463**, 72 (2010).
[11] M. D. LaHaye, O. Buu, B. Camarota, and K. C. Schwab, Science **304**, 74 (2004).
[12] R. G. Knobel and A. N. Cleland, Nature **424**, 291 (2003).
[13] A. D. O Connell, M. Hofheinz, M. Ansmann, R. C. Bialczak, M. Lenander, E. Lucero, M. Neeley, D. Sank, H. Wang, M. Weides, J. Wenner, J. M. Martinis, and A. N. Cleland, Nature **464**, 697 (2010).
[14] D. Vitali, P. Tombesi, M. J. Woolley, A. C. Doherty, and G. J. Milburn, Phys. Rev. A **76**, 042336 (2007).

[15] K. C. Schwab and M. L Roukes, Physics Today **58**, 36 (2005).
[16] F. Marquardt and S. M. Girvin, Physics **2**, 40 (2009).
[17] M. Aspelmeyer, Nature **464**, 685 (2010).
[18] M. Paternostro, D. Vitali, S. Gigan, M. S. Kim, C. Brukner, J. Eisert, and M. Aspelmeyer, Phys. Rev. Lett. **99**, 250401 (2007).
[19] D. Vitali, S. Gigan, A. Ferreira, H. R. Böhm, P. Tombesi, A. Guerreiro, V. Vedral, A. Zeilinger, and M. Aspelmeyer, Phys. Rev. Lett. **98**, 030405 (2007).
[20] J. Eisert, M. B. Plenio, S. Bose, and J. Hartley, Phys. Rev. Lett. **93**, 190402 (2004).
[21] A. Mari and J. Eisert, Phys. Rev. Lett. **103**, 213603 (2009).
[22] M. J. Woolley, A. C. Doherty, G. J. Milburn, and K. C. Schwab, Phys. Rev. A **78**, 062303 (2008).
[23] A. A. Clerk, F. Marquardt, and K. Jacobs, New J. Phys. **10**, 095010 (2008).
[24] F. Marquardt, J. P. Chen, A. A. Clerk, and S. M. Girvin Phys. Rev. Lett. **99**, 093902 (2007).
[25] J. M. Dobrindt, I. Wilson-Rae, and T. J. Kippenberg Phys. Rev. Lett. **101**, 263602 (2008).
[26] J. Eisert, PhD thesis (Potsdam, February 2001).
[27] G. Vidal and R. F. Werner, Phys. Rev. A **65**, 032314 (2002).
[28] M. B. Plenio, Phys. Rev. Lett. **95**, 090503 (2005).

Discussion and conclusions

Here I will do a global discussion about the scientific material presented in this thesis. First I will briefly summarize all the main results that have been achieved in each publication and afterwords I will try to give a global picture underling the connections among the different results.

- **Quantum effects in optomechanical systems [1]**

  This is a general review of the field of quantum optomechanics specially focused on the theory of mechanical ground state cooling and on the generation of entanglement involving mechanical, optical and atomic degrees of freedom. My contribution to this publication has been mostly on the analysis of the entanglement between spectral sidebands of output cavity modes and the motion of a vibrating mirror (Section 4) and on the study of optomechanical systems where two optical modes are driven at the same time (Section 5).

- **Gently modulating optomechanical systems [2]**

  Here a new method for generating squeezed mechanical states has been proposed. A squeezed state [34] is a quantum state where the uncertainty along one particular phase space direction is less than the vacuum fluctuations. Because of the Heisenberg principle, this noise reduction can only occur at the expense of having more noise along the orthogonal phase space direction, hence the name *squeezing*. Contrarily to ground state cooling, mechanical squeezing has not yet been experimentally achieved and it would represent a further step deep into the quantum regime. All previous proposals [7] required some experimental effort like: modulating the spring constant, driving with squeezed light or controlling with feedback loops. In this paper we have shown that all standard optomechanical setups currently used to cool the mechanical motion are potentially able to generate squeezed states. The idea is to simply modulate the amplitude of the driving laser field (this is much easier than

modulating the mechanical spring constant). For a particular choice of the modulation frequency (twice the mechanical one), non-trivial asymptotic cycles emerge generating strong degrees of mechanical squeezing. The appeal of this result is the simplicity of the proposed experimental apparatus since, with respect the state of the art of all laser cooling experiments, it only requires the addition of an amplitude modulator.

- **Directly estimating non-classicality [3]**

  In this paper we proposed a method for directly measuring "how much" a state is *non-classical*. By applying mathematical tools like classical [40] and quantum [38, 39] Bochner's theorems, we developed a direct operational test for rigorously certifying the negativity of the Wigner function of any continuous variable quantum system. With this new theoretical method we have been able to experimentally certify the non-classicality of a real quantum state of light. The proposed algorithm is very general and ready to be directly applied to optomechanical systems as soon as the preparation of mechanical non-classical states will be experimentally feasible.

- **Cooling by heating [4]**

  This paper introduces the quite counter-intuitive idea of "cooling by heating" in the sense of cooling a quantum system (in our case a mechanical resonator) by using hot thermal light. The technique of laser cooling of mechanical systems is well known and it is successfully used in many experiments [17, 19, 20, 21]. In this paper we have shown that, in some particular situations, the same task can be achieved without the need of a coherent laser but simply with incoherent thermal light. From a theoretical point of view we also introduced a new simulation method based on stochastic sampling of Gaussian quantum states with respect to stationary classical stochastic processes. This paper has been submitted to a peer review journal and it is currently under editorial evaluation. A news article about this work appeared in the popular science journal *Physics World* [42].

- **Opto- and electro-mechanical entanglement improved by modulation [5]**

  Here the modulation technique introduced in *Gently modulating optomechanical systems* has been exploited for a different task: improving the

steady state entanglement between a mechanical resonator and an optical or microwave cavity mode. We have shown that for appropriate modulation frequencies (non-trivially related to the hybridization of the energy levels of the system) large degrees of entanglement can be generated. The proposed method may be very convenient from an experimental point of view: entangled optomechanical states are very fragile with respect to temperature and this technique could provide a feasible solution to this obstacle.

The common theme connecting all the particular results is the attempt to investigate new methods for *preparing* and *measuring* signatures of quantum effects in optomechanical systems. In particular several new protocols have been proposed for *preparing* pure states, squeezed states and entangled states involving optical and mechanical modes. For each of this effects we proposed a feasible way of experimentally *measuring* it. In particular we developed a rigorous and quantitative algorithm for experimentally certifying the nonclassicality of continuous variable quantum states.

The possibility of controlling massive mechanical systems ($\sim 10^{15}$ atoms) into a quantum mechanical regime would have huge impact not only within the scientific community but it would open the door for many new technological and industrial applications. Ultra sensitive measurements of position or force are just two examples of a direct application of quantum optomechanics [43]. Other ideas in the field of classical or quantum information processing have been proposed [6] and, as usual when some new physical phenomenon is discovered, many new unpredictable technological applications are "there" waiting to be found. It is then clear that the main goal of the present research on optomechanics is to reach the ability of manipulating mesoscopic mechanical devices at the quantum level, or said in other words, *"putting mechanics into quantum mechanics"* [43]. This thesis is intended as a small contribution in this big challenge.

Bibliography

[1] C. Genes, A. Mari, D. Vitali and P. Tombesi, *Adv. At. Mol. Opt. Phys.* **57**, 33 (2009).

[2] A. Mari and J. Eisert, *Phys. Rev. Lett.* **103**, 213603 (2009).

[3] A. Mari, K. Kieling, B. M. Nielsen, E. S. Polzik and J. Eisert, *Phys. Rev. Lett.* **106**, 010403 (2011).

[4] A. Mari and J. Eisert, *arXiv:1104.0260*.

[5] A. Mari and J. Eisert, *arXiv:1111.2415*.

[6] F. Marquardt, S. M. Girvin, *Physics* **2**, 40 (2009).

[7] M. Aspelmeyer, S. Gröblacher, K. Hammerer, N. Kiesel, *J. Opt. Soc. Am.* **B 27**, A189-A197 (2010).

[8] M. Arndt *at al.*, *arXiv:quant-ph/0505187*, *Quantum Physics of Nature Conference* (Vienna, 2005).

[9] J. Kepler, *De cometis libelli tres* (A. Apergeri, 1619).

[10] E. Kalemci *et al.*, *Astrophys. J. Supp.* **169**, 75-82 (2007).

[11] J. C. Maxwell, *A Treatise on Electricity and Magnetism* (Clarendon, Oxford, 1874).

[12] E. Einstein, *Physikalische Zeitschrift Vol. 10 No.* **22**, 817 (1909).

[13] V. B. Braginsky, A. B. Manukin and M. Y. Tikhonov, *Sov. Phys. JETP* **31**, 829 (1970).

[14] C. Fabre *et al.*, *Phys. Rev.* **A 49**, 1337 (1994).

[15] S. Mancini and P. Tombesi, *Phys. Rev.* **A 49**, 4055 (1994).

[16] G. J. Milburn, K. Jacobs and D. F. Walls, *Phys. Rev.* **A 50**, 5256 (Dec 1994).

[17] S. Mancini, D. Vitali and P. Tombesi,*Phys. Rev. Lett.* **80**, 688 (1998).

[18] S. Bose, K. Jacobs and P. L. Knight, *Phys. Rev.* **A 56**, 4175 (1997).

[19] P. F. Cohadon, A. Heidmann and M. Pinard, *Phys. Rev. Lett.* **83**, 3174 (1999).

[20] C. H. Metzger and K. Karrai, *Nature* **432**, 1002 (2004).

[21] T. J. Kippenberg and K. J. Vahala, *Science* **321**, 1172 (2008).

[22] M. Aspelmeyer and K. C. Schwab, *New J. Phys.* **10**, 095001 (2008).

[23] A. Schlisser *et al.*, *Nature Physics* **5**, 509-514 (2009).

[24] J. Chan *et al.*, *Nature* **478**, 89 (2011).

[25] J. D. Teufel *et al.*, *Nature* **475**, 359 (2011).

[26] A. D. O'Connell *et al.*, *Nature* **464**, 697 (2010).

[27] W. Marshall, C. Simon, R. Penrose and D. Bouwmeester, *Phys. Rev. Lett.* **91**, 130401 (2003).

[28] J. Eisert, M. B. Plenio, S. Bose and J. Hartley, *Phys. Rev. Lett.* **93**, 190402 (2004).

[29] D. Vitali *et al.*, *Phys. Rev. Lett.* **98**, 030405 (2007).

[30] K. Stannigel *et al.*, *Phys. Rev.* **A 84**, 042341 (2011).

[31] O. Romero-Isart *et. al*, *Phys. Rev. Lett.* **107**, 020405 (2011).

[32] J. D. Thompson *et al.*, *Nature* **452**, 72-75 (2008).

[33] C. K. Law, *Phys. Rev.* **A 51**, 2537 (1995).

[34] C. W. Gardiner and P. Zoller, *Quantum Noise*, (Springer, Berlin, 2000).

[35] W. Vogel, D. G. Welsch, *Quantum Optics*, (WILEY-VHC, Berlin, 2006).

[36] J. Eisert and M. B. Plenio, *Int. J. Quant. Inf.* **1**, 479 (2003).

[37] S. L. Braunstein and P. van Loock, *Rev. Mod. Phys.* **77**, 513 (2005).

[38] C. D. Cushen and R. L. Hudson, *J. Appl. Prob.* **8**, 454 (1971).

[39] F. J. Narcowich, *J. Math. Phys.* **29**, 2036 (1988).

[40] S. Bochner, *Math. Ann.* **108**, 378 (1933).

[41] G. Teschl, *Ordinary differential equations and dynamical systems*, http://www.mat.univie.ac.at/∼gerald.

[42] H. Johnston, *Cooling with heat*, (PhysicsWorld, April, 2011).

[43] K. C. Schwab and M. L. Roukes, *Physics Today* **58**, 36 (2005).